ERDC TR-14-12

US Army Corps of Engineers®
Engineer Research and Development Center

ERDC
INNOVATIVE SOLUTIONS for a safer, better world

Experimental Evaluation of the Failure of a Seismic Design Category – B Precast Concrete Beam-Column Connection System

Jorge O. Torres-Alamo, Vincent P. Chiarito, and Henry L. Blake

December 2014

Engineer Research and Development Center

The US Army Engineer Research and Development Center (ERDC) solves the nation's toughest engineering and environmental challenges. ERDC develops innovative solutions in civil and military engineering, geospatial sciences, water resources, and environmental sciences for the Army, the Department of Defense, civilian agencies, and our nation's public good. Find out more at www.erdc.usace.army.mil.

To search for other technical reports published by ERDC, visit the ERDC online library at http://acwc.sdp.sirsi.net/client/default.

ERDC TR-14-12
December 2014

Experimental Evaluation of the Failure of a Seismic Design Category – B Precast Concrete Beam-Column Connection System

Jorge O. Torres-Alamo and Vincent P. Chiarito

Geotechnical and Structures Laboratory
U.S. Army Engineer Research and Development Center
3909 Halls Ferry Road
Vicksburg, MS 39180-6199

Henry L. Blake

Information Technology Laboratory
U.S. Army Engineer Research and Development Center
3909 Halls Ferry Road
Vicksburg, MS 39180-6199

Final report

Prepared for U.S. Army Engineer Research and Development Center
3909 Halls Ferry Road
Vicksburg, MS 39180-6199

Abstract

Modern cities across the United States choose to use multistory buildings in an attempt to optimize the available construction space. These structures are required by governing building codes to be designed for regional or site-specific seismic hazards that affect the resulting loads on moment resisting beam-column connections. These seismically designed connections and seismic structural systems provide resistance to shear and moment forces resulting from the seismic loads. But little is known about predicting their capacity in a brittle manner under a disproportionate collapse condition.

The U.S. Army Engineer Research and Development Center (ERDC) was tasked by the Department of Homeland Security under the Building Stabilization Program to conduct a full-scale experiment to test a precast concrete beam-column system to failure. This experiment was designed to evaluate the performance of precast frame systems in order to develop a methodology and obtain basic insight for predicting the brittle failure of precast beam-column connections under conditions related to a disproportionate collapse scenario. Understanding the parameters that affect the onset of brittle failure of these systems will lead to the development of new techniques allowing first responders to assess the stability of the structures in real time prior to entering for rescue operations.

Contents

Figures and Tables

Figures

Tables

Preface

The research reported herein was sponsored by the Department of Homeland Security, under the Building Stabilization Program. Dr. Mila Kennett was the Program Manager.

These experiments were conducted by personnel of the Geotechnical and Structures Laboratory (GSL) and the Information and Technology Laboratory (ITL) of the U.S. Army Engineer Research and Development Center (ERDC).

Dr. Stanley Woodson, Geosciences and Structures Division (GSD), was the ERDC Program Manager. The research was conducted by Jorge O. Torres-Alamo, Structural Mechanics Branch (SMB), and Vincent P. Chiarito, Structural Engineering Branch (StEB), all within the GSD, and Henry L. Blake, Information Technology Laboratory (ITL). This report was prepared by Torres-Alamo, Chiarito, and Blake.

During this investigation, Dr. Gordon W. McMahon was Chief, SMB; Terry R. Stanton was Chief, StEB; Bartley P. Durst was Chief, GSD; Dr. William P. Grogan was Deputy Director, GSL; and Dr. David W. Pittman was Director, GSL.

COL Jeffrey R. Eckstein was Commander and Executive Director of ERDC. Dr. Jeffery P. Holland was Director.

Unit Conversion Factors

Multiply	By	To Obtain
cubic feet	0.02831685	cubic meters
cubic inches	1.6387064 E-05	cubic meters
degrees (angle)	0.01745329	radians
feet	0.3048	meters
inches	0.0254	meters
pounds (force)	4.448222	newtons
pounds (force) per square foot	47.88026	pascals
pounds (force) per square inch	6.894757	kilopascals
pounds (mass)	0.45359237	kilograms
pounds (mass) per cubic foot	16.01846	kilograms per cubic meter
pounds (mass) per cubic inch	2.757990 E+04	kilograms per cubic meter
pounds (mass) per square foot	4.882428	kilograms per square meter
square feet	0.09290304	square meters
square inches	6.4516 E-04	square meters

1 Introduction

1.1 Background

Modern cities across the United States choose to use multistory buildings in an attempt to optimize the use of available construction space. These structures are required by law to be designed for seismic loads utilizing moment resisting beam-column connections. These seismically designed connections and seismic structural systems provide resistance to shear and moment resulting from both lateral and vertical earthquake forces. Despite these requirements, little is known about predicting the capacity of precast systems failing in a brittle manner under a disproportionate collapse condition.

The term disproportionate collapse is used to describe the behavior of a building when a primary structural element fails, resulting in the failure of adjoining structural elements, which, in turn, causes further structural failure. Some of the events that challenged the engineering community to develop new and advanced technologies to diminish the effects of a disproportionate collapse on infrastructure are the collapse of Ronan Point Apartment Tower in Newham, East London, on May 16, 1968; the Alfred P. Murrah Federal Building, caused by a truck bomb attack in Oklahoma City on April 19, 1995; and the World Trade Center towers on September 11, 2001, caused by the impact of large passenger jetliners (Shankar Nair March 2004).

The National Institute of Standard and Technology (NIST), the Precast Concrete Institute (PCI), and Metromont Corporation (MC) created a research team with the objective of developing a new beam-column system design resistant to disproportionate collapse events. This resistance to disproportionate collapse is achieved either implicitly, by establishing minimum levels of strength, continuity, and ductility, or explicitly, by (1) providing alternate load paths so that local damage is absorbed and major collapse is averted or (2) providing sufficient strength to specific structural members that are critical to global stability.

The U.S. Army Engineer Research and Development Center (ERDC) was tasked by the Department of Homeland Security, under the Building Stabilization Program, to conduct a full-scale experiment using the precast

concrete column connection specified for Seismic Design Category – B (SDC-B) with the objective of understanding the modes of failure. This understanding would lead to development of a methodology to predict the brittle failure of precast beam-column connections. Understanding the parameters that affect the onset of brittle failure of precast concrete structure systems will help to develop new techniques that allow first responders the ability to assess the stability of structures in real time before entering a damaged building for rescue operations. This effort will also help to improve the (UFC 4-023-03 2005)and quantify large displacement behavior of precast structural elements for enhancing building structural health monitoring.

1.2 Objectives

The objectives of the experiment were to evaluate the performance of the full-scale precast structural system and obtain data from which a methodology could be developed to predict the brittle failure of precast beam-column connections under a disproportionate collapse condition. In addition to this, the experimental data will also be used to validate a numerical model developed by NIST.

1.3 Scope

These objectives were met by testing two precast concrete beam-column subassemblies (each with two beams, two end columns, and a center stub column) designed by NIST, MC, and PCI. There are two distinct designs for the precast concrete beam-column subassemblies, one each for Seismic Design Categories D and B (SDC-D and SDC-B), respectively. Each experiment investigated a single design. This report documents the failure performance of the precast beam-column assembly designed for SDC-B. The response of the SDC-D assembly will be documented in a companion report.

The precast assembly for SDC-B consisted of two deep rectangular concrete beams supported by two concrete columns at the ends of the beams and a column stub at center. The assembly was subjected to a concentrically loaded displacement-controlled force at the center of the column stub. This simulated the structure's behavior under a column removal scenario. It was expected that catenary action would develop where the beams respond in a tensile membrane manner. The test was terminated on reaching the collapse mechanism of the assembly. Active instrumentation was installed

on the specimens and monitored throughout the test to investigate structural response during experiment execution. A data acquisition system was used to record the gauge data. Video and still photography obtained structural response and damage images during experiment execution.

Results of this test will help provide an improved understanding of typical behavior of a precast multistory building undergoing loss of an essential supporting member caused by an unforeseen event.

2 Experiment Description

2.1 Prototype building design

NIST, working with a panel of practicing structural engineers across the United States, developed the overall configuration and dimensions of the prototype SDC-B and SDC-D buildings to be considered in this research program. For simplicity of design and analysis, a 10-story office building with a rectangular plan was chosen as the prototype structure. For this study, two precast concrete frame buildings were designed, each with plan dimensions of 125 ft by 125 ft with 5 bays in both longitudinal and transverse directions. The detailed design of the building was provided by a consulting engineering firm Metromont Corporation 2010. This innovative design was developed with the objective of reducing the brittle failure of precast concrete beam-column connections in conventional buildings due to a loss of an essential supporting member. The lateral loads were resisted by exterior moment resisting frames. All interior frames were designed to support gravity loads only. Figure 1 shows an elevation view of the prototype building.

Figure 1. East-west elevation of the prototype precast concrete building (Sadek 2010).

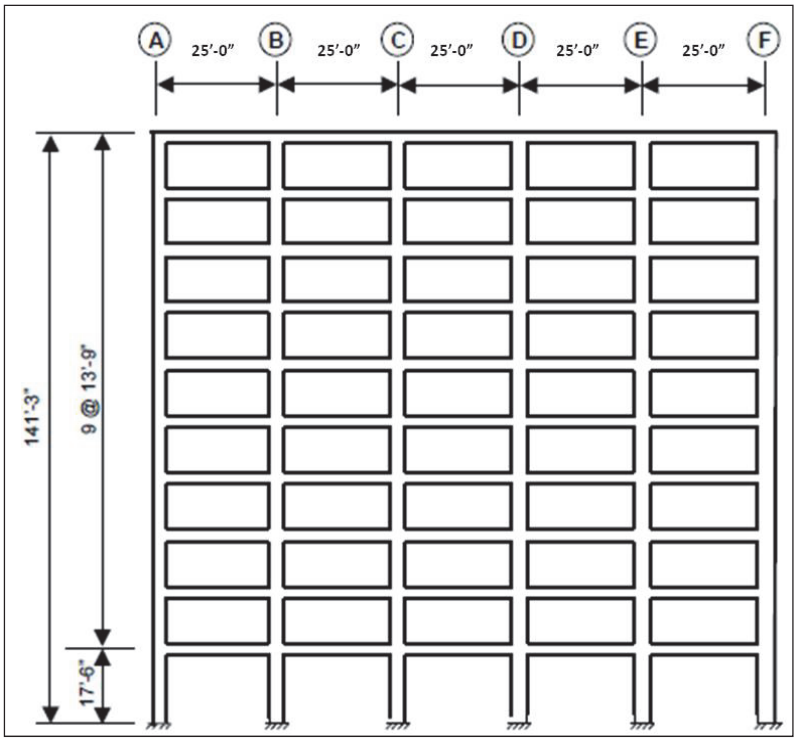

Figure 2 shows the front elevation view of the schematic layout of the test specimen. The experimental test assembly represents a precast reinforced concrete beam-column connection from the fourth floor of a 10-story building.

Figure 2. SDC-B front view.

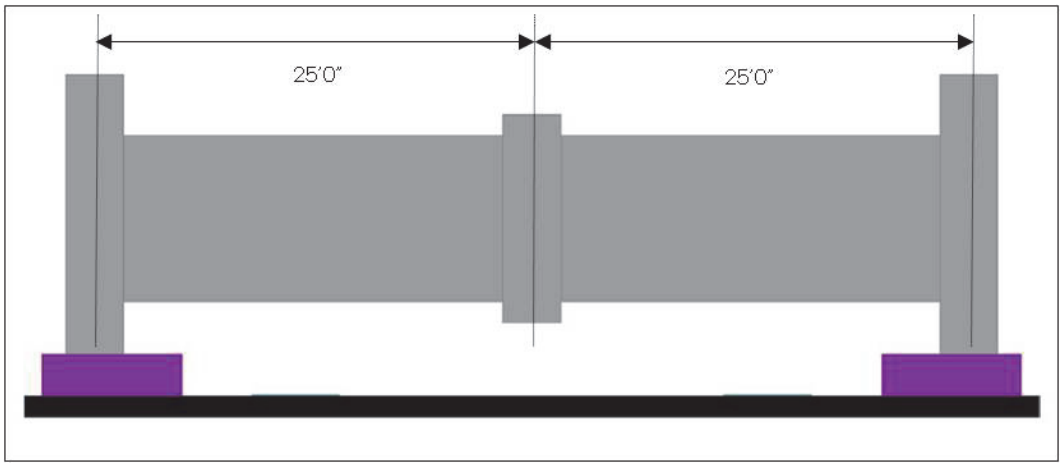

2.2 Experimental reaction structure

A schematic view of the test setup used for the SDC-B specimen is shown in Figure 3. The vertical load was applied to the top of the center column/stub by single hydraulic ram acting through a load cell and a steel plate. In Figure 3, it is also observed that the horizontal movements of the steel plate were restrained by four steel columns positioned at each corner of the plate.

A special roller-bearing support arrangement at the four corners of the plate allowed free vertical displacement of the plate along the four steel columns. The steel plate also restrained the horizontal movements of the top center column/stub, thereby keeping the applied load in the vertical direction and limiting eccentricity of the load. A pair of steel plates at the lower end of the center column/stub, on each face, restrained out-of-plane motion. Two 50-ft-long steel girders shown in green in Figure 3 were connected by a four short steel beams shown in Figure 4. These girders were also used to restrain the end columns from buckling or moving horizontally.

A hydraulic ram with a capacity of 600 kips and a 20-in. stroke (Figure 5) was used to apply a vertical downward load to the center column of the test specimen. The load was applied under ram displacement control at a rate of 1 in. per minute.

Figure 3. SDC-B reaction structure.

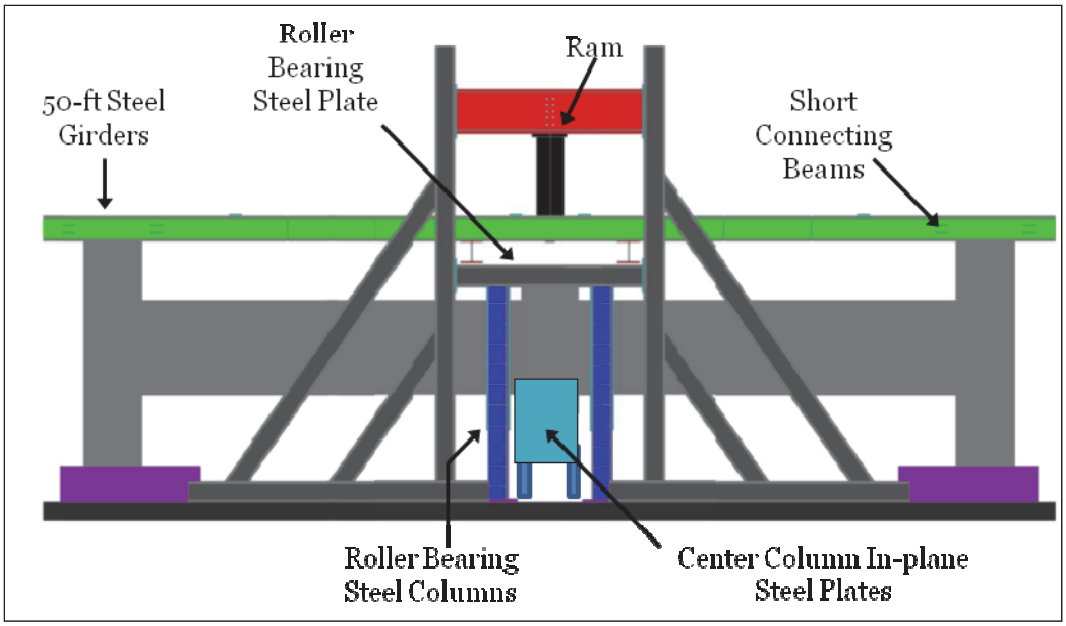

Figure 4. Reaction structure restrains short beams or girders.

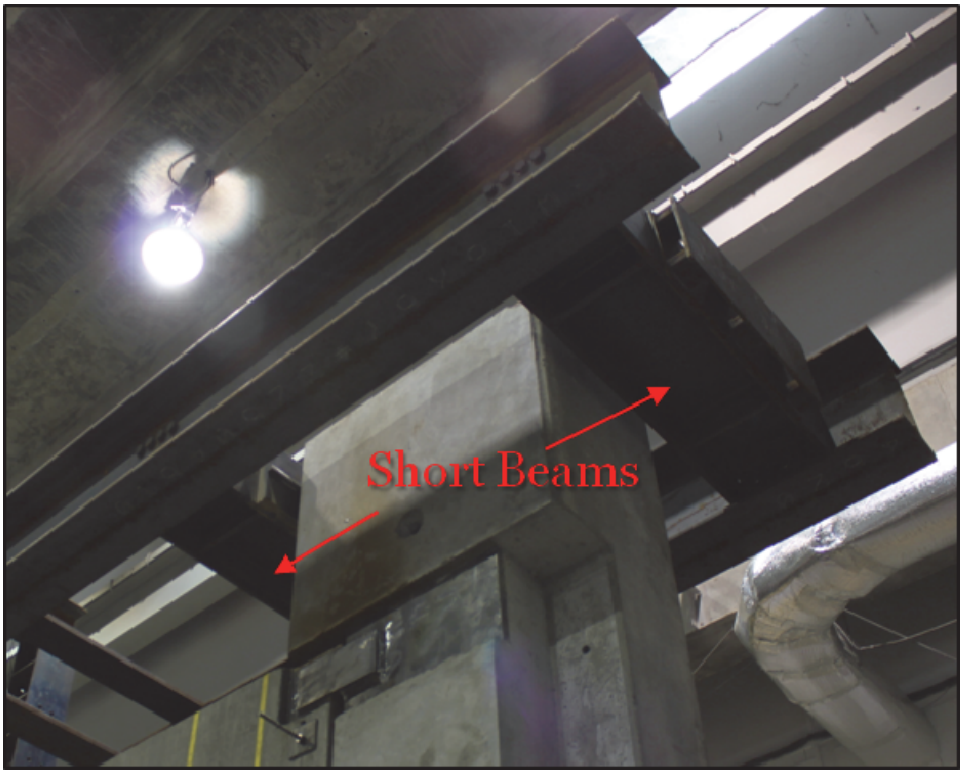

Figure 5. View of the 600-kip hydraulic ram.

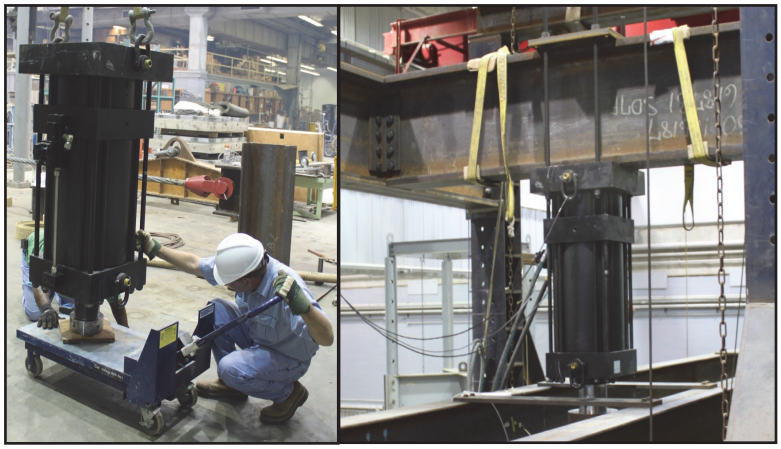

2.3 Seismic design category – B specimen description/test setup

2.3.1 Overview of test specimen SDC-B

Figure 6 shows an elevation view of the setup, member sizes, and beam-to-column connection details for the SDC-B specimen. All beams and columns were constructed of concrete with a 7,000-psi unconfined compressive strength at 28 days and strengthened with (ASTM A706 n.d.) steel reinforcing bars.

Figure 6. SDC-B front elevation view of the experimental setup.

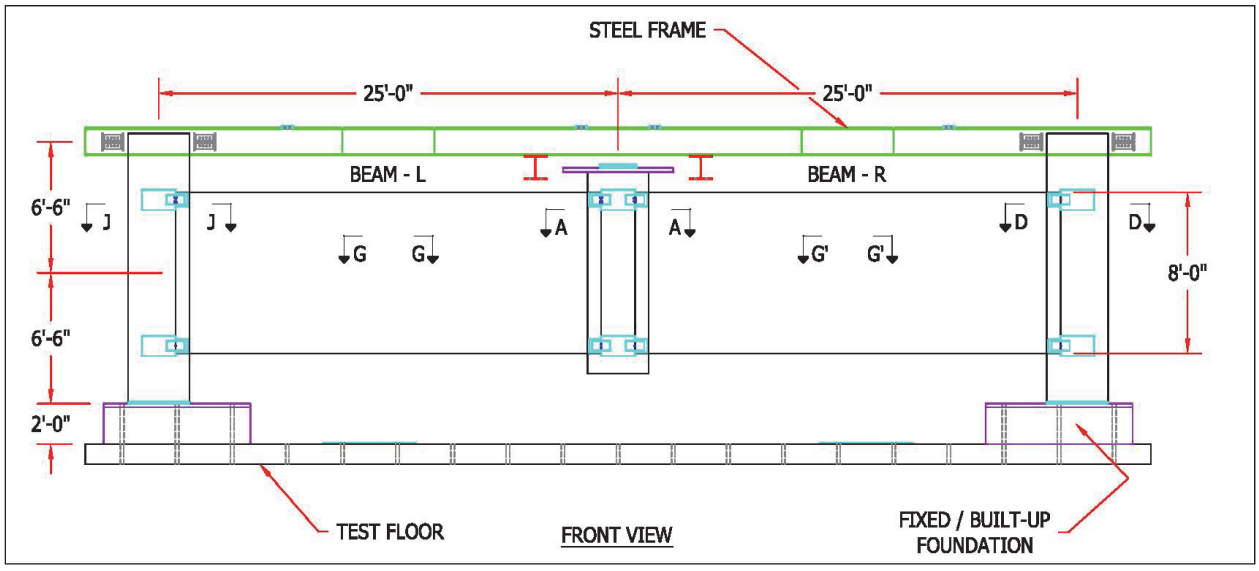

Figure 7 shows the layout of the two end columns used in SDC-B experiment. These columns were fully welded around the bottom surface to a steel plate connected to a concrete slab foundation using threaded rods.

Figure 7. SDC-B end columns.

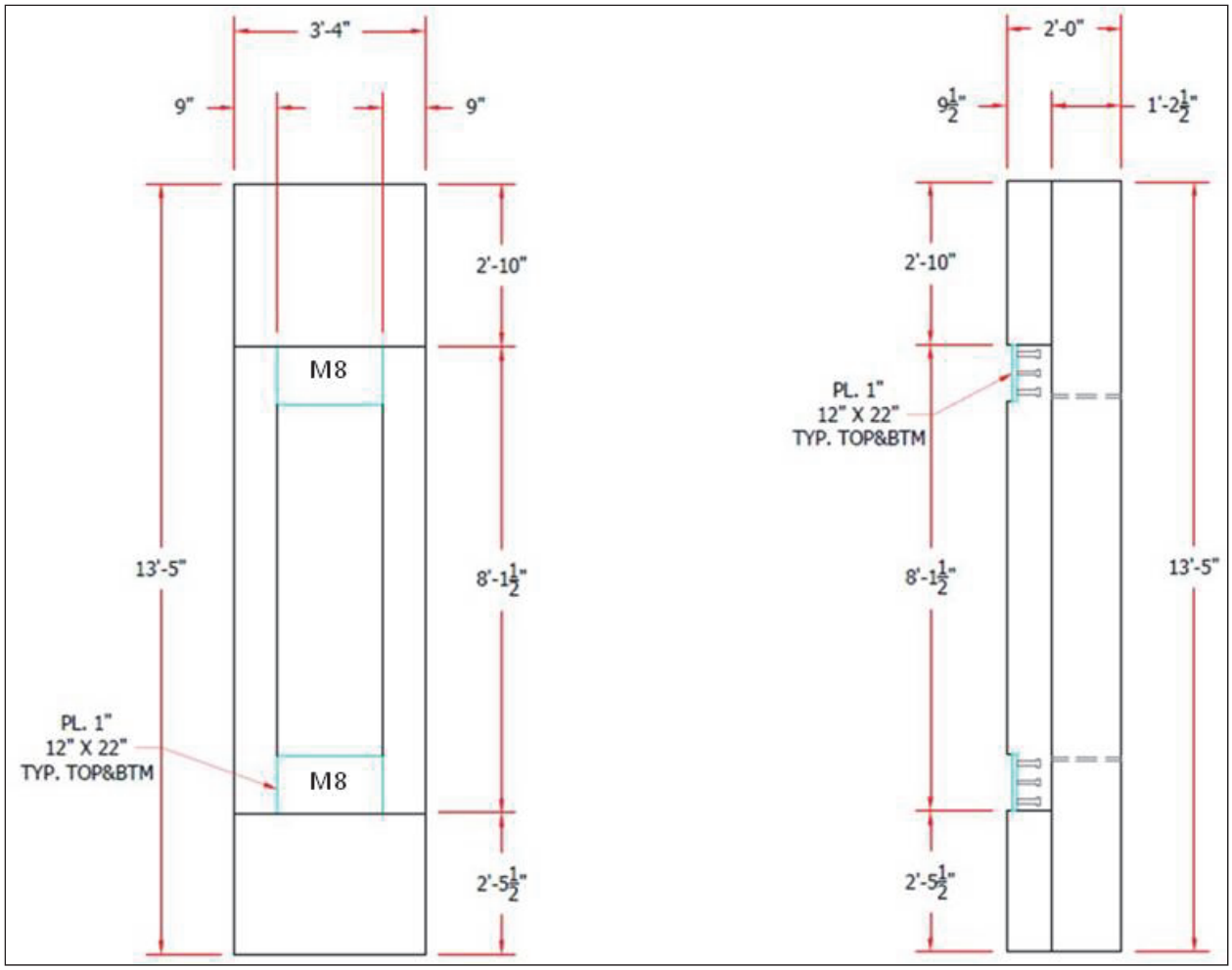

Figure 8 illustrates the layout of the center column/stub used on SDC-B. The center column was connected to the concrete beams using ductile steel connecting plates.

2.3.2 Beam – column connections

As shown in Figure 7 and Figure 8, each beam has two 1-in.-by-12-in.-by-22-in. (ASTM A36 n.d.) steel plates embedded to the concrete. Each plate was anchored using nine 1-in.-by-4-in. Headed Concrete Anchors (HCA) nelson studs.

The beams also had 8-in.-by-6-in.-by-1-in.-by-8-in.-long. ASTM A36 embedded angles on each corner (see Figure 9). Every angle had anchor bars welded to it as well. Figure 10 specified the welding details utilized. On the bottom embedded angles (M7) of each beam were two 6-ft-long #10 (ASTM A706 Gr. 60) anchor bars, and on the other two top-corner

embedded angles (M6) were two 7.67-ft-long #10 anchor bars. Anchor bars were a key design parameter for the SDC-B test specimen. Two #10 steel reinforcing bars were used to provide tensile resistance and anchor the embedded steel connection plates to the ends of the moment resisting beam-column connection. Details of these connections are shown in Figure 11. Each beam was placed on the column on top of a 0.5-in. bearing pad and connected to the columns using 1-in.-by-5.5-in.-by-12-in. connecting A36 steel plates welded to the embedded angles in each of the corners of the beams and to the embedded plate on the columns shown in Figure 12. Figure 13 illustrates a typical view of the beam-column connection method. These ductile connection steel plates were made of ASTM A36 steel. In addition, four torsion rods were installed through the beam-column connections. The purpose of these rods is to maintain the system aligned by resisting torsion forces on the beams.

Figure 8. SDC-B center column/stud.

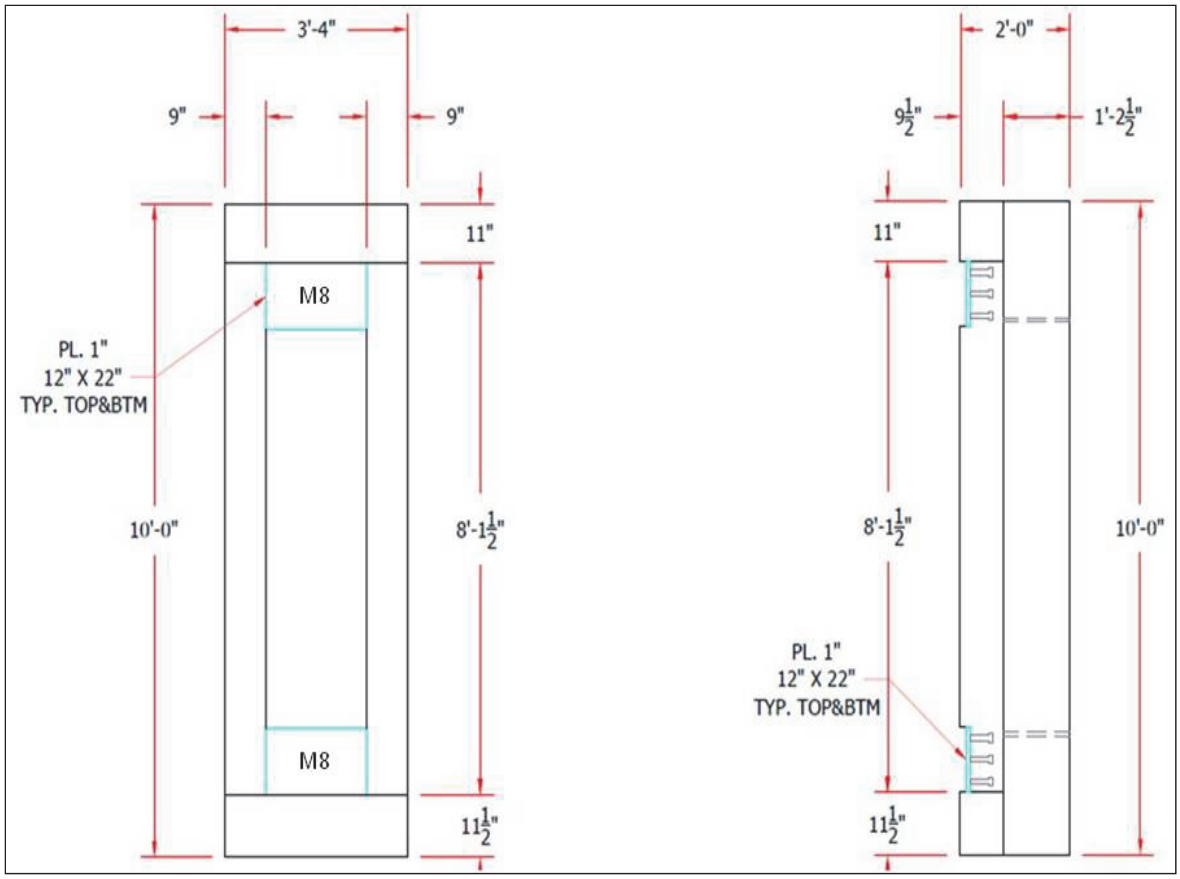

Figure 9. SDC-B typical layout of the concrete beams.

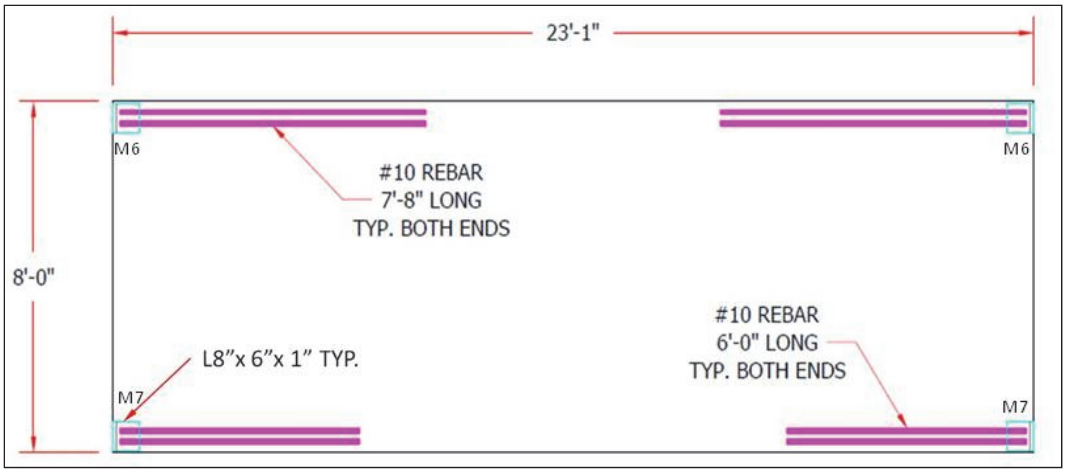

Figure 10. Welding details on M6 and M7 beam embedded angles.

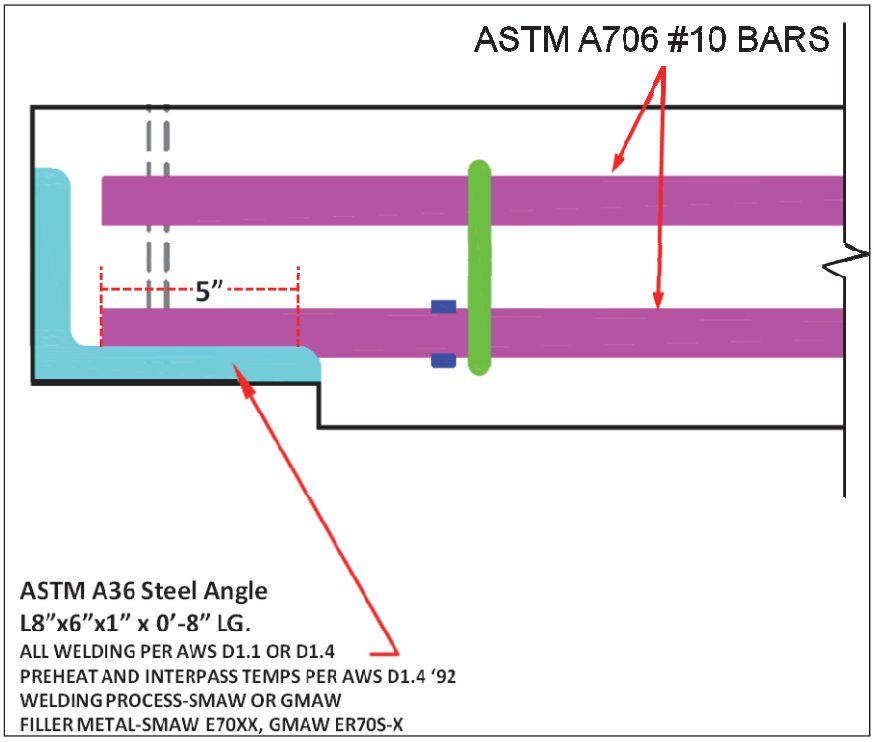

Figure 11. Detail of the connection plate attached with the number 10 rebars.

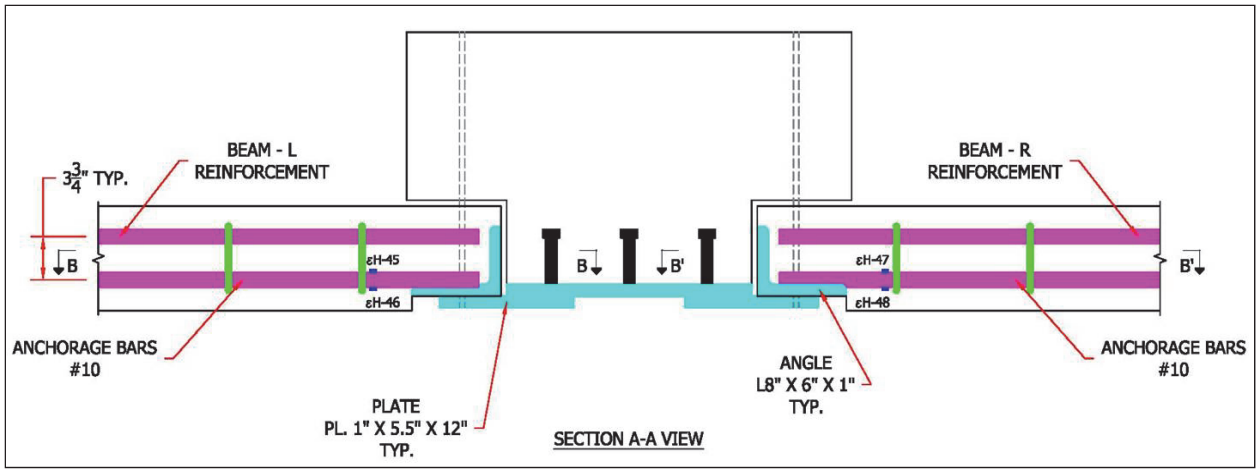

Figure 12. Assembling of SDC-B test specimen.

Figure 13. A36 ductile connecting plate and torsion rod beam connecting elements.

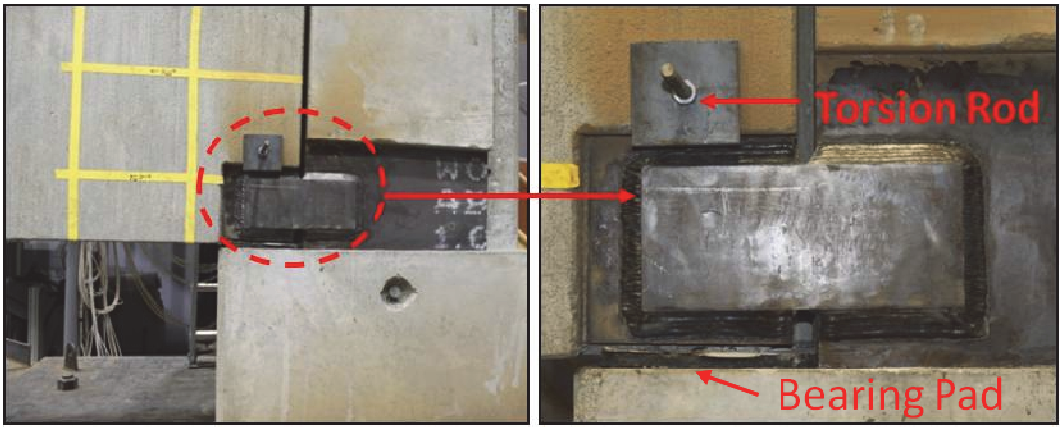

3 Instrumentation

3.1 Pseudo-static response channels

A total of 71 recording channels were used in the instrumentation plan for SDC-B, including 16 at a high-speed sample rate of 2 MHz. The data included information on the applied load, displacements, rotations, strains on reinforcement bars and the exterior steel connections plates, tension in the torsion bars connecting the beams to the columns, and acoustic emissions near the center column stub-beam connections. Table 1 describes the type of measurement and number of channels for each of the instrumentation components.

Table 1. Instrumentation matrix for SDC-B.

Type of Gauge	Measurement Number	Number of Channels
Load Cell	L-95A	1
Differential Pressure Gauge	L-95B	1
“String Potentiometer” Gauges	D-83, 85, 86, 88	4
Linear Variable Differential Transformer (LVDT)	LVDT-81, 90	2
Inclinometers	R-91, 92, 93, 94	4
Internal Strain Gauges	Ɛh-41 - 127	16
Rosette External Strain Gauges		24
Single External Strain Gauges		9
Load Cells for Torsion Bar Tensile Loads	T1, T2	2
Acoustic Emission Sensors	AE1, AE2	2
Accelerometers	L1, L2	6
Total		71

3.1.1 Load cell and differential pressure gauge

A hydraulic ram was used to apply a vertical downward static load to the center column of the test specimens while the load was recorded using an external 400-kip load cell installed at the end of the stroke (Figure 14). A differential pressure sensor inside the 600-kip servo-hydraulic actuator (ram) was used to record the hydraulic pressure exerted on the piston rod. Figure 15 illustrates where the ram was anchored during the test.

Figure 14. SDC-B 400-kip load cell and differential pressure gauge.

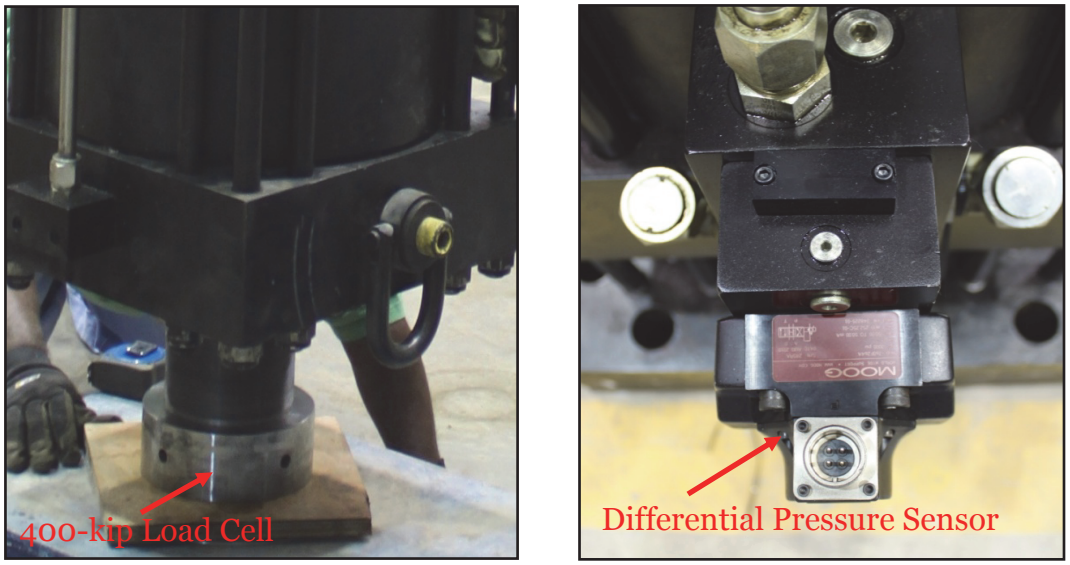

Figure 15. SDC-B hydraulic static ram installation.

3.1.2 Displacement gauges

Six displacement gauges were used in the test (Figure 16). Four sensors were string potentiometers with a 72-in. range and 0.001-in. accuracy; these sensors measured the vertical displacements. In addition, two linear variable differential transformers (LVDTs) located at mid-elevation of the end columns measured displacements in the horizontal direction throughout the test.

Figure 16. SDC-B layout of the displacement gauge locations.

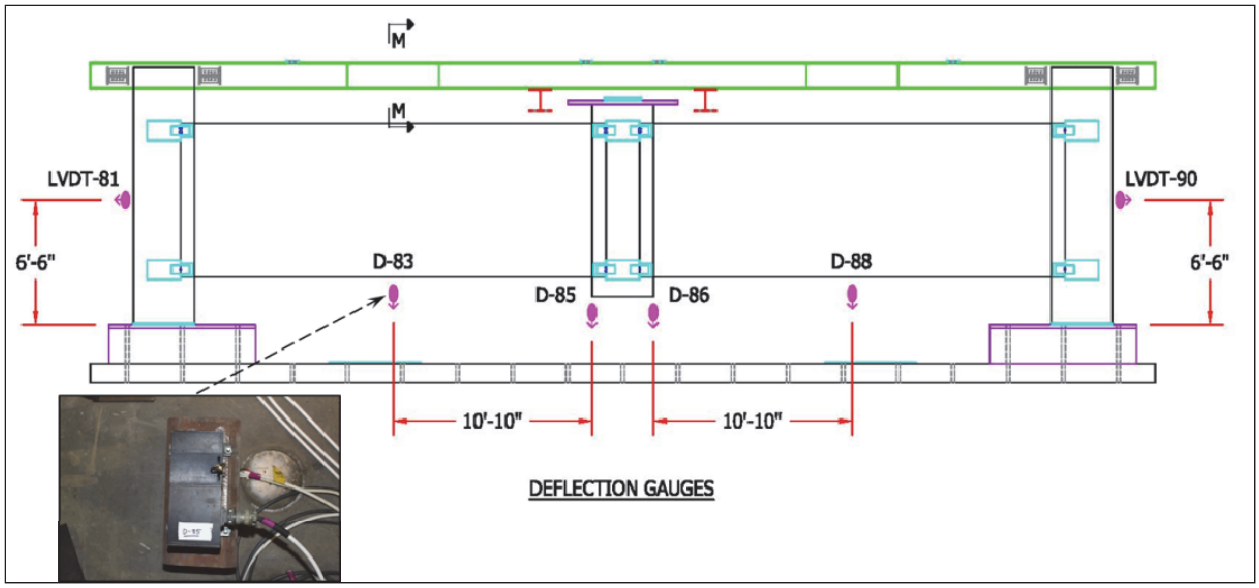

3.1.3 Inclinometers

Four inclinometers were used on SDC-B (Figure 17). The inclinometers were installed at 18-in. offsets from the columns on top of the concrete beams in each corner for a total of two rotational gauges on each beam. These gauges measured the rotation near the supports of the frame system.

Figure 17. SDC-B layout of the inclinometer locations.

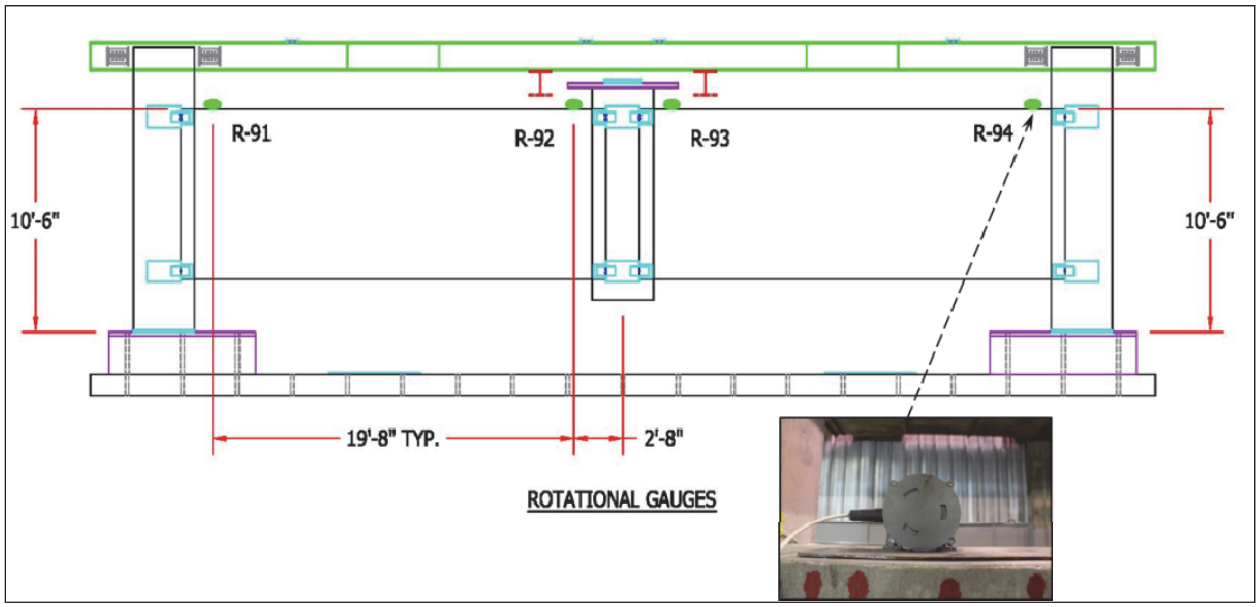

3.1.4 Internal strain gauges

Each beam contained eight internal strain gauges placed on steel reinforcing bars. Beam L contained two internal strain gauges at the right bottom corner of the beam attached to the #10 (ASTM A615 n.d.) top anchor bar of M7, two at the left top corner attached to the #10 top anchor bar of M6, and four at mid-span on the outer most #4 (ASTM A615) reinforcing bars, (two gauges on top and two on bottom). Beam R contained two internal strain gauges at the left bottom corner of the beam attached to the #10 top anchor bar of M7, two at the right top corner attached to the #10 top anchor bar of M6, and four at mid-span on the outer most #4 bars (two on the top and two on the bottom). All of the internal strain gauges were installed in pairs at three and nine o'clock of the rebar cross-section area. Figures 18 through 21 show layouts of the concrete beam with the respective locations of the internal strain gauges used in the test.

Figure 18. SDC-B Beam L internal strain gauges on steel bars M6 and M7.

Figure 19. SDC-B Beam L internal strain gauges on mid-span.

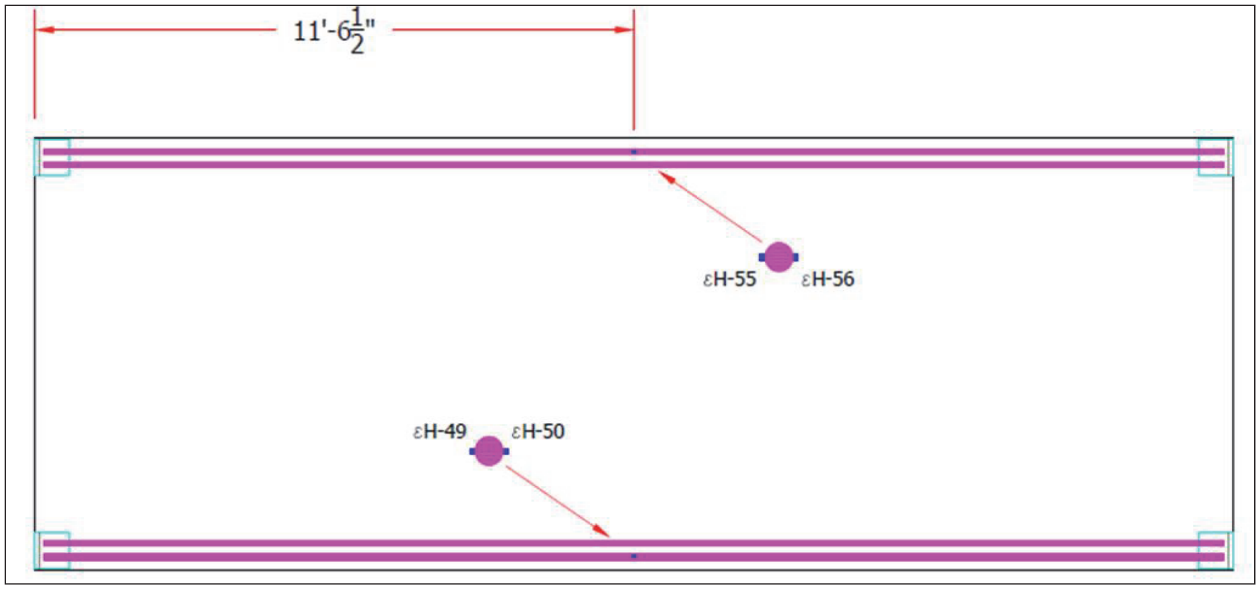

Figure 20. SDC-B Beam R internal strain gauges on steel bars M6 and M7.

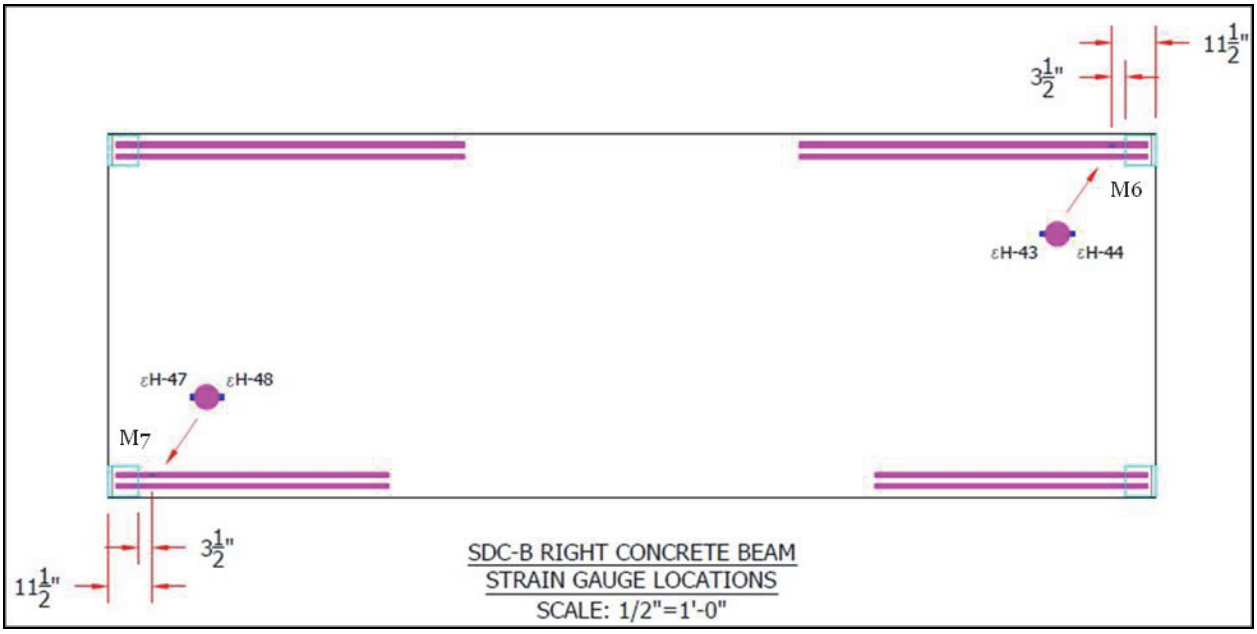

Figure 21. SDC-B Beam R internal strain gauges on mid-span.

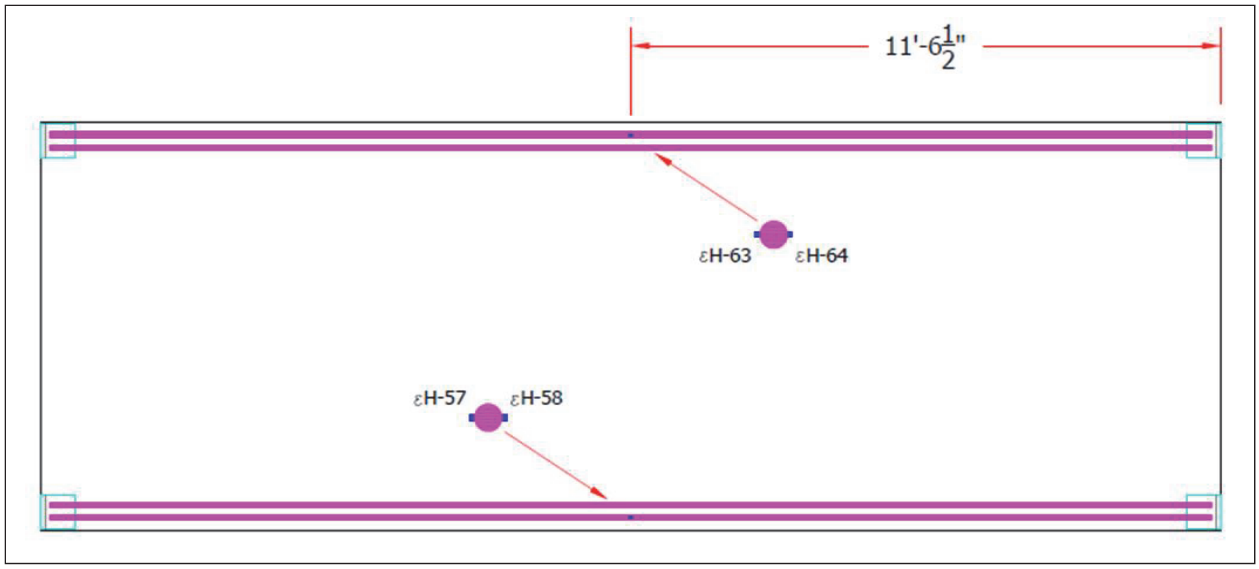

3.1.5 External strain gauges

A total of 33 external strain gauges were used on SDC-B. The strain gauges were installed on the ductile steel connecting plates used in the beam-column connections. On some of these plates, 45-deg Strain Rosettes (consisting of three strain gauges) were used instead of three horizontal single strain gauges. Figure 22 shows an overview layout of each location of the external strain gauges on the ductile connecting plates. Each of these ductile connecting plates had a specific strain gauge arrangement. Figures 23 through 30 show the strain gauge configurations used on each of the steel ductile connecting plates.

Three single strain gauges were also installed at mid-span on one of the top 50-ft-long girders that braced the outermost columns. These gauges measured the axial strain in this girder. The strain in these bracing girders is due to external forces caused by deformation of the end columns toward each other in the near vertical plane of the beam deformation. Figure 31 shows the location of each of the single strain gauges installed on the top girder.

Figure 22. Locations external strain gauges for SDC-B.

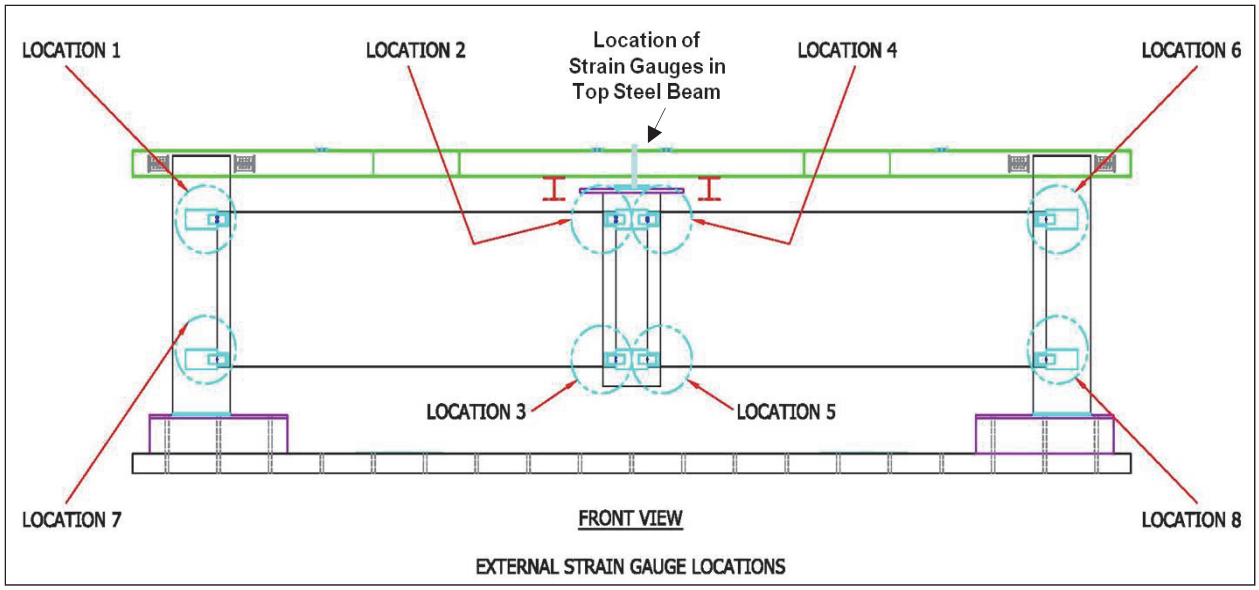

Figure 23. SDC-B external strain gauges at Location 1.

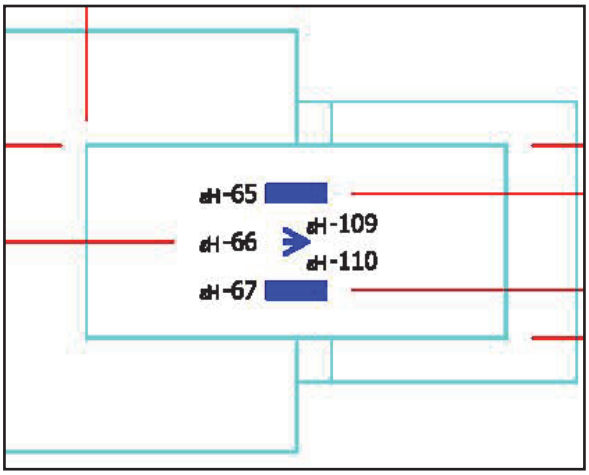

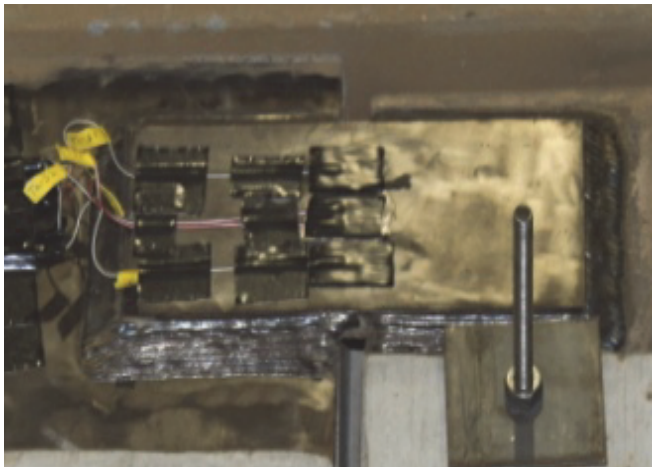

Figure 24. SDC-B external strain gauges at Location 2.

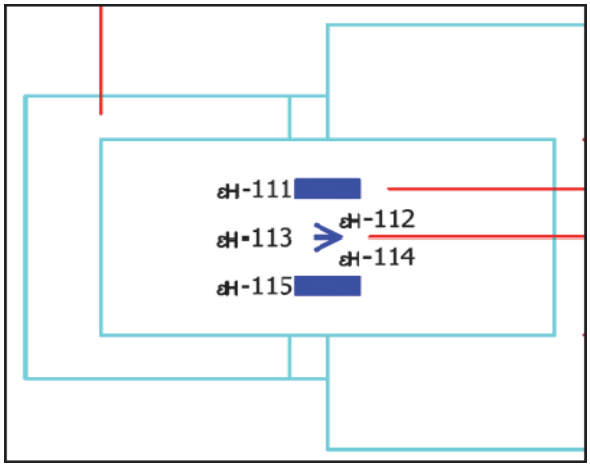

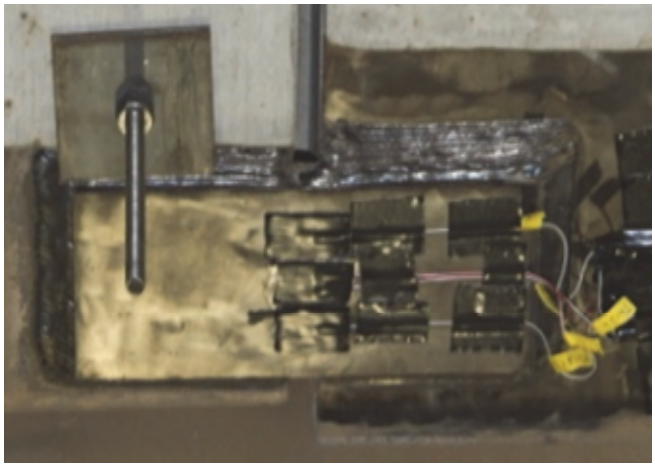

Figure 25. SDC-B external strain gauges at Location 3.

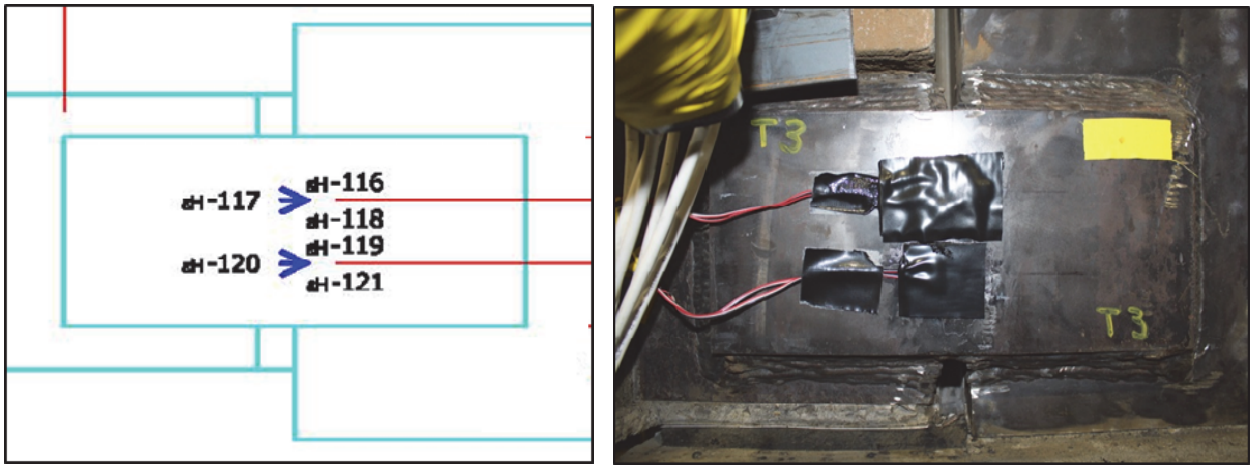

Figure 26. SDC-B external strain gauges at Location 4.

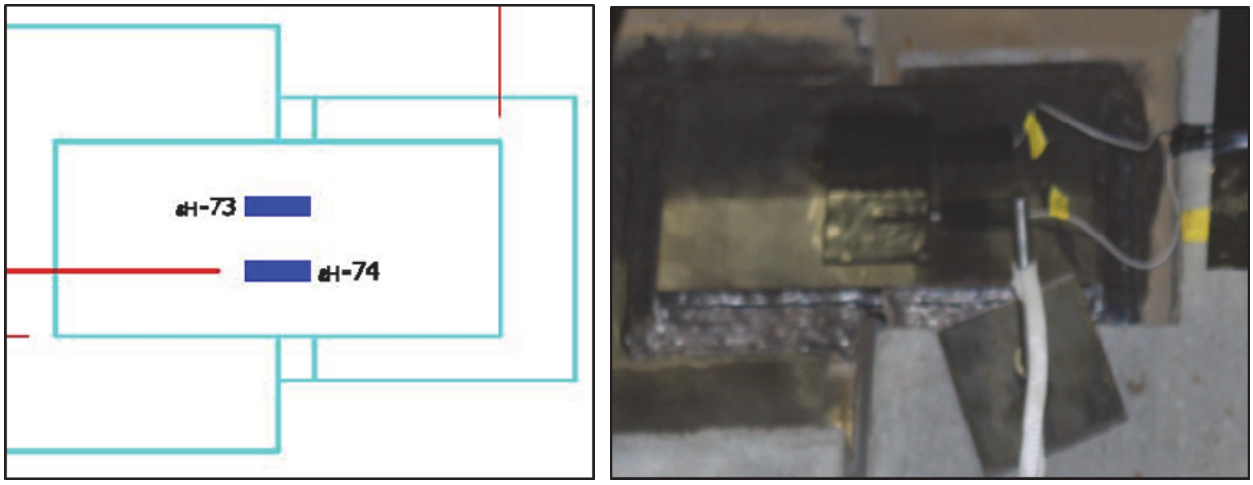

Figure 27. SDC-B external strain gauges at Location 5.

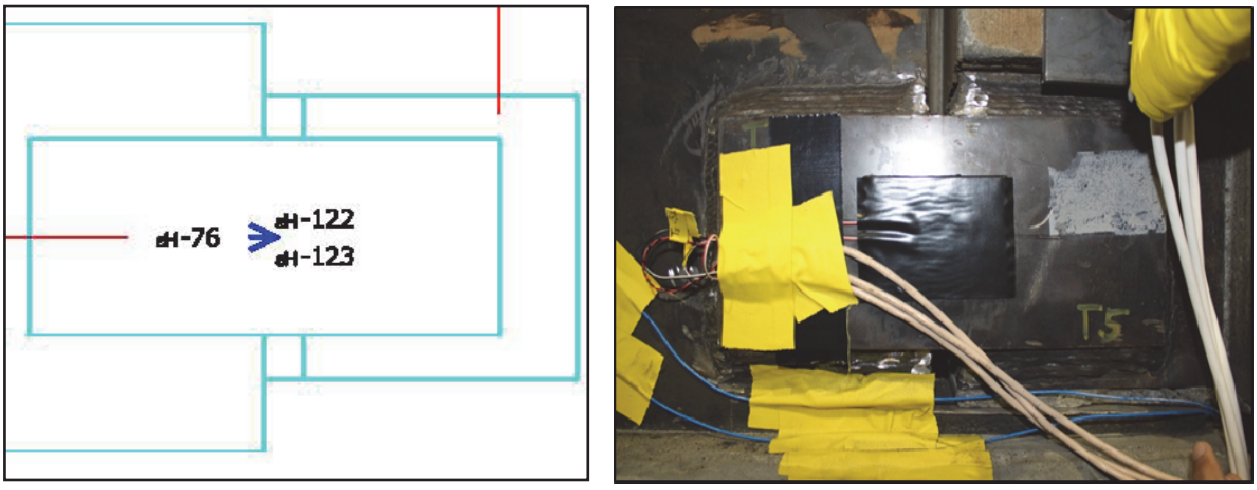

Figure 28. SDC-B external strain gauges at Location 6.

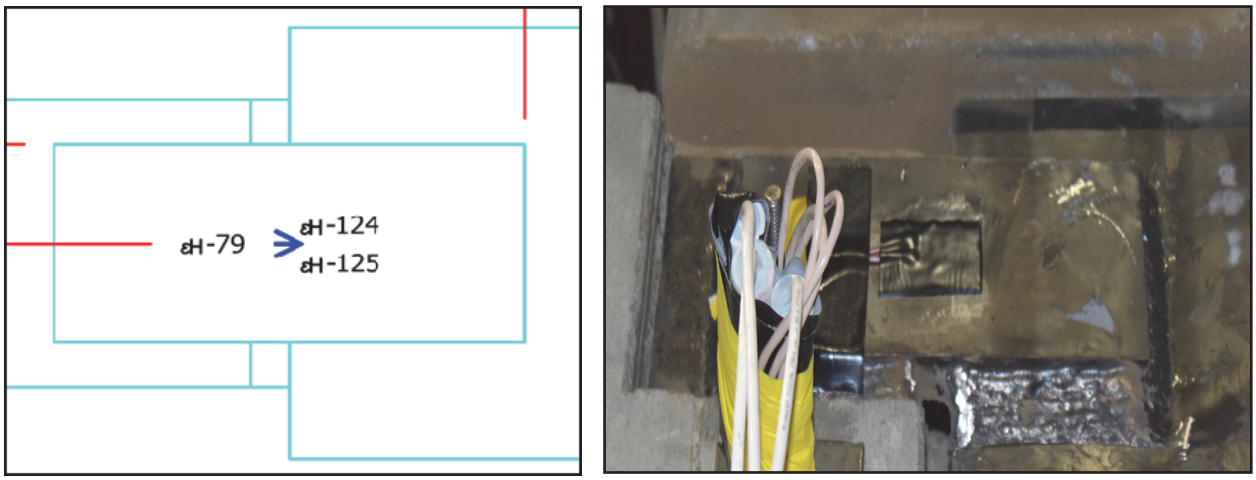

Figure 29. SDC-B external strain gauges at Location 7.

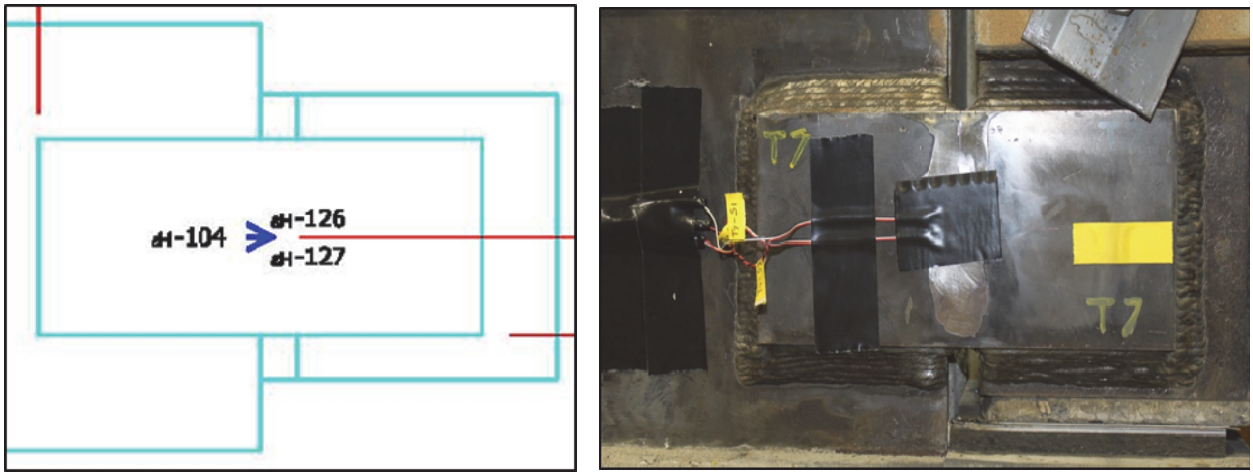

Figure 30. SDC-B external strain gauges at Location 8.

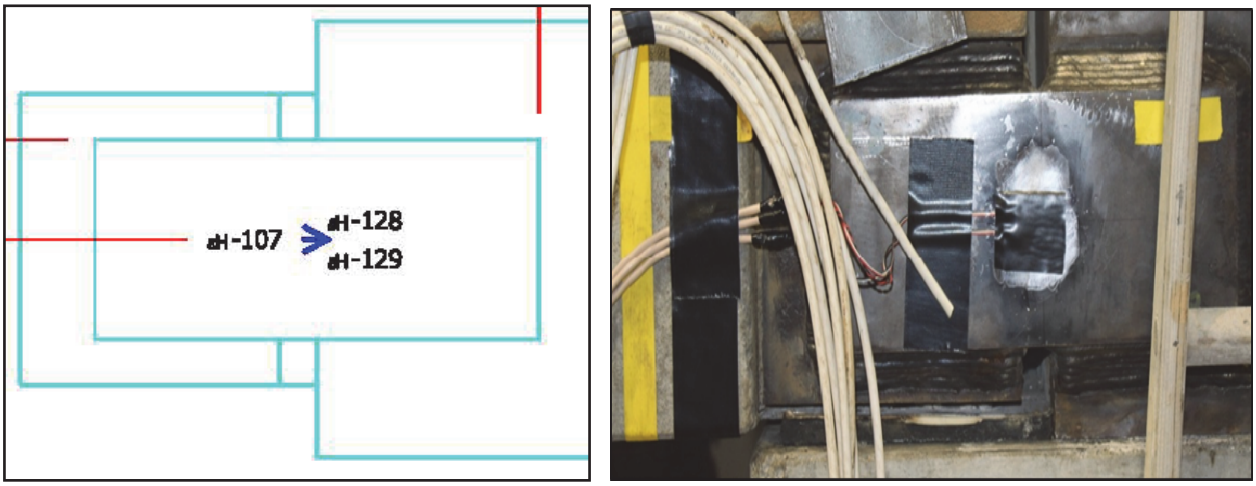

Figure 31. Cross-section view of SDC-B external strain gauge on top steel girder.

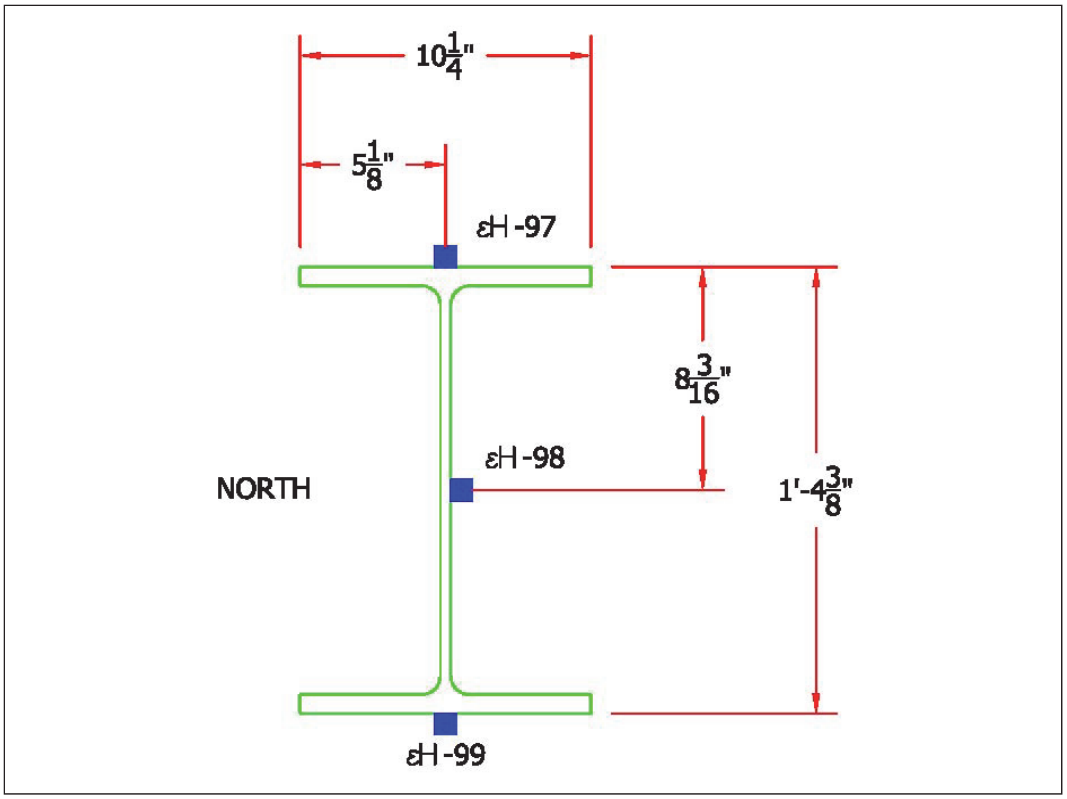

3.1.6 Tension in torsion bars

Two load cells were installed on the two bottom center torsion rods of SDC-B (Figure 32). The purpose of these cells was to measure any change in the tension force in the torsion rods caused by a misalignment of the beam-column system during test execution.

3.2 High-frequency response channels

To accomplish the primary objective of this investigation, 14 sensors were recorded at the highest available sampling rate of 2 million samples per second (MHz). The sensors included two acoustic emission sensors, six accelerometers, one load cell, and five strain gauges. Some of these channels were dual recorded at the lower sample rate (40 Hz) for most of the channels (pseudo-static measurements) and at 2 MHz. Table 2 shows the list of channels recorded at 2 MHz and the sensor types.

Figure 32. Layout of load cells on torsion bars for SDC-B.

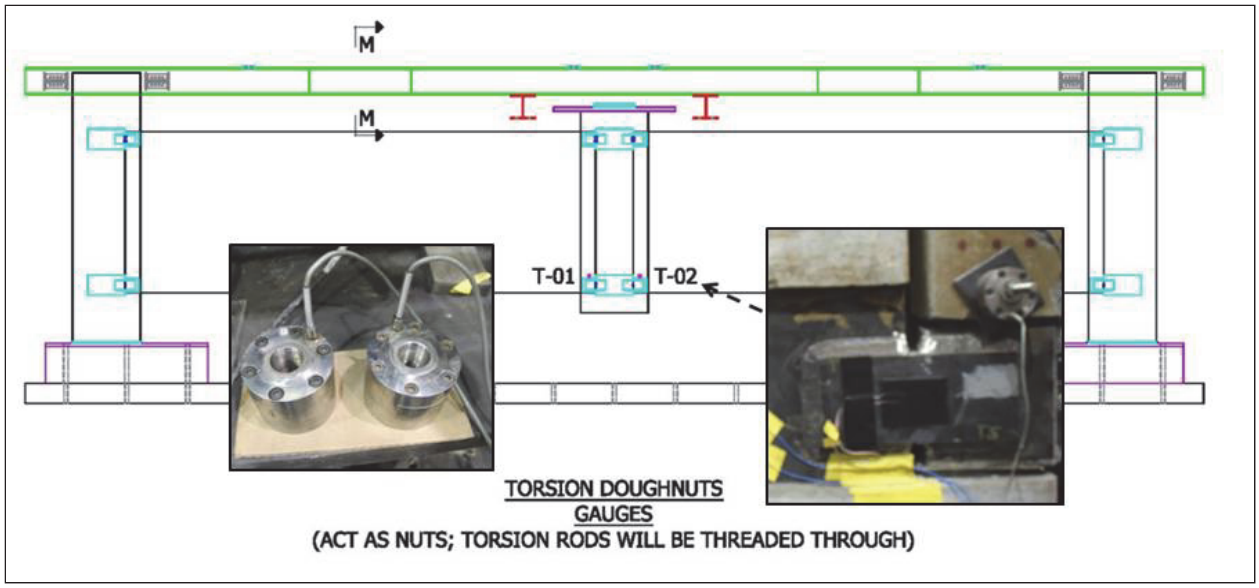

Table 2. High-speed (2 MHz) channel matrix.

Channel No.	Channel Name	Sensor Type
1	L1A	Accelerometer
2	L1B	Accelerometer
3	L1C	Accelerometer
4	L2A	Accelerometer
5	L2B	Accelerometer
6	L2C	Accelerometer
7	AE1	Acoustic Emission
8	AE2	Acoustic Emission
9	L-95A	Load Cell
10	M7-45 (εh-45)	Strain
11	M7-47 (εh-47)	Strain
12	T3-S1 (εh-116)	Strain
13	T3-S2 (εh-117)	Strain
14	T3-S3 (εh-118)	Strain

3.2.1 Acoustic emission sensors

Two acoustic emission (AE) sensors were monitored during the execution of SDC-B. Figure 33 shows one of the AE sensors. These AE sensors (Model SE900-MWB) were manufactured by Dunegan, and both were powered by a Model 500J 15-volt supply. Both AE sensors were installed on the bottom steel plate embedded in the center column/stub. The purpose of the AE

sensors was an attempt to record information on the pattern and growth of acoustic emissions resulting during test execution and potentially correlate these results with the observed and measured damage states inferred from analyses or other recorded data. These data were to be used to help in the understanding of progressive collapse behavior due to a brittle failure in the connections of a precast concrete building. Figure 34 shows the locations of the AE sensors on the test specimen.

Figure 33. SDC-B acoustic emission sensor (Score Atlanta Inc. 2011).

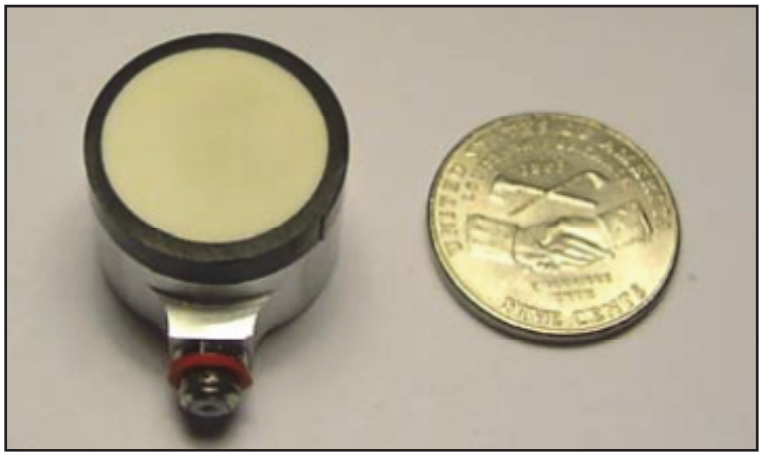

Figure 34. SDC-B acoustic emission sensor locations.

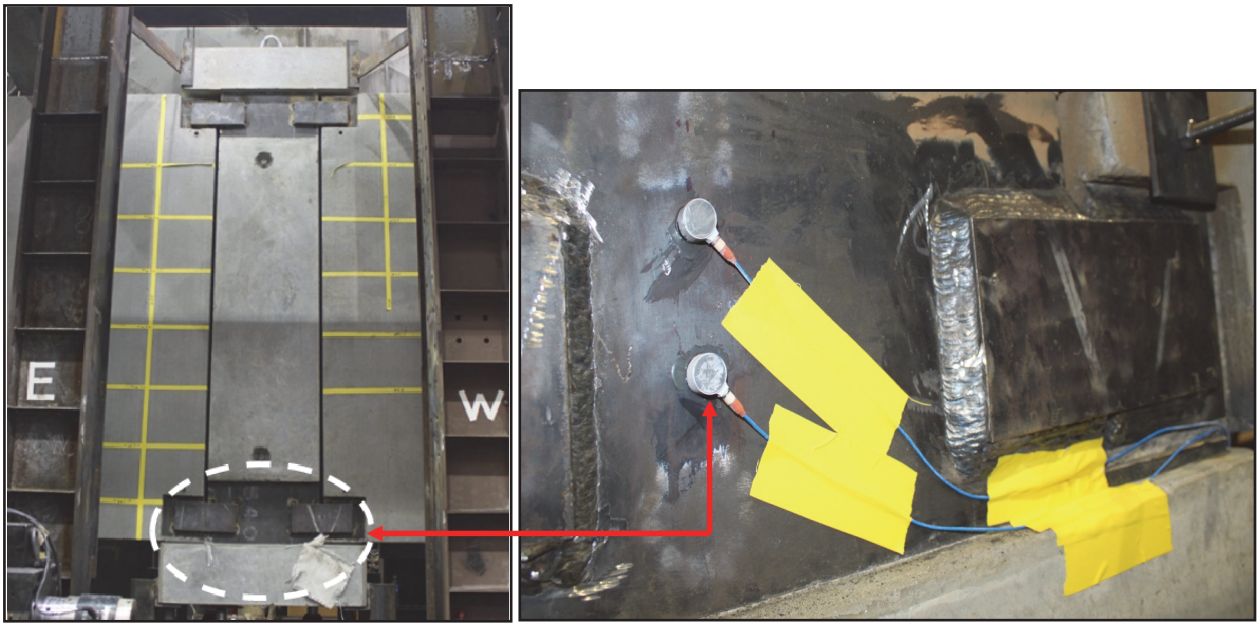

3.2.2 Accelerometers

Six accelerometers were installed on SDC-B as part of the investigation. They were strategically installed along the bottom centerline of the beams,

as shown in Figure 35. The purpose of the accelerometers was to assess whether global instability could be determined, e.g., gross changes in the dynamic properties, linear or nonlinear, during the execution of the test. Changes in linear dynamic properties assume a priori that no nonlinear system response exists. Thus, any changes observed in the data, ignoring the inclusion of hypothesized nonlinear contributions, would result only in changes of an assumed linear system. This assumption of the linear-only model was not expected to be correct; thus, it was expected that a follow-on effort would be required to assess the data from both the accelerometers and the AE sensors in some coupled manner. Another feature of the accelerometers was that the frequency response was below that of the AE sensors and thus thought to provide a more complete frequency domain picture of the release of energy caused by damage growth during the test.

Figure 35. SDC-B accelerometer locations.

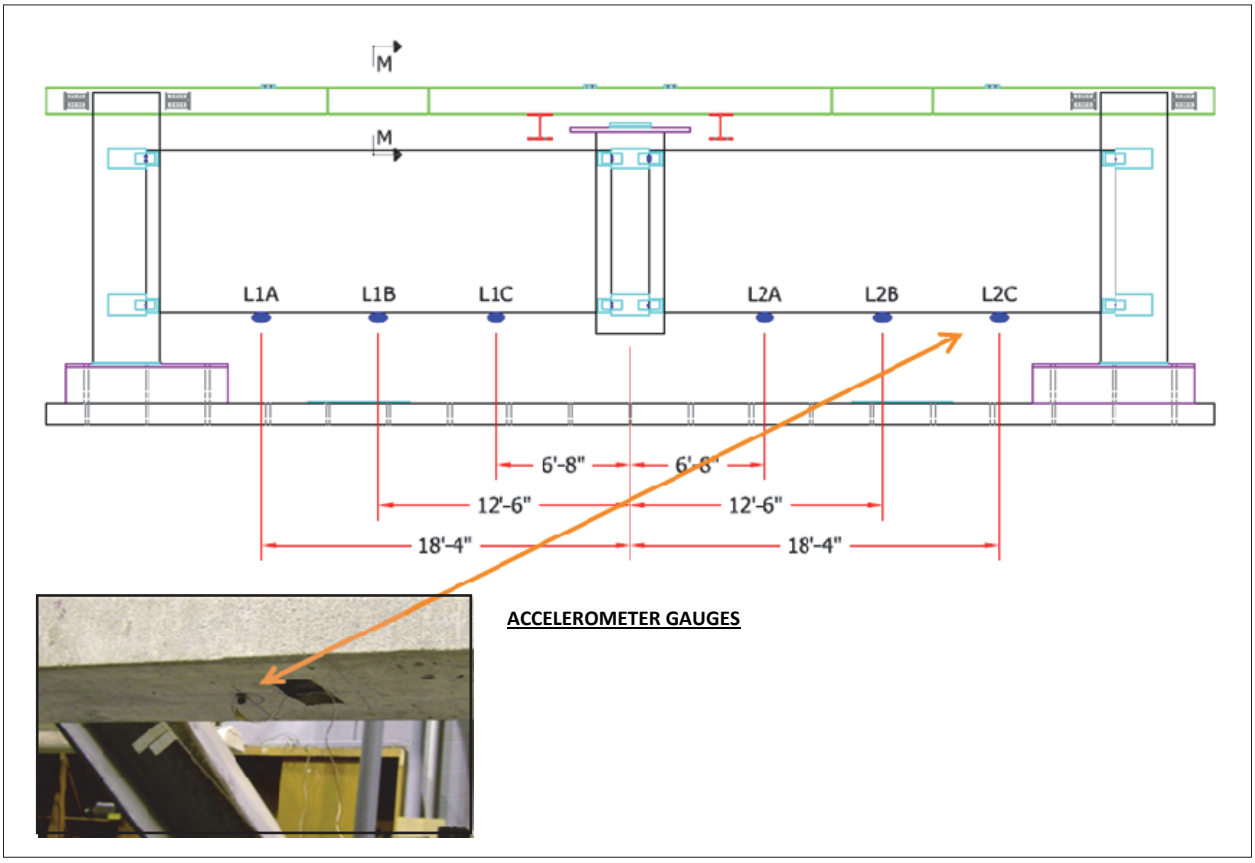

4 Experimental Results

4.1 Overview

The experiment was conducted October 5, 2011. An existing reaction structure described in Chapter 3 was used to test SDC-B under static load. The experimental procedure is described in Appendix B: Experiment Procedure was followed throughout the execution of the test.

The data collected in this experiment were recorded using two separate data acquisition systems recording at different sample rates. The pseudo-static response was recorded on a Synergy system at a frequency of 40 Hz with a minute-based (min.) time scale. The high-frequency response was recorded using a similar data acquisition system but at a sample rate of 2 MHz with a millisecond (ms) time scale. The offset in minutes from the zero trigger point in the pseudo-static data is noted in the title of each transient data plots.

4.2 Observed failure modes of SDC-B

This section presents the observations and interpreted results describing the execution of the SDC-B test. The experimental results include the observed behavior and failure modes along with response measurements from the displacement transducers, inclinometers, strain gauges, and load cell. Figures 36 and 37 show pretest and posttest views, respectively, of the experimental specimen.

Two different gauges were used to measure the applied vertical load to the specimen, an external 400-kip load cell and an internal pressure gauge in the MTS ram. Figure 38 shows a comparison of the values obtained by the two gauges. The coefficient of correlation between both recorded data, is r=0.997. The relative closeness of the points to the line where the two gauges have the same value indicates minor differences between the two measurements.

Therefore any of the two load measurements could be used to discuss the performance of the specimen. In this report L-95A was used to plot the gauge curves. Figure 39 shows the relationship between the applied load (y_1) and the center vertical displacement (y_2) of the specimen and time (x).

Figure 36. Pretest view of SDC-B experimental specimen.

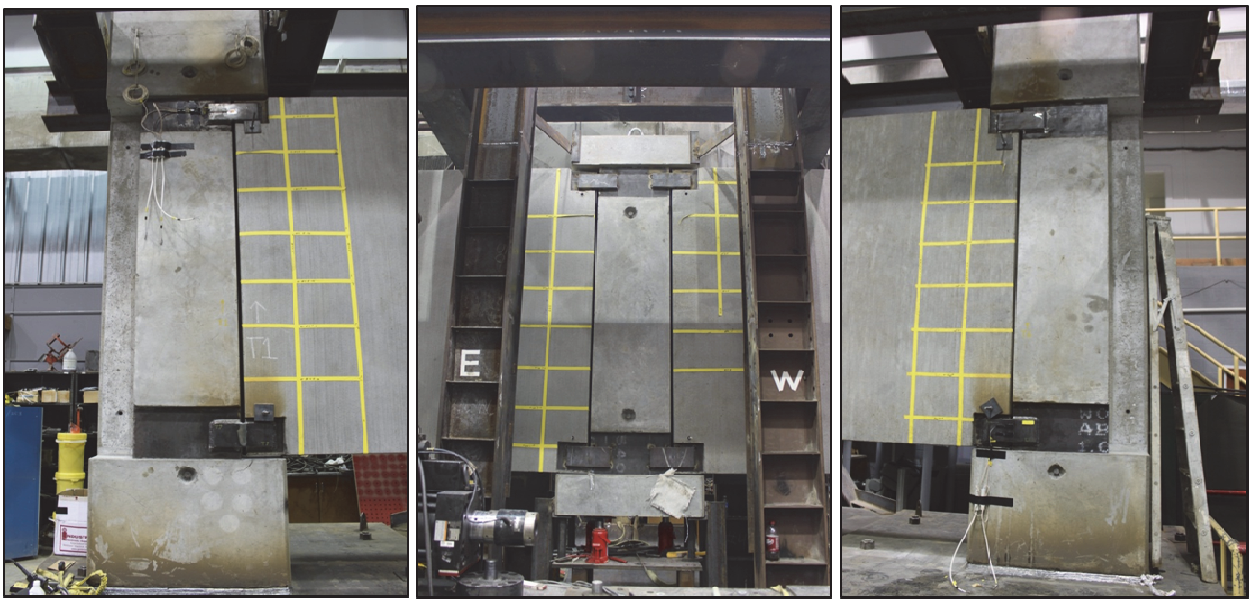

Figure 37. Posttest view of SDC-B experimental specimen.

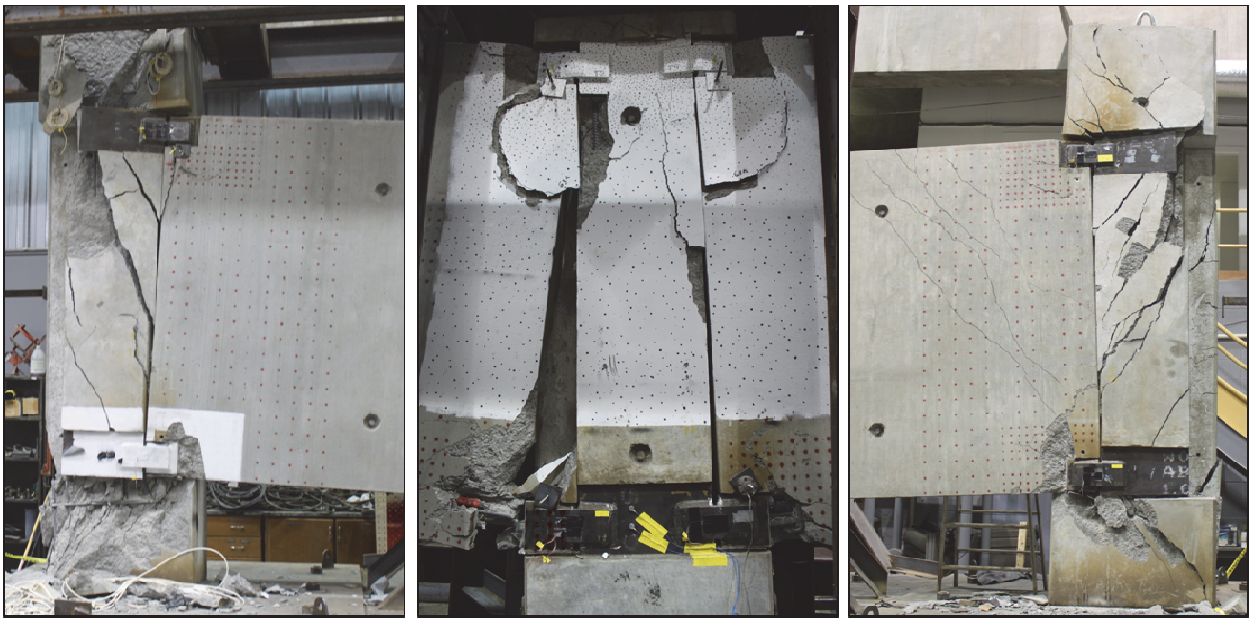

The maximum load and vertical center column/stud displacement were 175-kip (at 216-min.) and 18-in. (at 295-min.), respectively.

The overall failure modes of the specimen can be recapped in four main events (I, II, III and IV). Each of these events is identified in green on Figure 39. All of these events are linked to failure modes observed in the specimen at different stages of the test.

Figure 38. Load Cell vs MTS Ram Internal Pressure Gauge Correlation.

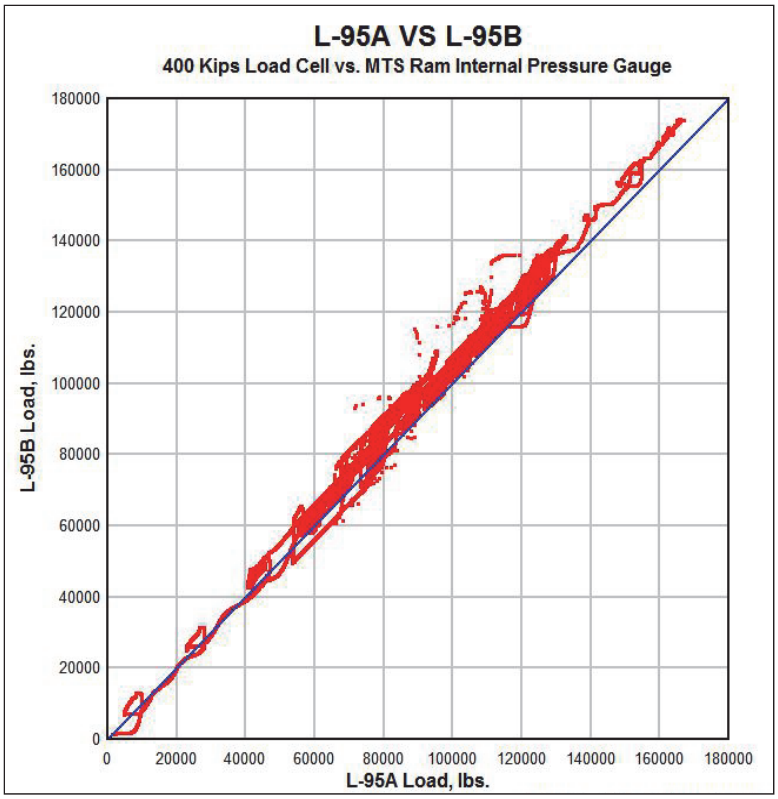

Figure 39. Load (y_1) and center vertical displacement (y_2) vs. time (x).

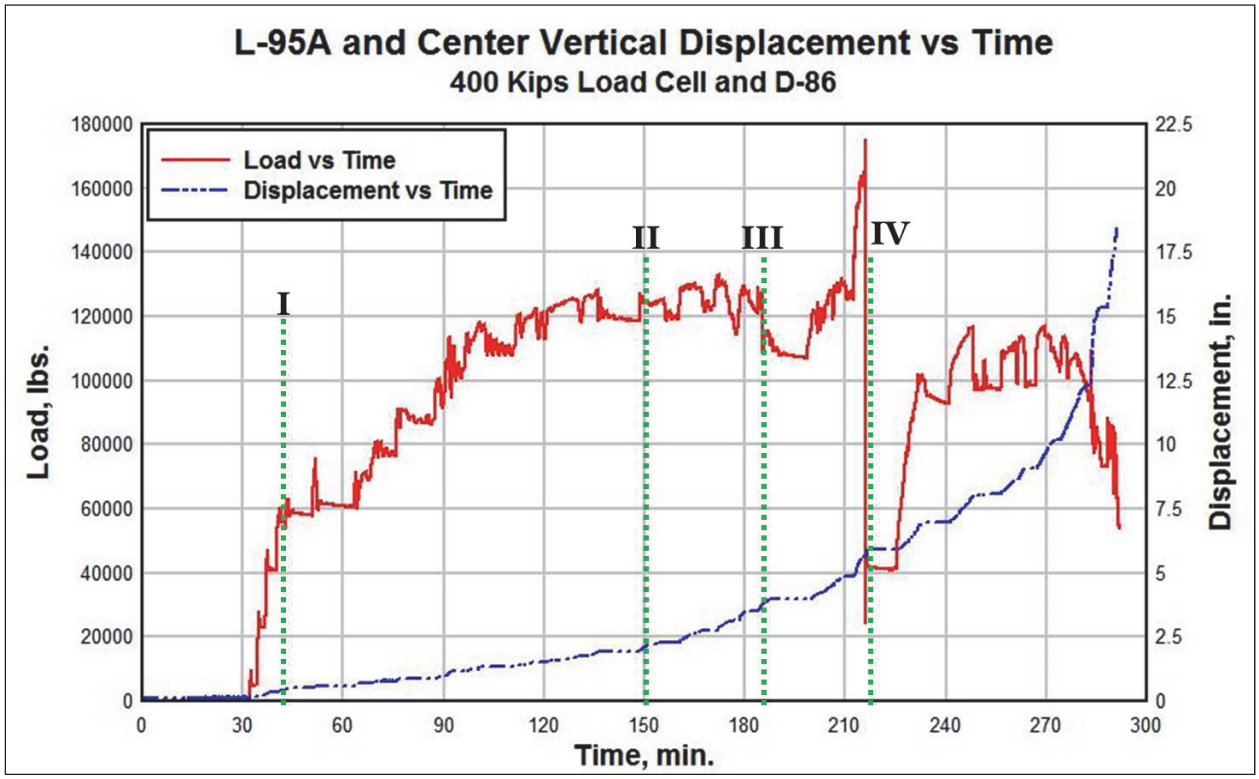

The first event (I) is linked to the initial cracks observed on the specimen. The cracks were first observed when the system reached the 63 kips vertical load mark and had a vertical center displacement of 0.5 in. (at 42 min). Figure 40 illustrates the crack pattern exhibited on the top center corner of the beams. At the time the specimen began to flexure, the top part of the beams started acting in compression against the center column creating cracks around the stress concentration area. At the same time the end columns began to crack and bend due to the high magnitude bending moments at the support. Figure 41 exhibited the posttest structural damage of the end columns. The direction of the cracks in the columns is an indication of horizontal movement toward the center column/stud. The end columns reacted to the lateral-torsional response and began to bend out of the plane of the beam-column system. This caused the system to exceed its yielding strength and exhibit plastic behavior, resulting in permanent deformation. These occurrences explain the displacement differential from 42 min to 150 min of test time.

The second event (II) is linked to a brittle failure of the bottom anchor bar welded to the (M7) embedded angle in the left beam. Figure 42 shows the location of the ruptured anchor bar. The tensile failure of the bar occurred when the system reached the 125-kip vertical load mark and had a vertical center displacement of 2.1 in. (at 150 min). The brittle failure of this bar caused the system to become more unstable resulting in a gradual change in center deflection without a significant change in applied load. This event was also captured by the strain rosettes gauges on the ductile connection plate #3, and the strain gauges located on the M7 top anchor bar (εh-45 and 46). Figure 43 depicts the change in strain on the connection plate#3 due to the brittle failure of the (M7) bottom anchor bar.

Figure 44 depict the change in strain on the strain gauges (εh-45 and 46). This increase in strain could potentially be an indicator of an abrupt increase of tensile force on the top anchor bar and bending moment on the ductile plate #3 due to the brittle failure of the bottom anchor bar. The system continued deforming in a plastic behavior.

The third event (III) could be linked to a connection failure of M8 steel plate and the left (east) end column. At the time the system reached the 128-kip vertical load mark and had a vertical center displacement of about 4.0 in. (at 185.5 min), the spalled concrete began to fall from both of the end columns.

Figure 40. Posttest front view of the SDC B top center column.

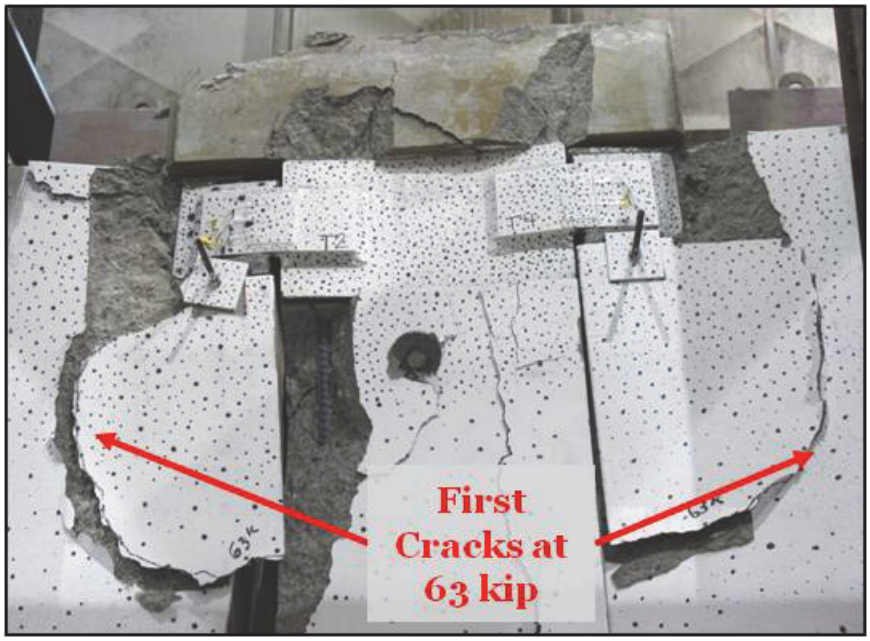

Figure 41. Posttest front view of end columns.

Figure 42. Location of M7 anchor bars in Beam L, brittle failure.

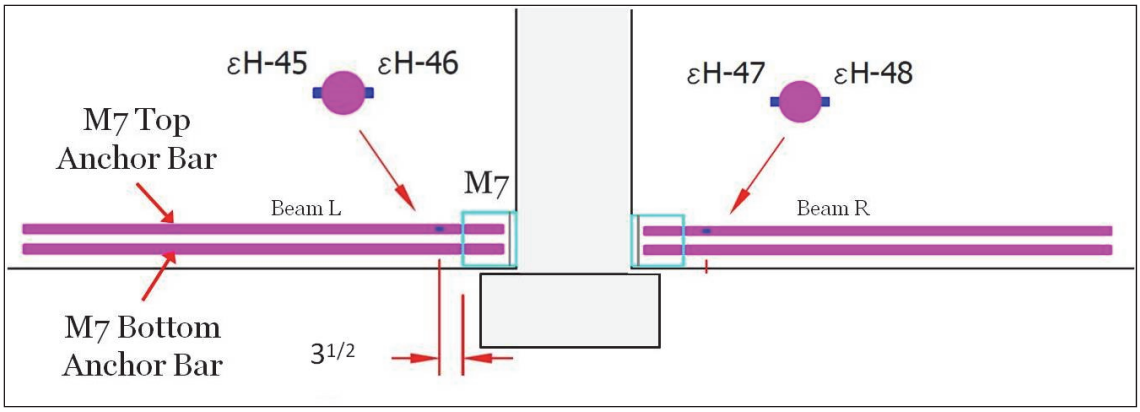

Figure 43. Ductile plate#3, brittle failure of bottom anchor bar of M7 in Beam-L.

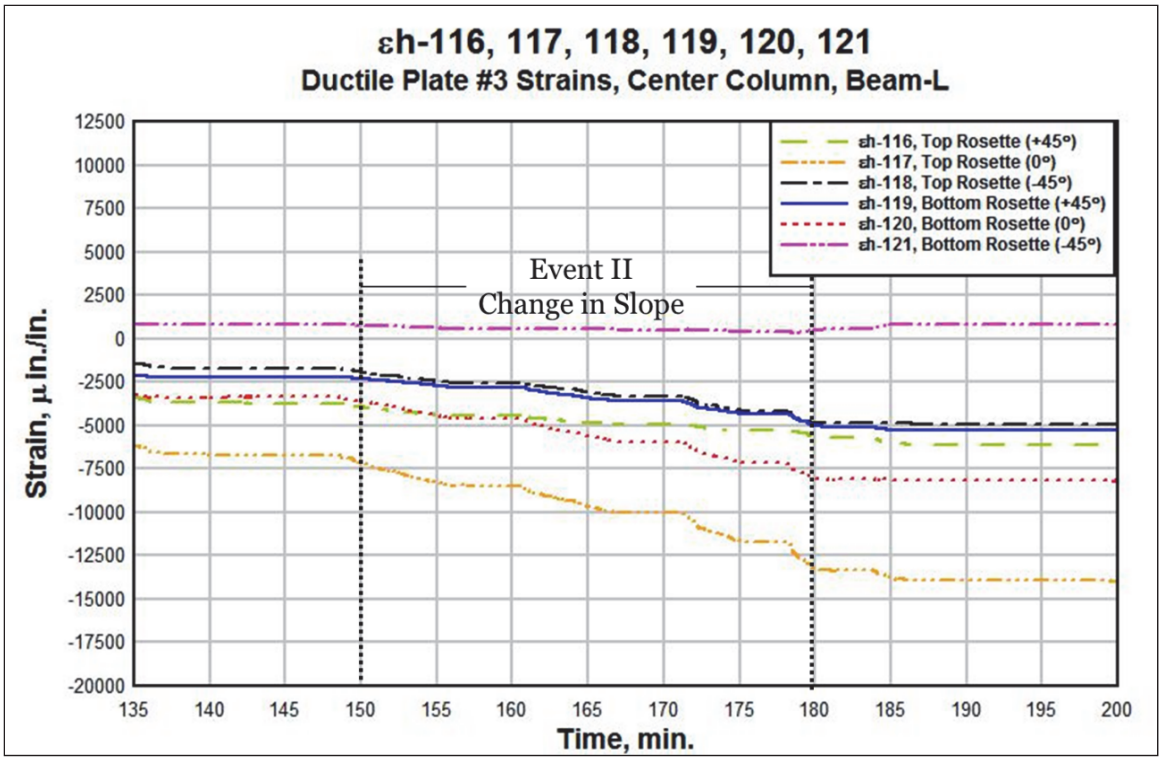

Figure 44. Strain (εh-45, 46), brittle failure of bottom anchor bar of M7 in Beam-L.

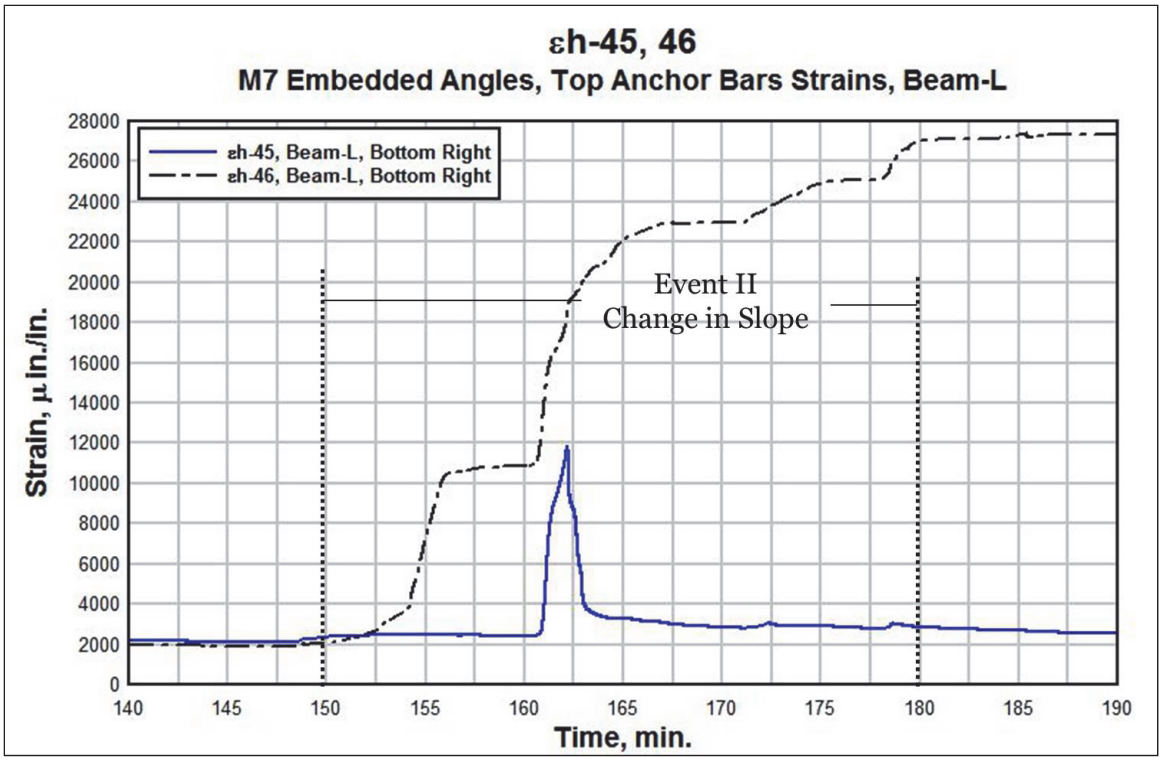

Each of the M8 plates were embedded to the columns using 1-in.-by-4-in. HCA nelson studs, Appendix A: SDC-B Instrumentation Drawings. The top left end column plate (M8) was pulled out of the concrete due to the high magnitude bending moments that cracked the column and consequently reduced the connection strength of the nelson studs and the concrete. Figure 39 show that the system ability to carry load reduced, however it ramped again. Figure 45 shows the structural damage of the left end column.

This event was also captured by the strain gauges on the ductile connection plate #1, (Figure 46) and the strain gauges mounted on the M6 top anchor bar (εh-41 and 42) in the left beam, (Figure 47). A sudden increase in strain can be observed in the ductile plate, contrarily at the top M6 anchor bar that shows a reduction in strain due to the connection failure of M8.

The fourth event (IV) is directly related to the failure of the top anchor bar of the (M7) embedded angle in the left beam. Please refer to Figure 42 for the location of the M7 top anchor bar. The bar failed when the system reached its capacity at the 175.5-kip load mark and had a vertical center displacement of 5.8 in (at 216 min.). Figure 48 illustrates both of the ruptured M7 anchor bars.

Figure 45. Left (east) end column, failure of top embedded plate M8.

Figure 46. Ductile plate #1, failure of top embedded plate M8.

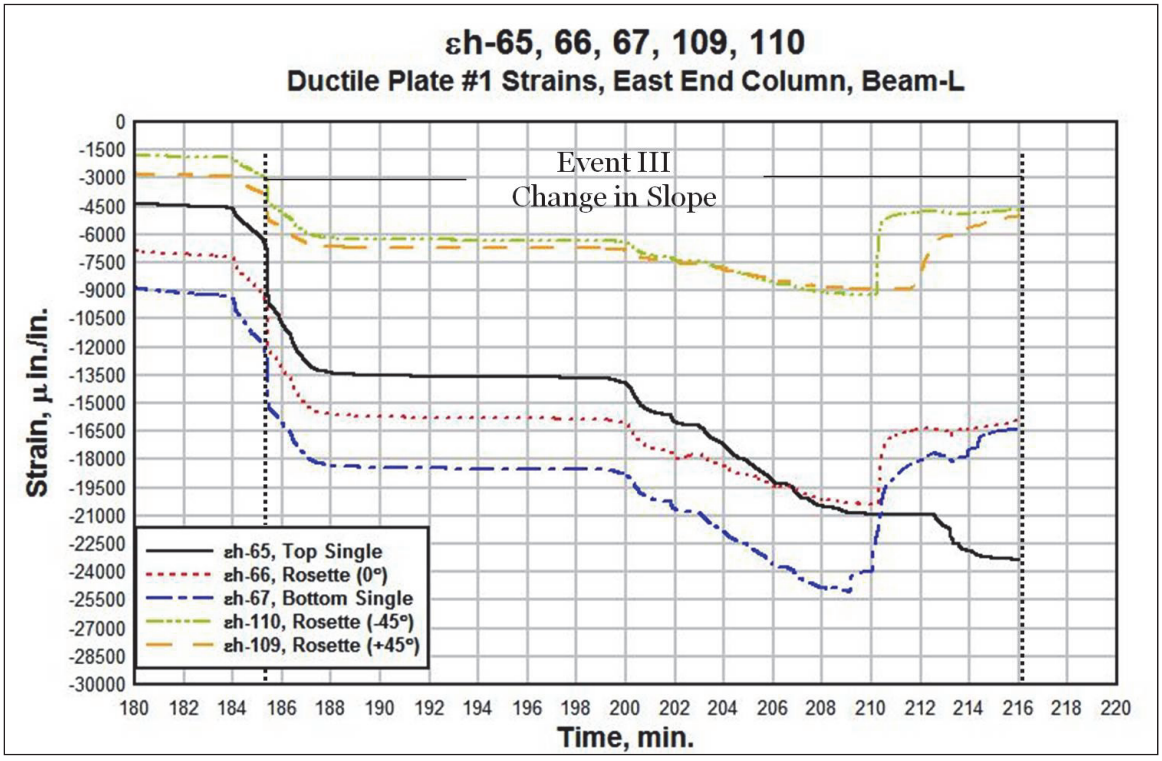

Figure 47. Strain (εh-41, 42), failure of top embedded plate M8.

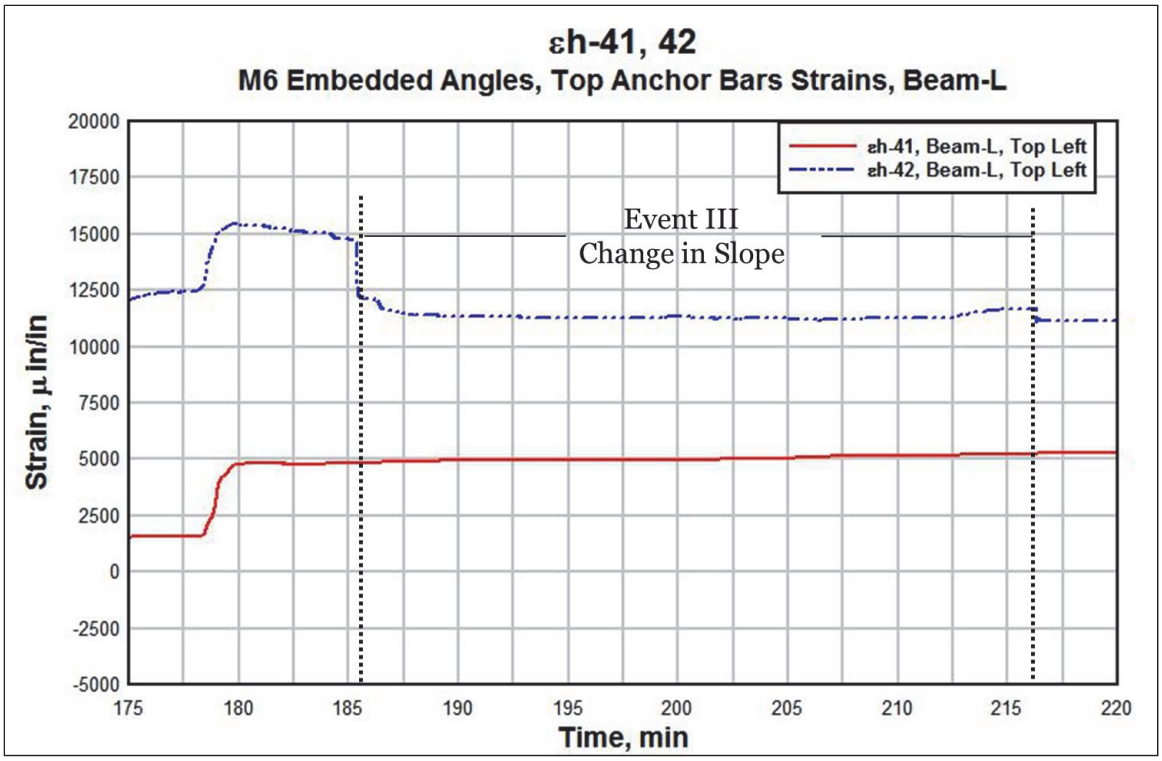

Figure 48. Posttest views of SDC-B ductile connecting plate (Location #3) T-3, M7 (Beam-L).

The bar ruptured at a strain (ε_u) of 0.029 in./in. at 216 min (Figure 49). The average tensile strain (ε_{tu}) of the A706 (Grade 60) for #10 bars was 0.18 in./in., (Appendix E: SDC-B Reinforcement A706 Samples Tensile Test Data); more than six times higher than (ε_u). The connection design between the anchor bars and the embedded angles (M6 and M7) could

explain the reason why these bars failed prematurely. All of the anchor bars in the specimen were welded to the embedded angles (M6 and M7) on each corner of the beams. This welding process could have potentially developed a "heat affected zone" in the bars that change its mechanical properties, causing both to behave as a brittle material when subjected to high magnitude tensile/bending loads.

Figure 49. Brittle failure of top anchor bar M7 embedded angle on Beam L.

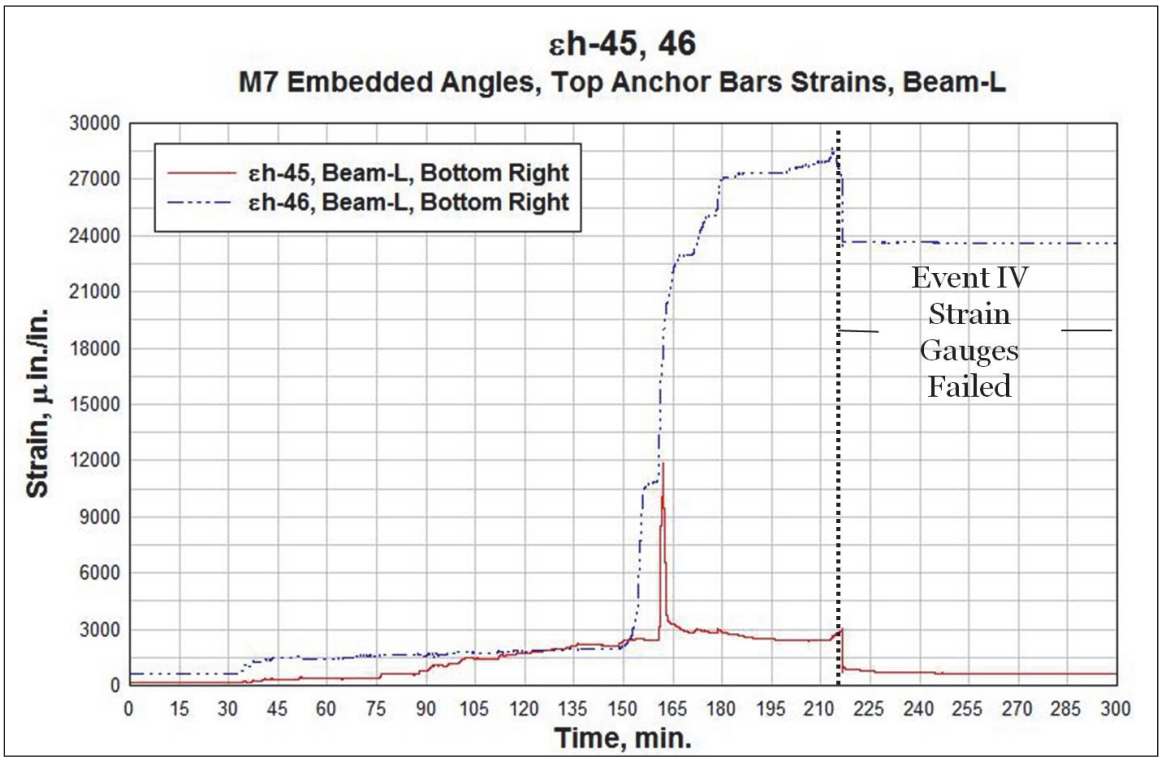

Figure 50 shows a close-up view of the fractured surface of both M7 anchor bars. Flat surface, very little necking, chevron marks, and crystallization are some of the characteristics found on the fracture surface of the bars. These characteristics are typically found on brittle failure materials affected by "heat affected zones."

The brittle failure of this bar caused the system to experience a sudden drop in load (Figure 39). This behavior could potentially be explained by two different theories. First, because the test was executed under a displacement control scenario, the specimen could've potentially bounced at the time the top M7 anchor bar ruptured resulting in a misread in the load cell. Second, the behavior could be also the result of a dynamic response of the system due to the loss of a principal structural member. Although no significant vertical displacement was captured during this event, clearly the load cell's

loss of contact with the center column/stud resulted in a misreading. Either could potentially explain the unexpected behavior of the strain data captured at the outmost bars of the beams. This event was also captured by the strain rosettes gauges on the ductile connection plate #3, and the strain gauges located on the top anchor bar (εh-45 and 46). Figure 51 depicts the change in slope on the ductile plate#3 due to the brittle failure of the (M7) top anchor bar. Figure 49 shows the strain in the (M7) top anchor bar.

Figure 50. Close up view of the fractured surfaces of both failed anchorage bars.

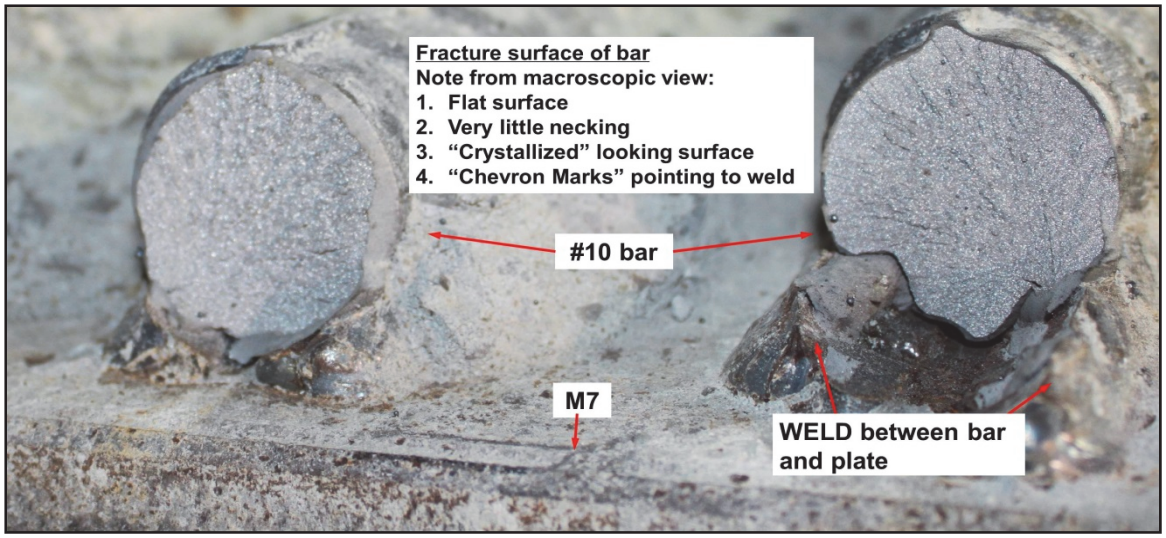

Figure 51. Ductile plate #3, failure of top anchor bar of M7 in Beam L.

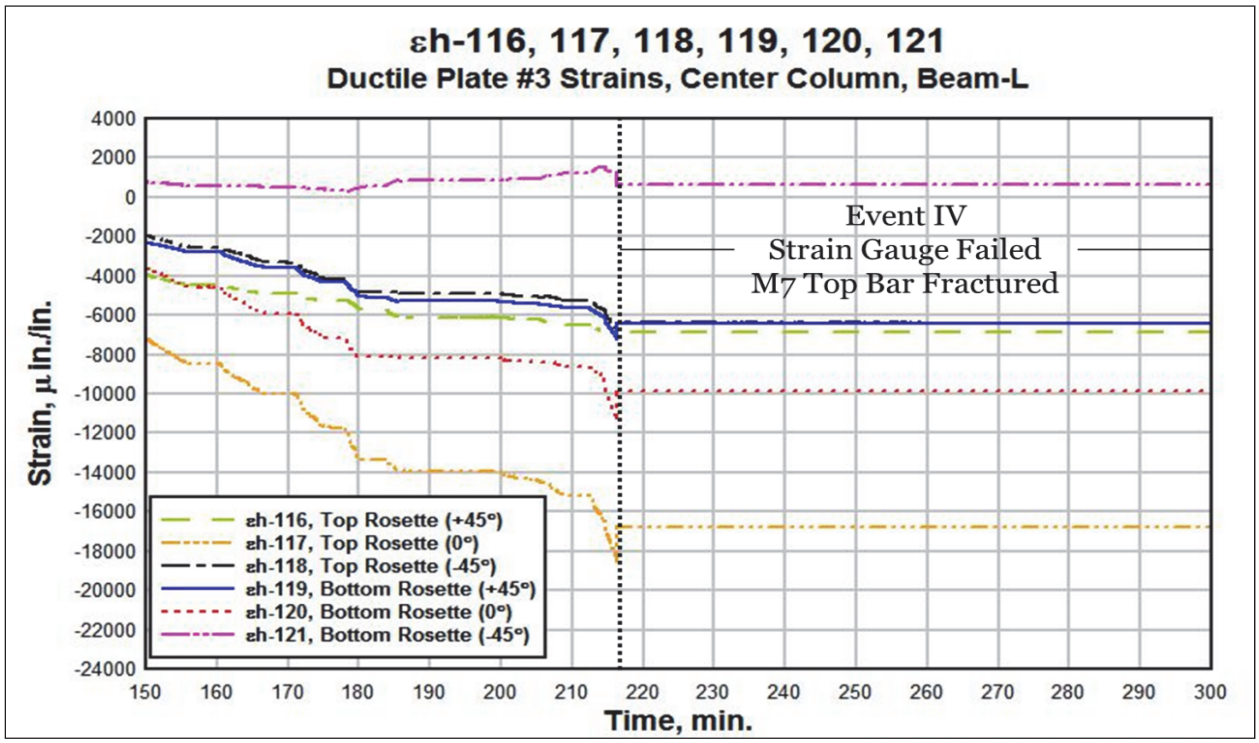

Also an increase in rotation of the center stud toward the right end column was observed soon after the M7 top anchor bar failed. Figure 52 illustrates the misalignment of the center stud from the center line towards the right (west) end column. Figure 53 depicts the displacement profiles of the beams (D-83 through D-88) at different load measurements. In this figure, dotted lines are used to connect the measured deflections. Notice how the differences between the displacement measurements on each side of the center column increase once the system reached its capacity and the top M7 anchor bar fractured.

Figure 52. Posttest center stud rotation toward the right (west) end column.

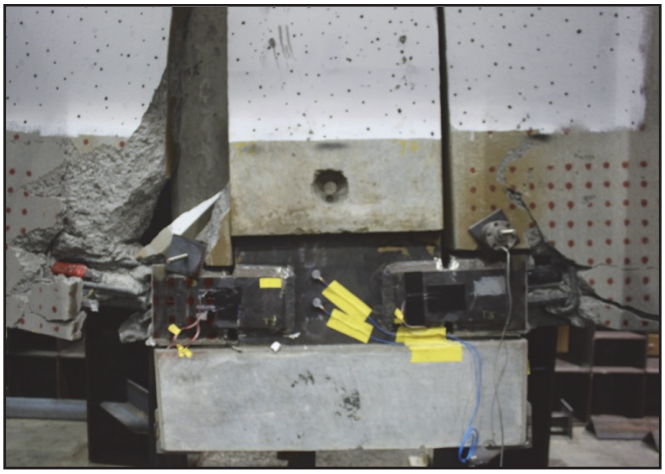

Figure 53. Vertical displacements of SDC-B during test execution.

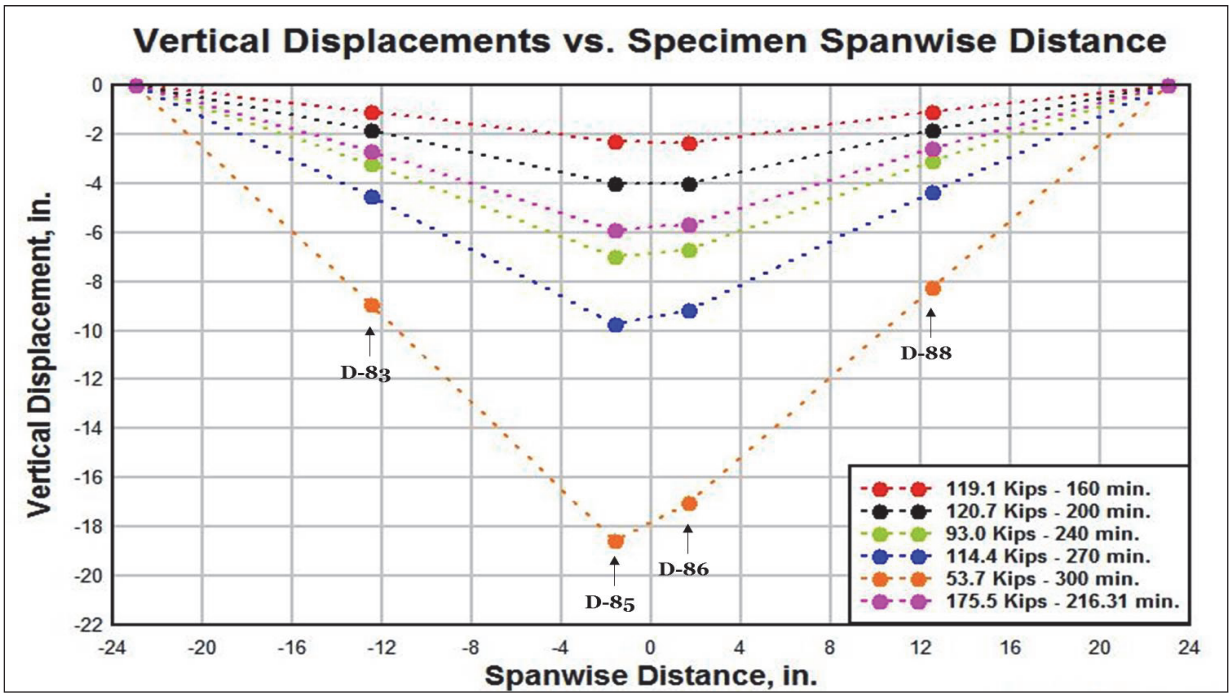

4.3 Overall performance evaluation of SDC-B

In the early stage of the response, the behavior was dominated by flexure. With increased vertical displacement, yielding occurred at the connecting steel plates at the beam-column connections, and axial tension developed in the beams, indicating catenary behavior. The axial tension in the beams continually increased until the test was stopped. Figure 54 shows the load versus the center column deflection with response states denoted as A, B, C, and D.

Figure 54. SDC-B load vs. central displacement.

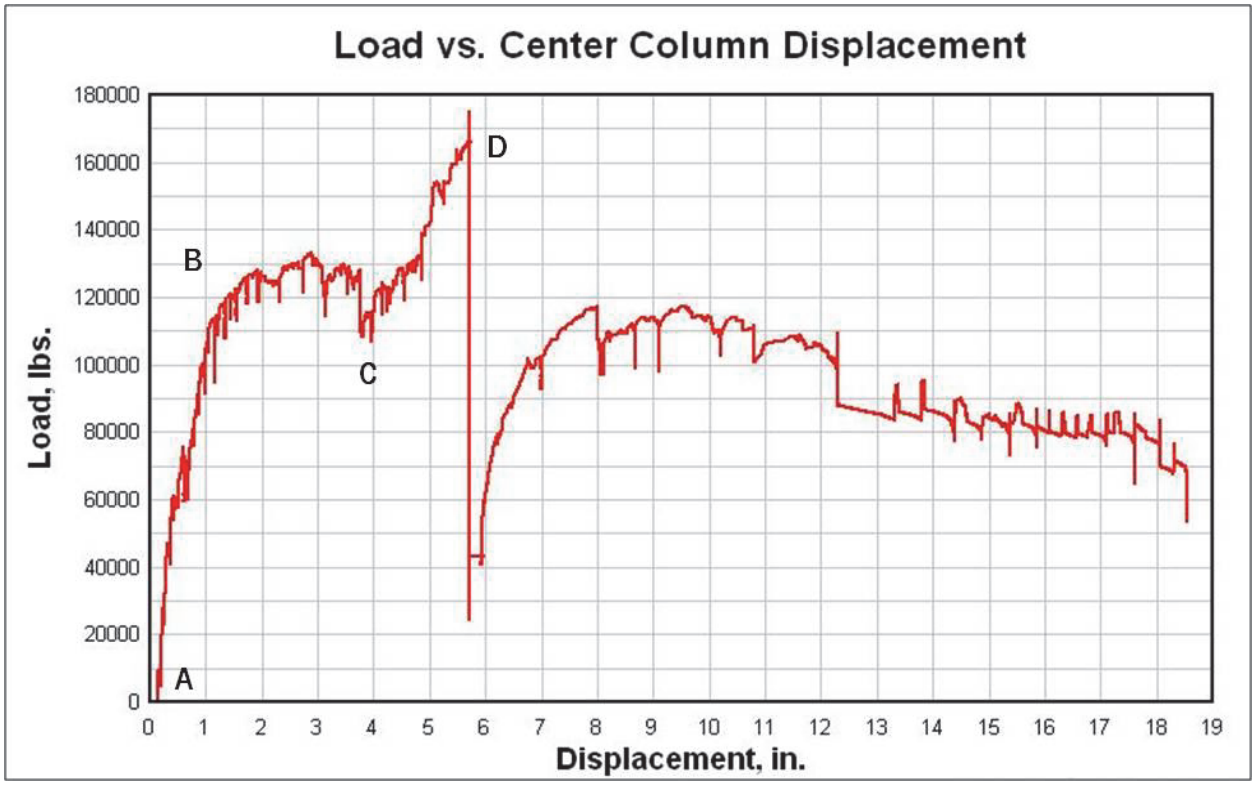

The system behaved elastically from response state A to B; and with the help of compressive field, the system reached an enhanced load capacity at response state B. As the deflection increased beyond response state B, the system exceeds the elastic region and began to deform in a plastic behavior. The load carried by the system decreased rapidly because of a reduction in the compressive field. The end columns react to this lateral-torsional response and are bending out of the plane of the beam-column setup (Figure 55). Consequently, the specimen began to crack and spalled concrete began to fall out due to the high magnitude bending moment at the supports, (Figures 6 and 18). As state C approached, the membrane forces

in the center of the system changed from compression to tension, and the M7 bottom anchor bar and all of the torsion rods failed. The specimen began to rotate out-of-plane. Beyond response state C, the beams carried load by the reinforcement acting as a plastic tensile membrane with full-depth cracking of concrete in the center connection due to the large displacement, (Figure 56). The system continued carrying further load with an increase in deflection until, at response state D, the bottom M7 anchor bar fractured. The tensile membrane increased the ultimate load by more than 30 percent.

Figure 55. Posttest view of bottom of end columns, spoiled concrete.

Figure 56. Posttest views of the bottoms of the SDC-B beams, full-depth cracks.

Near the end of the compressive membrane action range, the system transitioned to almost a pure state of tension membrane under large deflections. The system formed a catenary behavior. Even though none of the ductile connection plates failed, (Figures 57 to 64), the top anchor bar welded to the bottom left connection of the center stud (M7) failed, (Figure 48). Once both M7 anchor bars fractured, the ductile connection plate #1 was no longer interacting with the system. Therefore, the bending moment was redistributed to the remaining (7) ductile plates, causing the system to rotate even more toward the right end column. The system continued being loaded until it reached a total center vertical displacement of 18.5 in.

Figure 57. Posttest ductile connecting plate (T-1).

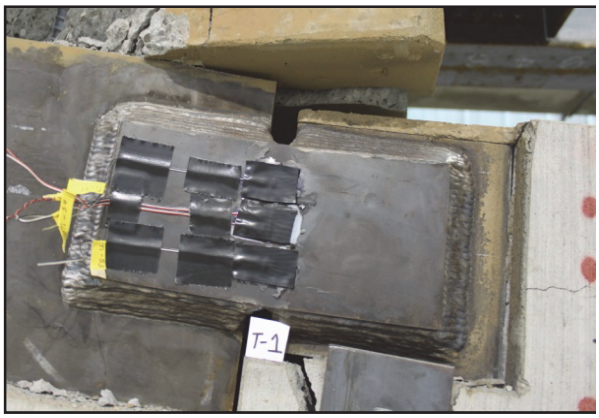

Figure 58. Posttest ductile connecting plate (T-2).

Figure 59. Posttest ductile connecting plate (T-3).

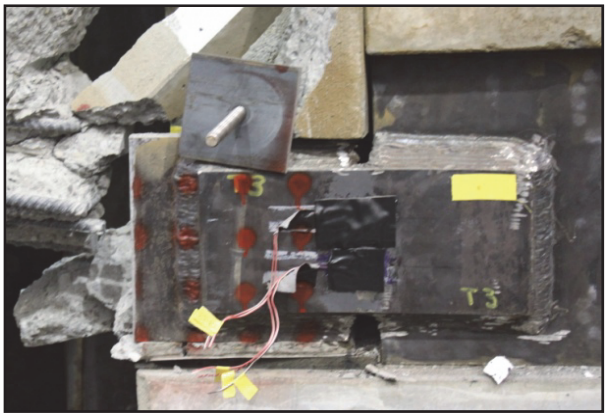

Figure 60. Posttest ductile connecting plate (T-4).

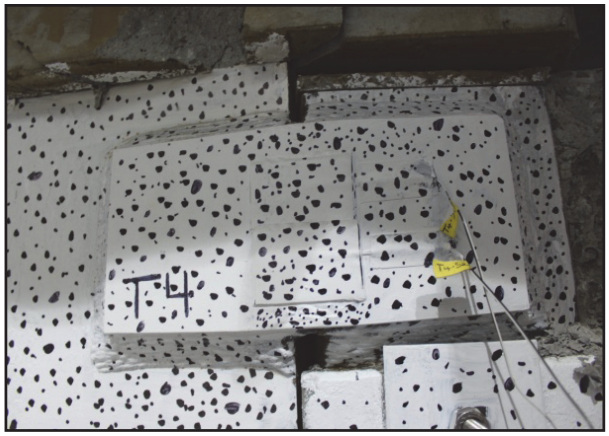

Figure 61. Posttest ductile connecting plate (T-5).

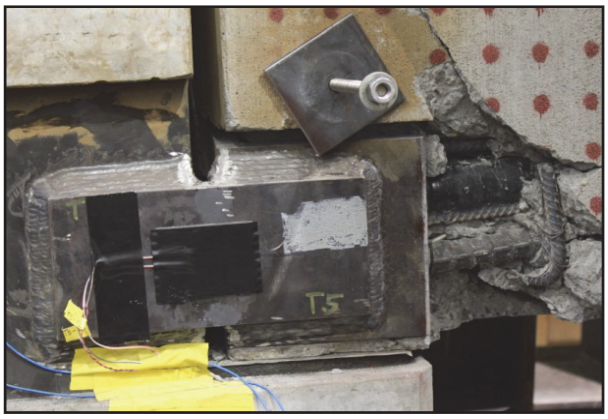

Figure 62. Posttest ductile connecting plate (T-6).

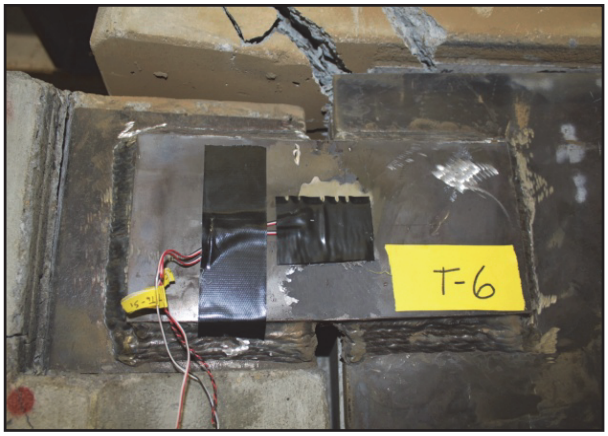

Figure 63. Posttest ductile connection plate (T-7).

Figure 64. Posttest ductile connecting plate (T-8).

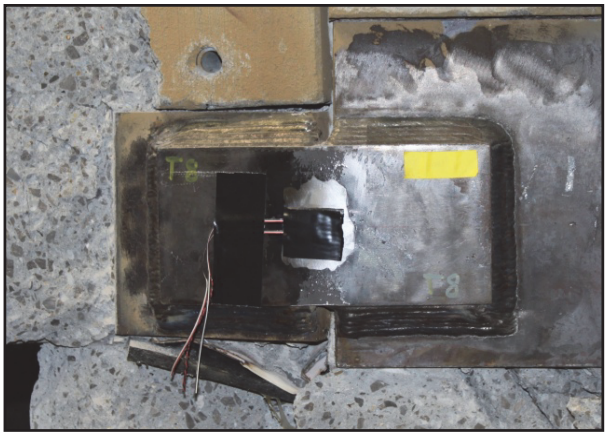

4.4 Pseudo-static response data

Table 3 provides a summary of the data recorded at 40 samples per second (40 Hz) and includes the channel description, type, location, and the peak values throughout the execution of the test.

Table 3. Summary of SDC-B pseudo-static response data.

Precast Concrete Beam-Column Connection Experiment SDC-B			
Measurement No.	Measurement Type	Measurement Location	Measured Peak Value/Time
L-95A	Applied Load	400 K Load cell/MTS ram positioned at the center of the center column	175.5 kip/216 min
L-95B	Pressure	MTS Ram Internal Pressure Gauge	181.7 ksi/216 min

Precast Concrete Beam-Column Connection Experiment SDC-B			
Measurement No.	Measurement Type	Measurement Location	Measured Peak Value/Time
D-83	Displacement	Beam-L, At mid span measured from bottom face/center line of beam-column connection	8.9 in./291 min
D-85	Displacement	Center column, Left measured from bottom face/center line of beam-column connection	18.5 in./291 min
D-86	Displacement	Center column, Right measured from bottom face/center line of beam-column connection	17.0 in./291 min
D-88	Displacement	Beam-R, At mid span measured from bottom face/center line of beam-column connection	8.3 in./291 min
LVDT-81	Displacement	East end column, At mid-point of column	-0.16 in./273 min
LVDT-90	Displacement	West end column, At mid-point of column	0.22 in./216 min
R-91	Rotation	Beam-L, East end column	-0.60 in./216 min
R-92	Rotation	Beam-L, Center column	0.2 in./214 min
R-93	Rotation	Beam-R, Center column	-3.9 in./290 min
R-94	Rotation	Beam-R, West end column	-5.1 in./290 min
εh-41	Strain	Beam-L, Top anchor bar at top left M6 embedded angle	7500 με/284 min
εh-42	Strain	Beam-L, Top anchor bar at top left M6 embedded angle	15500 με/179 min
εh-43	Strain	Beam-R, Top anchor bar at top right M6 embedded angle	14000 με/283 min
εh-44	Strain	Beam-R, Top anchor bar at top right M6 embedded angle	12000 με/283 min
εh-45	Strain	Beam-L, Top anchor bar at bottom right M7 embedded angle	12000 με/162 min
εh-46	Strain	Beam-L, Top anchor bar at bottom right M7 embedded angle	29000 με/213 min
εh-47	Strain	Beam-R, Top anchor bar at bottom left M7 embedded angle	24500 με/216 min
εh-48	Strain	Beam-R, Top anchor bar at bottom left M7 embedded angle	24000 με/216 min
εh-49	Strain	Beam-L, Outermost bottom bar at mid-span	150 με/290 min
εh-50	Strain	Beam-L, Outermost bottom bar at mid-span	120 με/205 min
εh-57	Strain	Beam-R, Outermost bottom bar at mid-span	100 με/296 min
εh-58	Strain	Beam-R, Outermost bottom bar at mid-span	160 με/297 min
εh-55	Strain	Beam-L, Outermost top bar at mid-span	45 με/290.9 min

Precast Concrete Beam-Column Connection Experiment SDC-B			
Measurement No.	Measurement Type	Measurement Location	Measured Peak Value/Time
εh-56	Strain	Beam-L. Outermost top bar at mid-span	100 με/291 min
εh-63	Strain	Beam-R, Outermost top bar at mid-span	100 με/216 min
εh-64	Strain	Beam-R, Outermost top bar at mid-span	90 με/216 min
εh-65	Strain	East end column - Beam-L, Shear tab #1, Top single	-23300με/216 min
εh-66	Strain	East end column - Beam-L, Ductile Plate #1, Rosette (0°)	-20400 με/210 min
εh-67	Strain	East end column - Beam-L, Ductile Plate #1, Bottom single	-25000 με/210 min
εh-109	Strain	East end column - Beam-L, Ductile Plate #1, Rosette (+45°)	-8900 με/210 min
εh-110	Strain	East end column - Beam-L, Ductile Plate #1, Rosette (-45°)	-9300 με/210 min
εh-111	Strain	Center column - Beam-L, Ductile Plate #2, Top single	9500 με/116 min
εh-112	Strain	Center column - Beam-L, Ductile Plate #2, Rosette (+45°)	7800 με/180 min
εh-113	Strain	Center column - Beam-L, Ductile Plate #2, Rosette (0°)	15000 με/180 min
εh-114	Strain	Center column - Beam-L, Ductile Plate #2, Rosette (-45°)	7000 με/180 min
εh-115	Strain	Center column - Beam-L, Ductile Plate #2, Bottom single	17000 με/127 min
εh-116	Strain	Center column - Beam-L, Ductile Plate #3, Top Rosette (+45°)	-7000 με/216 min
εh-117	Strain	Center column - Beam-L, Ductile Plate #3, Top Rosette (0°)	-18500 με/216 min
εh-118	Strain	Center column - Beam-L, Ductile Plate #3, Top Rosette (-45°)	-6700 με/216 min
εh-119	Strain	Center column - Beam-L, Ductile Plate #3, Bottom Rosette (+45°)	-7000 με/216 min
εh-120	Strain	Center column - Beam-L, Ductile Plate #3, Bottom Rosette (0°)	-12000 με/216 min
εh-121	Strain	Center column - Beam-L, Ductile Plate #3, Bottom Rosette (-45°)	1500 με/216 min
εh-73	Strain	Center column - Beam-R, Ductile Plate #4, Top single	1500με/186 min
εH-74	Strain	Center column - Beam-R Ductile Plate #4, Bottom single	40000 με/90 min

Precast Concrete Beam-Column Connection Experiment SDC-B			
Measurement No.	Measurement Type	Measurement Location	Measured Peak Value/Time
εh-76	Strain	Center column - Beam-R, Ductile Plate #5, Rosette (0°)	-10400 με/216 min
εh-79	Strain	West end column - Beam-R Ductile Plate #6, Rosette (0°)	-6110 με/216 min
εh-104	Strain	East end column - Beam-L, Ductile Plate #7, Rosette (0°)	16200 με/158 min
εh-107	Strain	West end column - Beam-R Ductile Plate #8, Rosette (0°)	17500 με/175 min
εh-122	Strain	Center column - Beam-R Ductile Plate #5, Rosette (+45°)	-2000 με/216 min
εh-123	Strain	Center column - Beam-R, Ductile Plate #5, Rosette (-45°)	-5700 με/216 min
εh-124	Strain	West end column - Beam-R, Ductile Plate #6, Rosette (+45°)	-1000 με/216 min
εh-125	Strain	West end column - Beam-R, Ductile Plate #6, Rosette (-45°)	-2400 με/216 min
εh-126	Strain	East end column - Beam-L, Ductile Plate #7, Rosette (+45°)	8000 με/158 min
εh-127	Strain	East end column - Beam-L. Ductile Plate #7, Rosette (-45°)	7800 με/158 min
εh-128	Strain	West end column - Beam-R, Ductile Plate #8, Rosette (+45°)	8800 με/175 min
εh-129	Strain	West end column - Beam-R, Ductile Plate #8, Rosette (-45°)	7000 με/175 min
εh-97	Strain	Top lateral steel brace beam for columns, Center of top flange	-75 με/180 min
εh-98	Strain	Top lateral steel brace beam for columns, Mid-height of interior web	-65 με/172 min
εh-99	Strain	Top lateral steel brace beam for columns, Center of bottom flange	-55 με/163 min
T1	Torsion Load Cell	Center column-Beam-L, Bottom Torsion load cell	7.3 kip/180 min
T2	Torsion Load Cell	Center column-Beam-R, Bottom Torsion load cell	53.5 kip/214 min

4.4.1 Displacement measurements

Figure 65 shows all of the vertical displacements recorded versus the applied concentric load throughout the execution of SDC-B. The maximum vertical displacements at each gauge were 8.9 in. (D-83), 18.5 in. (D-5), 17.0 in. (D-86), and 8.3 in. (D-88), resulting in a center column average vertical displacement of 17.8 in.

Figure 65. Beam vertical displacements from gauges D–83, D-85, D-86, and D-88.

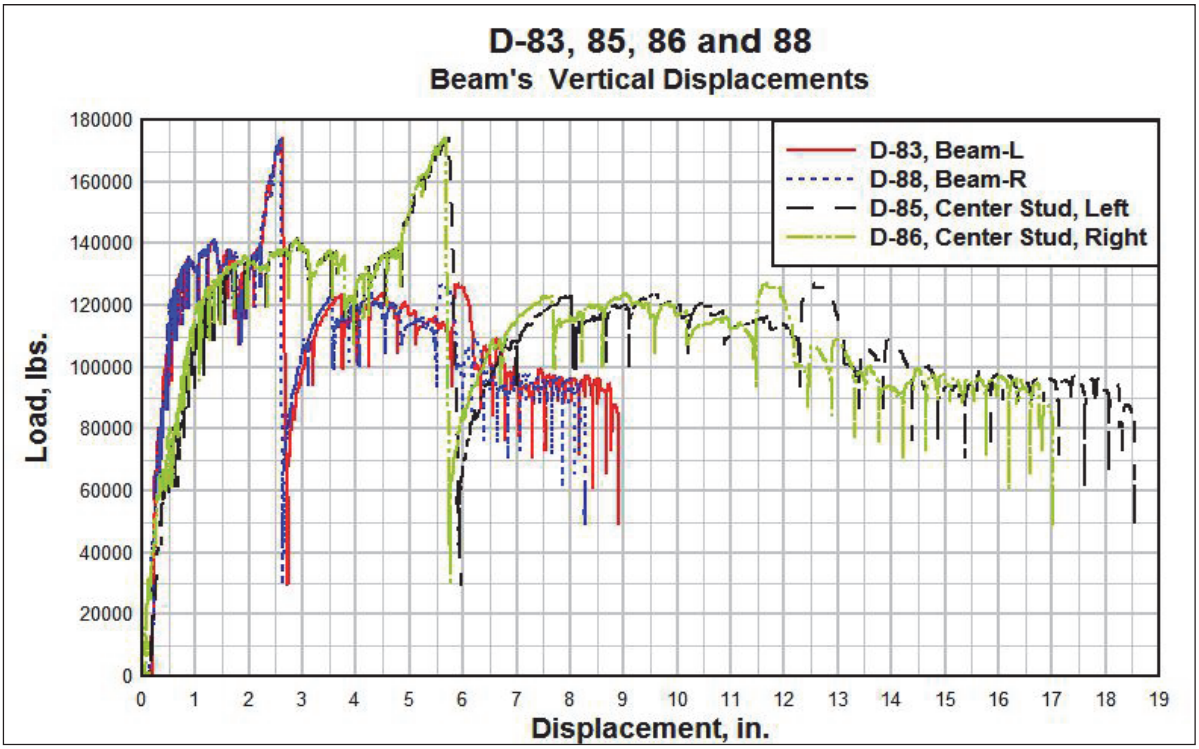

Figure 66 shows the horizontal displacements of the end columns measured at mid-height of the beams. In the plot, positive values indicate an inward displacement. It's clear that the end columns maintained an inward and largely symmetric displacement throughout the test. However, during the posttest forensic exam it was observed that the LVDTs shifted from their original position. This variable could have potentially affected the reading of the horizontal measurements, especially during the final stages of the test.

4.4.2 Inclinometer measurements

During the experiment, inclinometers R-91 and R-92 malfunctioned due to a cutoff in the instrumentation line by a spalled concrete fragment from the test specimen. Figure 67 shows the angles of rotation in degrees at the columns versus the applied load. The rotations at time that the system

reached capacity were -1.4 deg (R-93) and -1.0 deg (R-94). The maximum rotational values were -4 deg (R-93) and -5 deg (R- 94). Figure 68 shows the maximum rotation of the right end column.

Figure 66. Horizontal displacement of end columns (LVDTs 81 and 90).

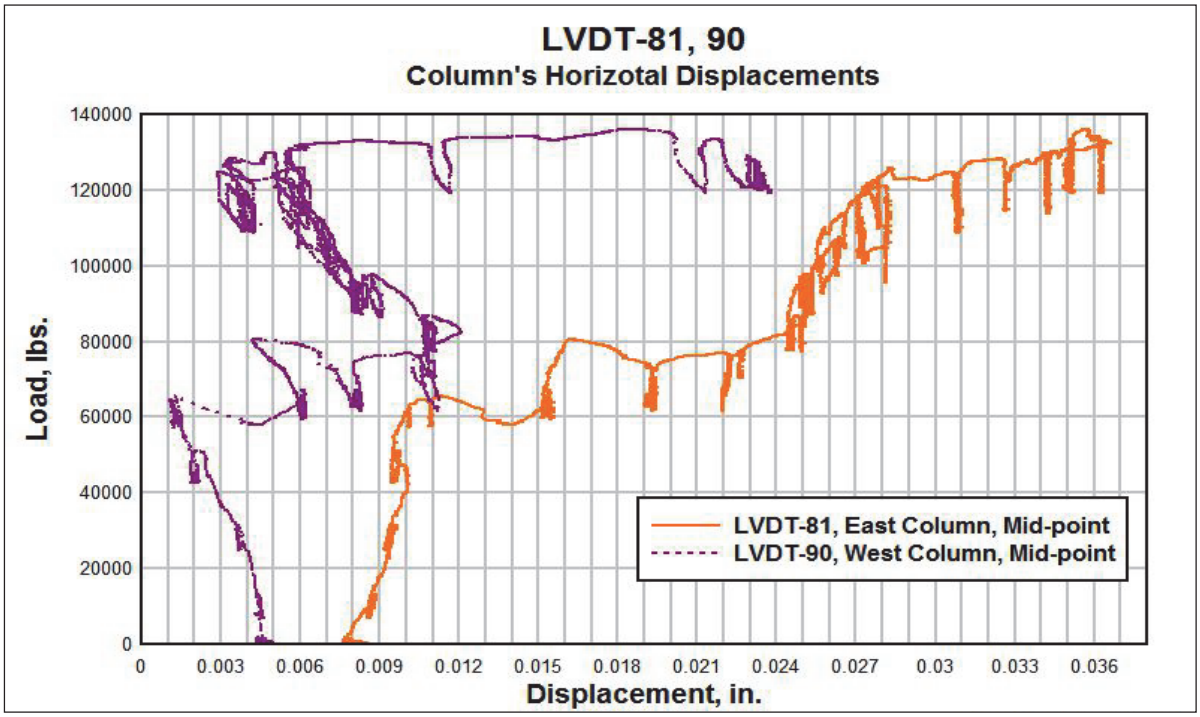

Figure 67. Beam endpoint rotations.

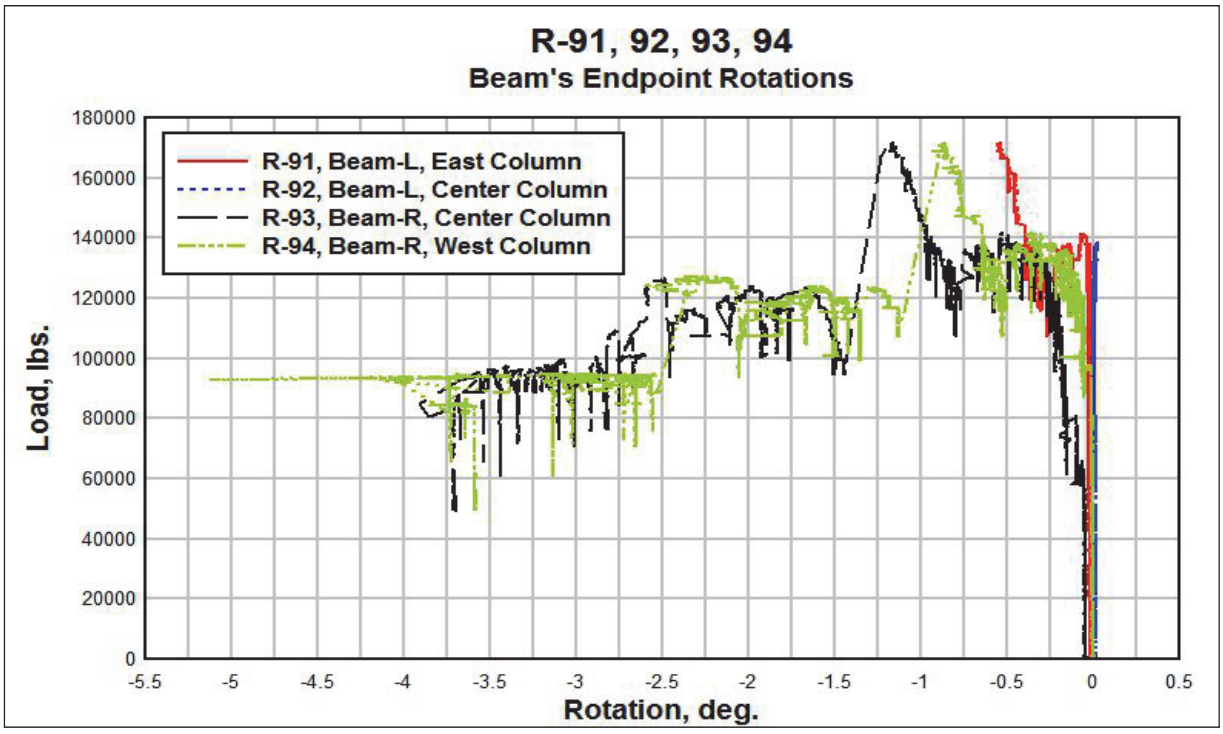

Figure 68. Rotation at right end column (gauge R-94).

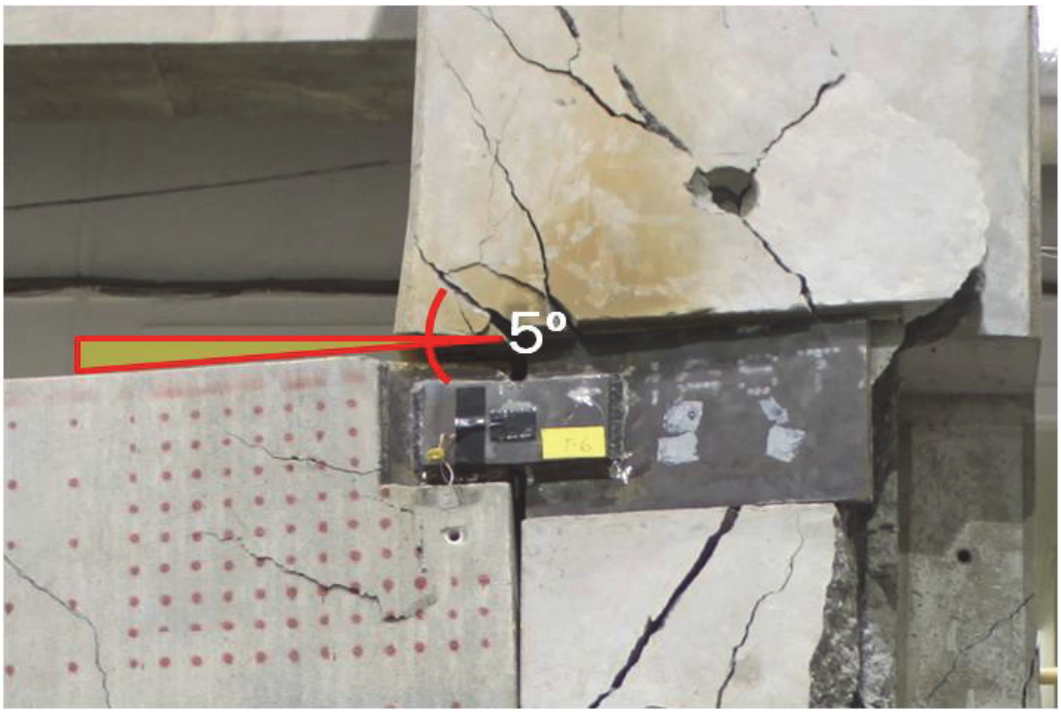

4.4.3 Strain measurements

Figure 69 shows the recorded strains at the anchor bars located at the upper end corners of the beams (M6) versus the applied load. Each of the curves in the graph exhibits a positive behavior, implying that these #10 anchor bars were mostly in tension throughout the entire execution of the test.

The strains in the top anchor bars located at the bottom center corners of the beams (M7) are shown in Figure 70. These bottom #10 anchor bars were also in tension throughout the test. Both anchor bars located at the left beam failed due to the high deformation caused by high tensile stress levels.

Figures 71 and 72 show the internal strain of the outer-most bars of the beams. All strain measurements in the outer-most bars (Figures 19 and 21) were significantly less than the nominal yield strain of A706 (0.2% or 0.002 in./in.), indicating that at mid-span, the beam remained in the elastic range throughout the test. Figure 72 shows how the tensile strains in the beam increased as the vertical displacement of the center column increased until the anchor bars in location 3 failed at the approximate testing time of 216.31 min (Figure 18).

Figure 69. Strains in top anchor bars in M6 embedded angle.

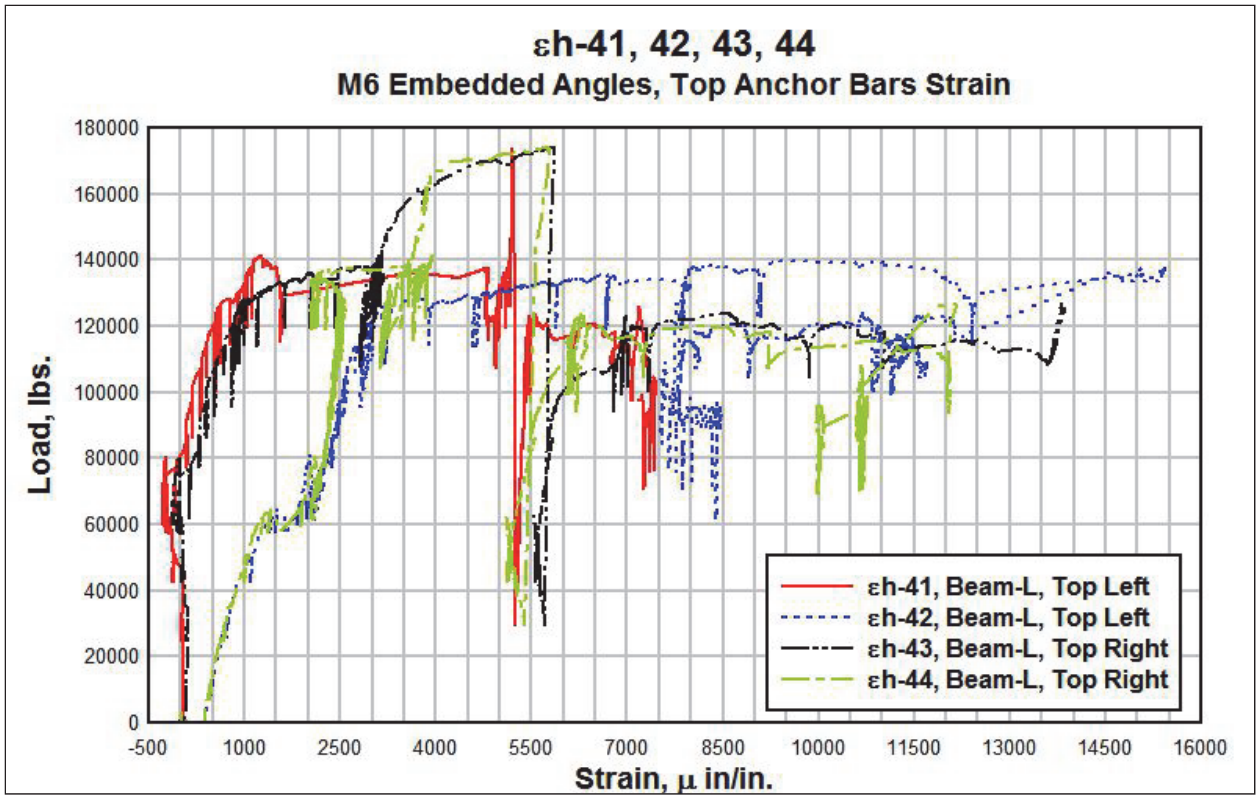

Figure 70. Strains in top anchor bars in M7 embedded angle.

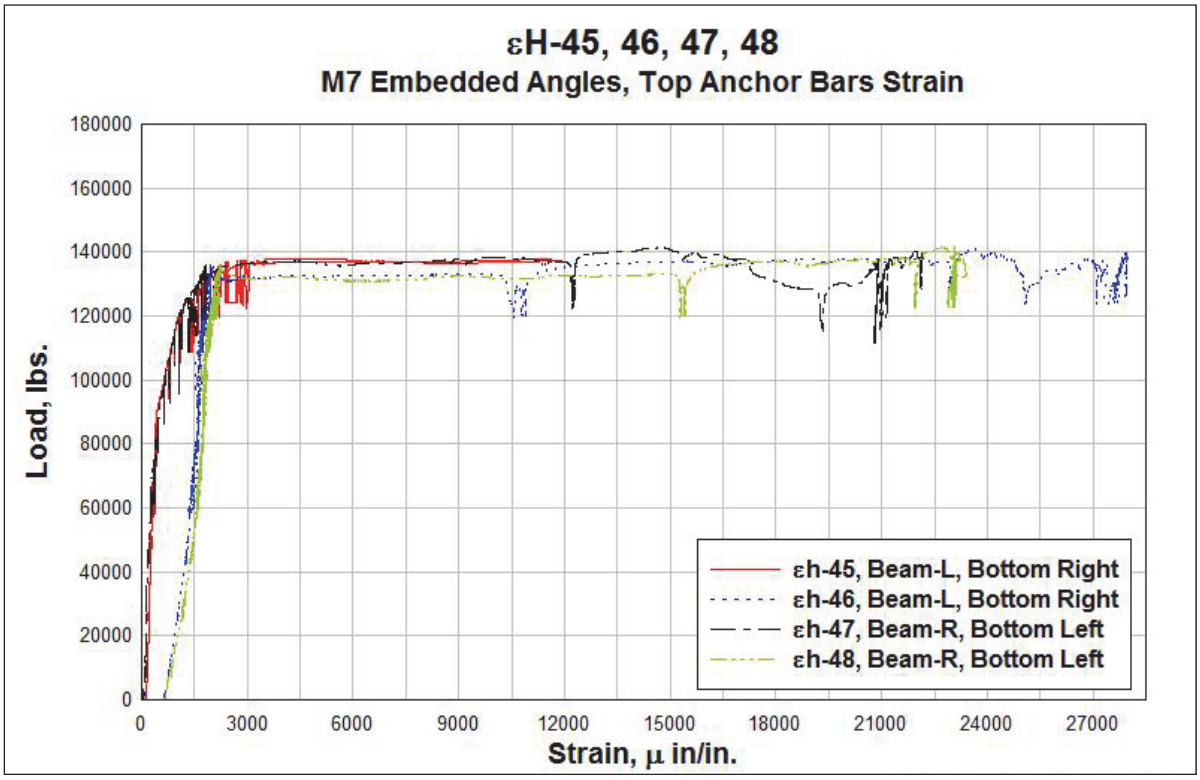

Figure 71. Strains in outer-most top bars at mid-span.

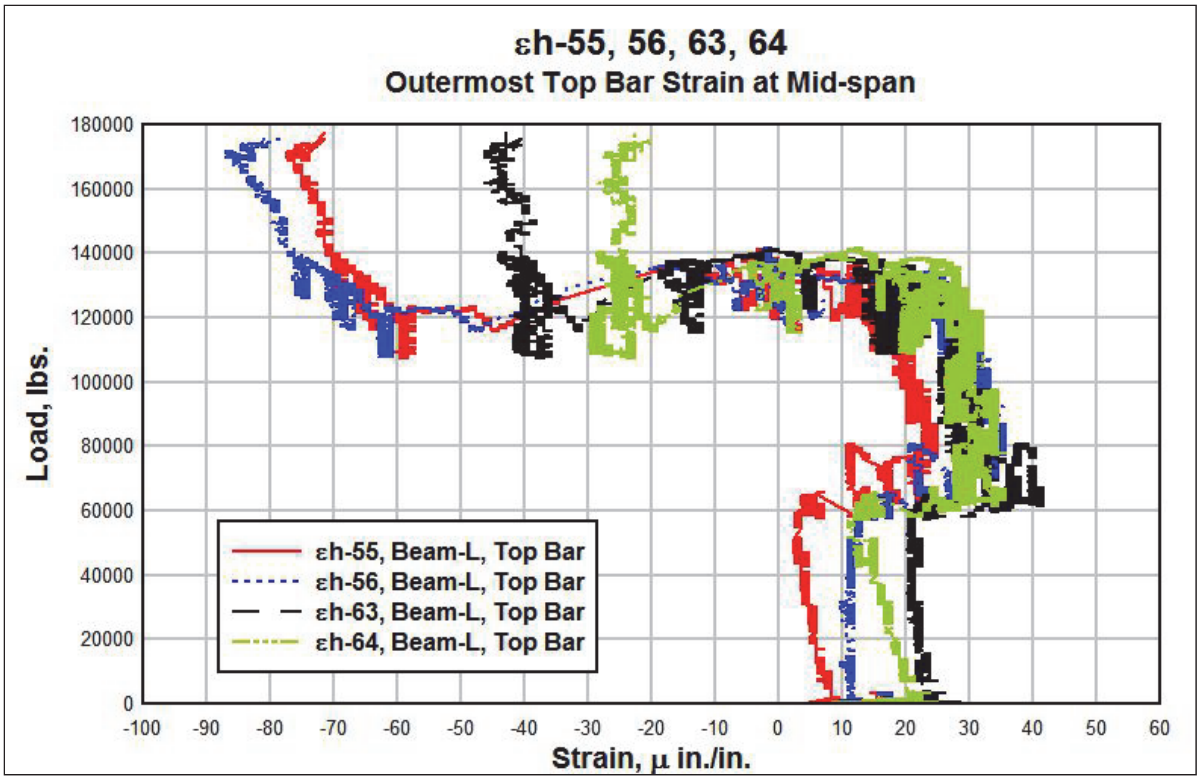

Figure 72. Strains in outer-most bottom bars at mid-span.

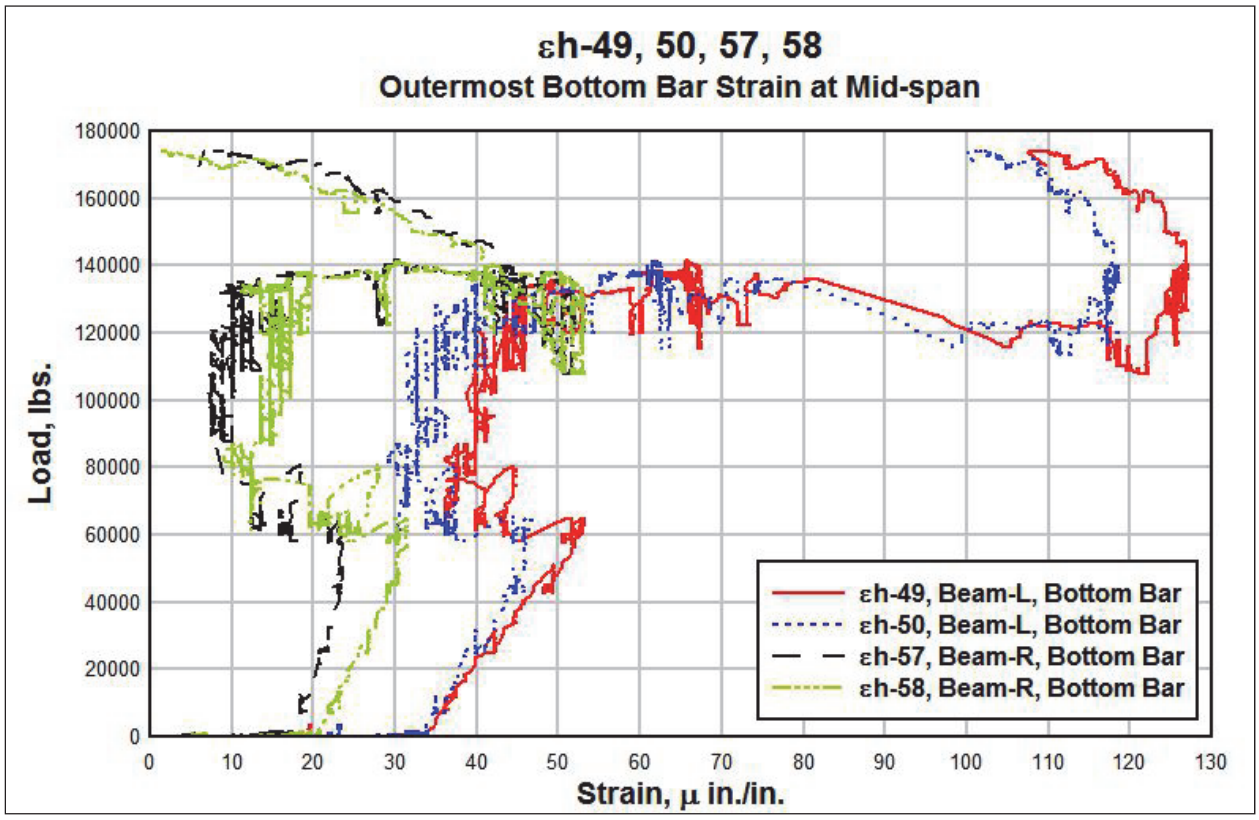

A total of 33 external strain gauges were placed at selected locations among the eight steel connecting plates in SDC-B. Figures 73 through 80 show the recorded strains in each of the ductile connection plates versus the applied load. Figure 81 shows the recorded strains in top lateral steel brace beam.

A total of eight rosettes were mounted on seven different ductile connection plates. Figure 82 illustrates the name arrangement and geometry given to each rosette's axis in order to define the 2D state of strain and calculate the principal strain and its orientation. The following arrangement was utilized in this report: Gauge A (ε_a) at (-45°), Gauge B (ε_b) at (0°), and Gauge C (ε_c) at (+45°).

Table 4 shows the principal strains (ε_1 and ε_2) and its orientation (ϕ_p) recorded on the ductile connection plate #1, at location #1. The tabulated data were taken from the peak values captured during the test. In this case the ductile connection plate #1 peak values were taken when the test reached the 139-kip mark at 210 min of test. These values could potentially be linked to the system's continuous out-of-plane behavior due to the failure of the M8 embedded plate on the top left end column, at 186 min of test.

Figure 73. Strains in shear tab #1, east end column, Beam L.

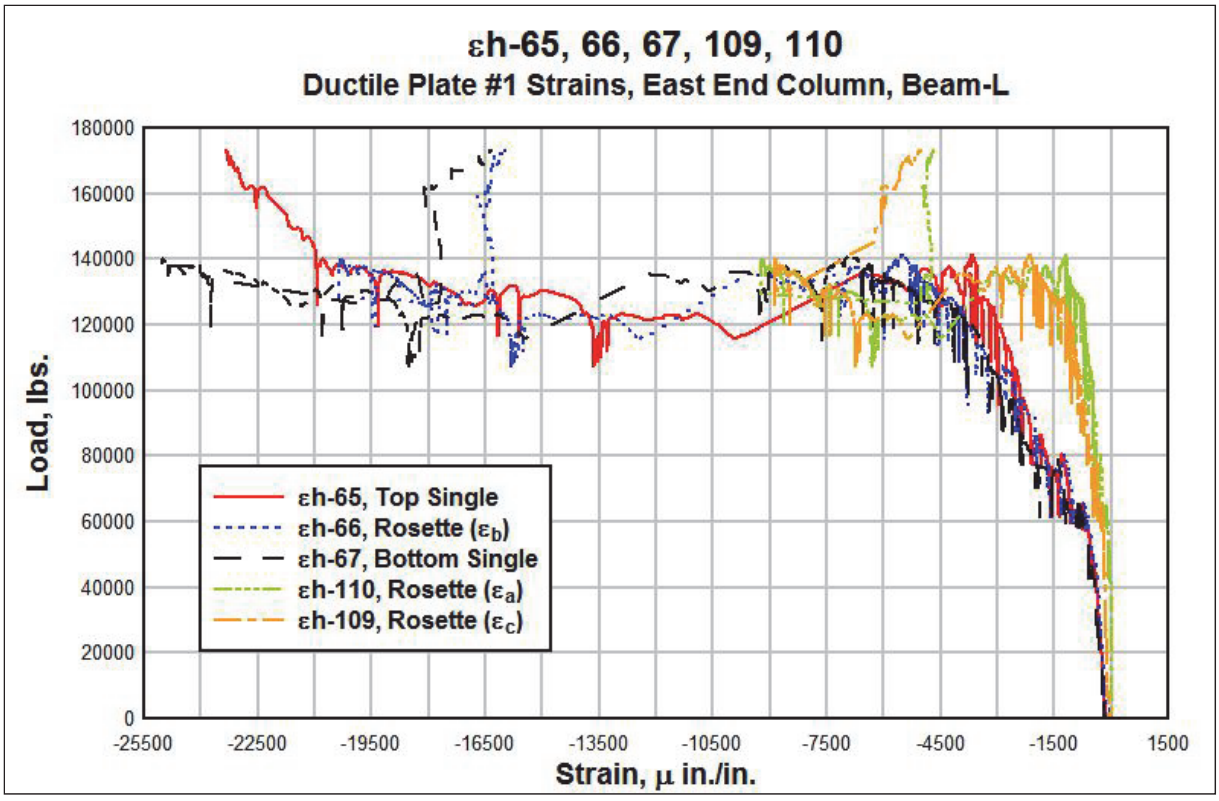

Figure 74. Strains in shear tab #2, center column, Beam L.

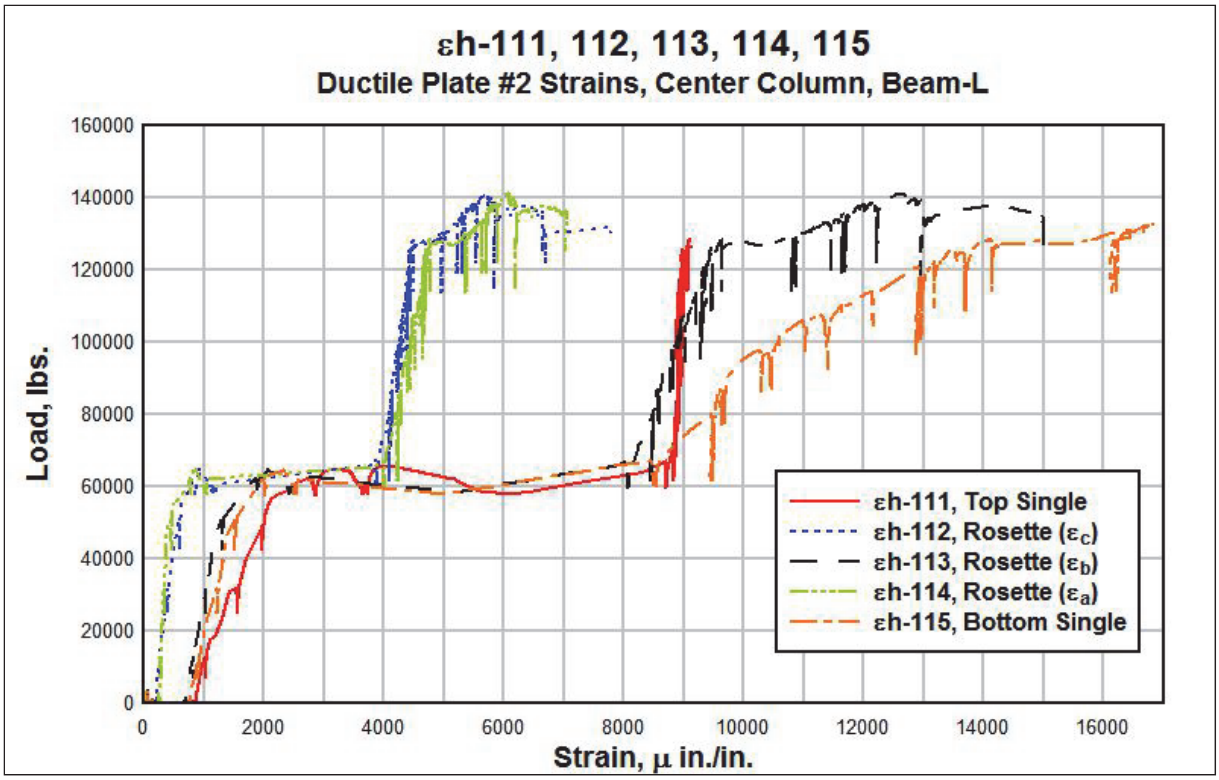

Figure 75. Strains in shear tab #3, center column, Beam L.

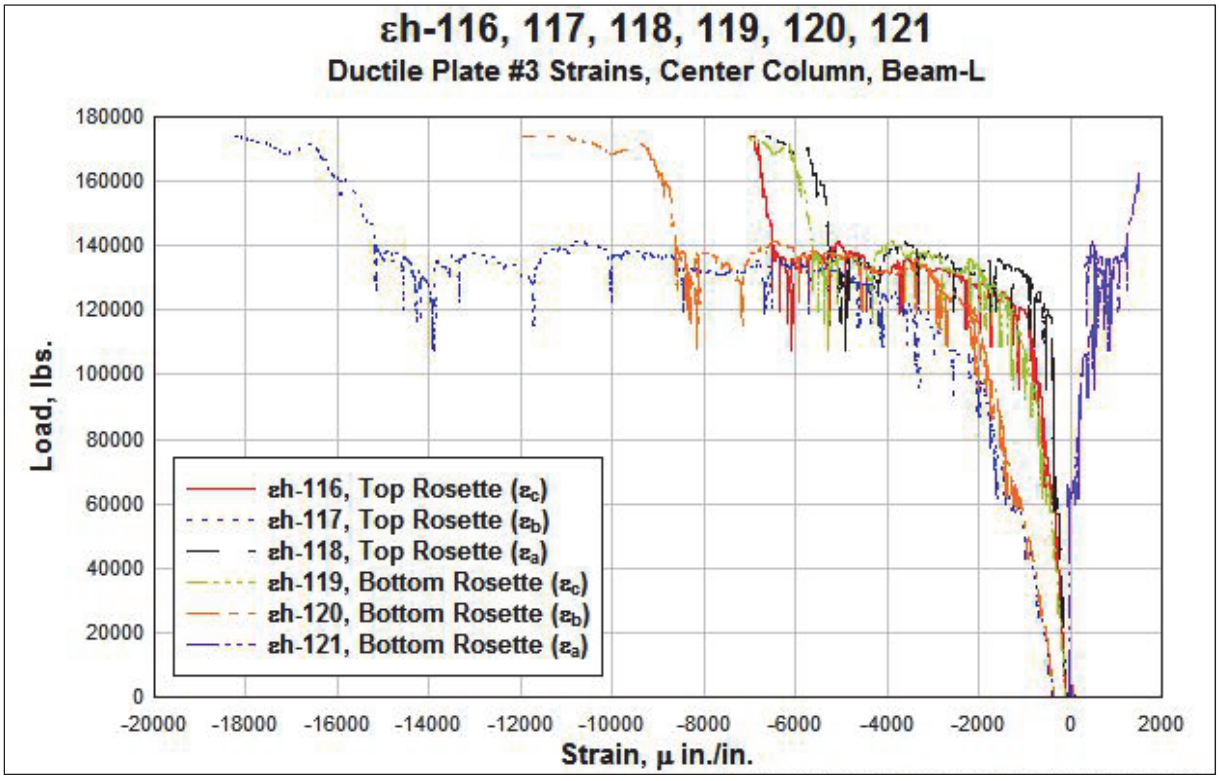

Figure 76. Strains in shear tab #4, center column, Beam R.

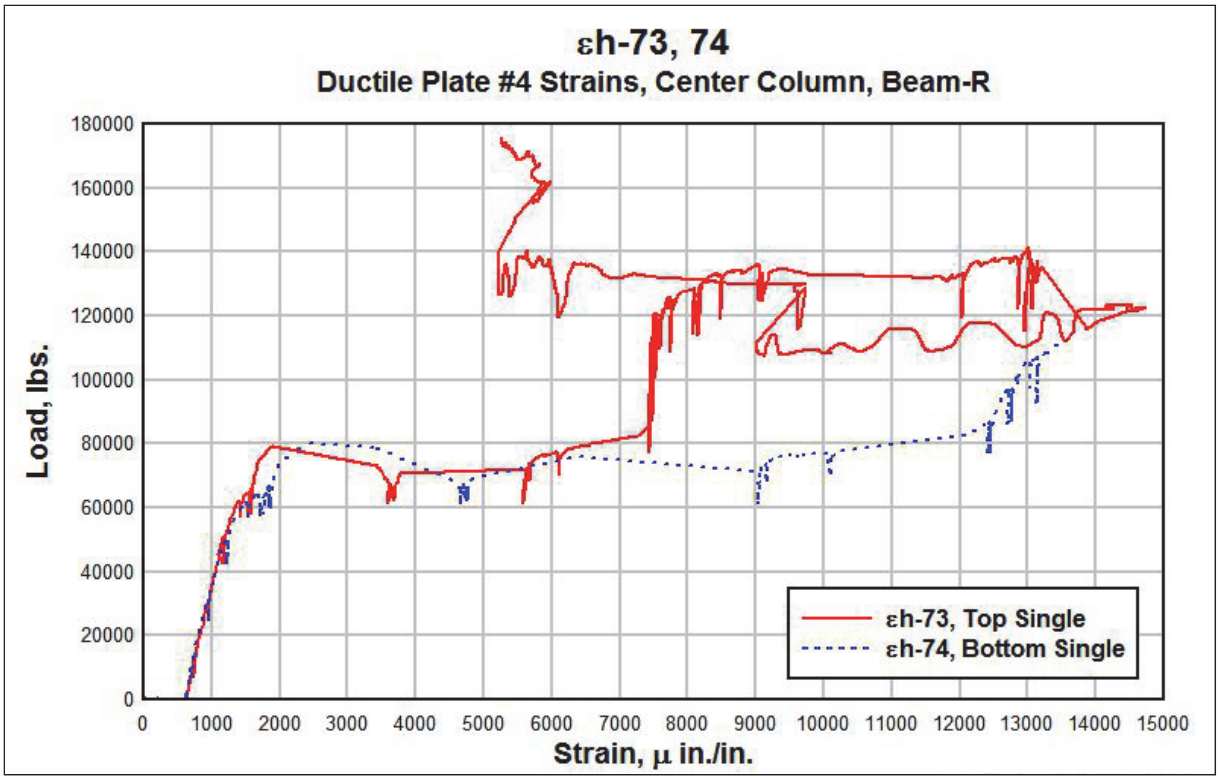

Figure 77. Strains in shear tab #5, west end column, Beam R.

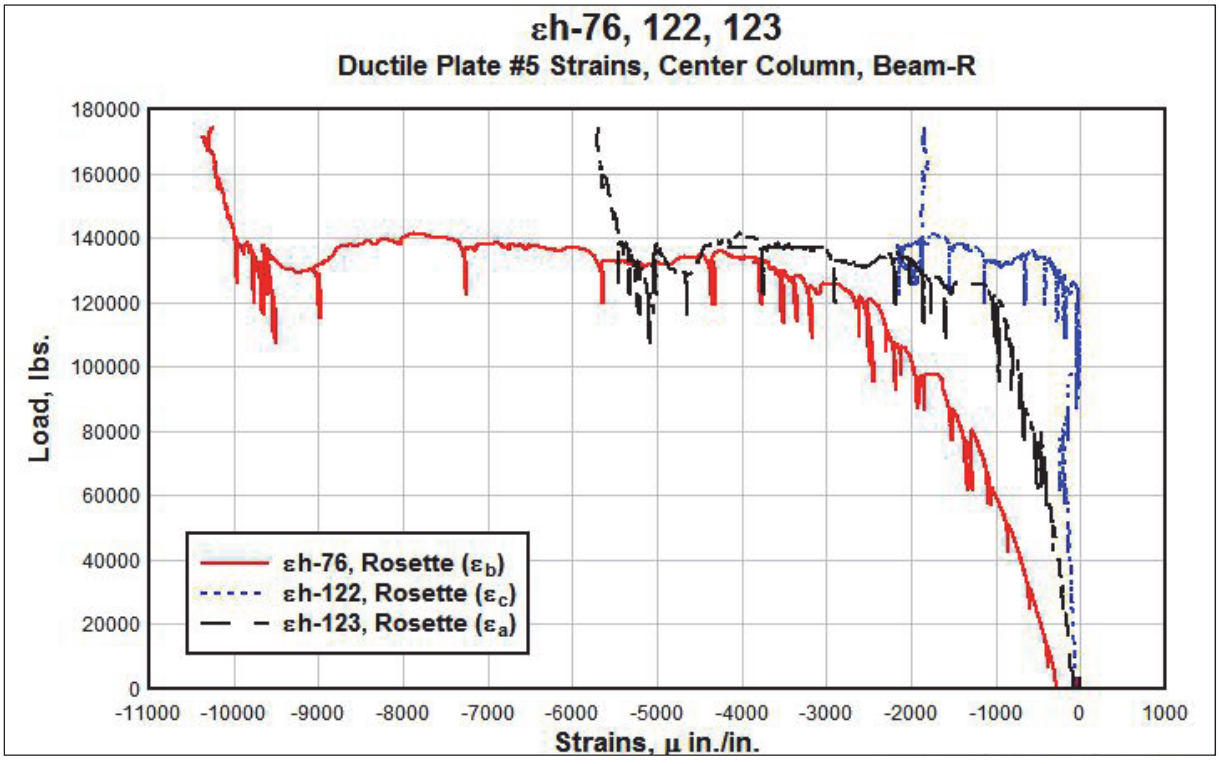

Figure 78. Strains in shear tab #6, center column, Beam R.

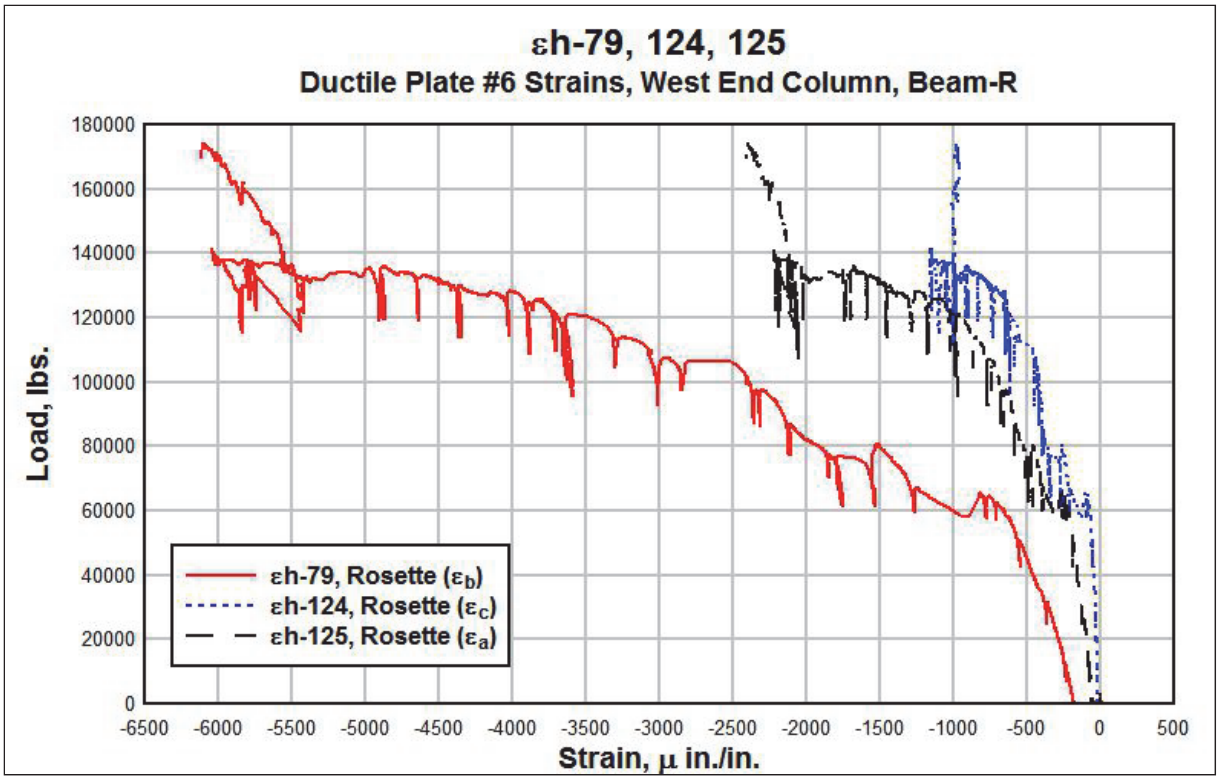

Figure 79. Strains in shear tab #7, east end column, Beam L.

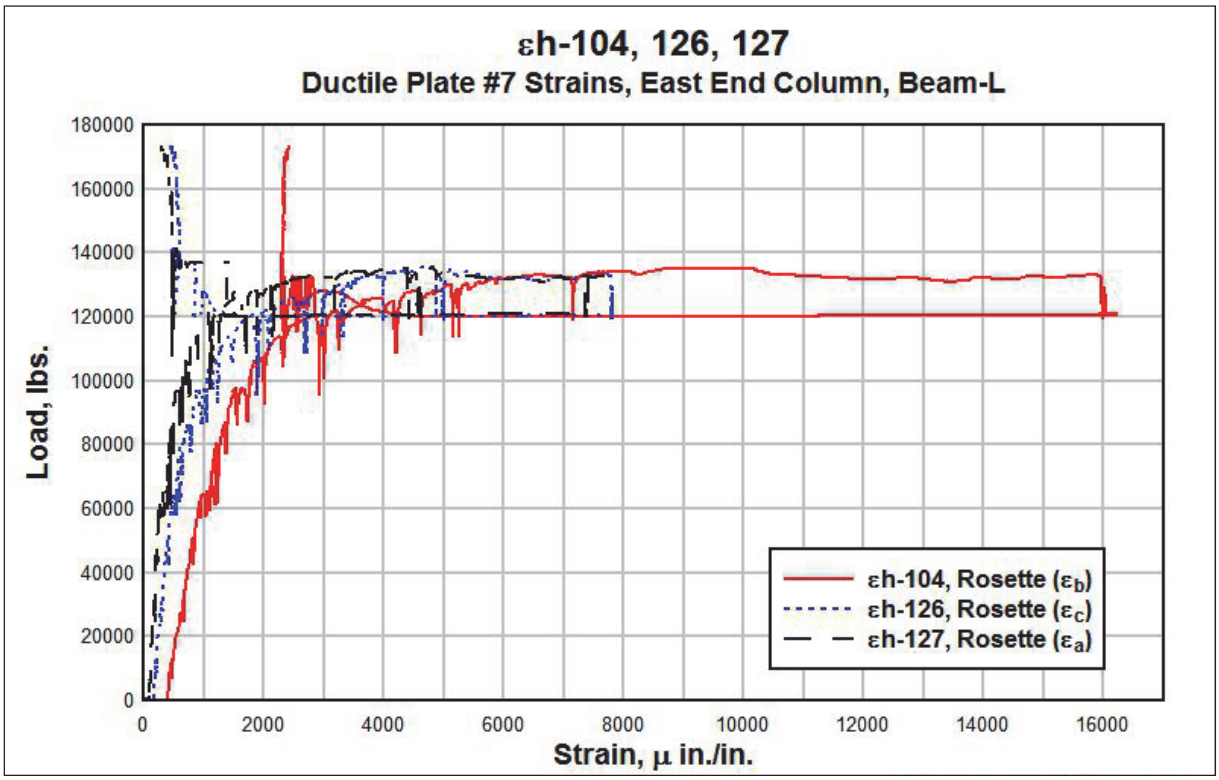

Figure 80. Strains in shear tab #8, west end column, Beam R.

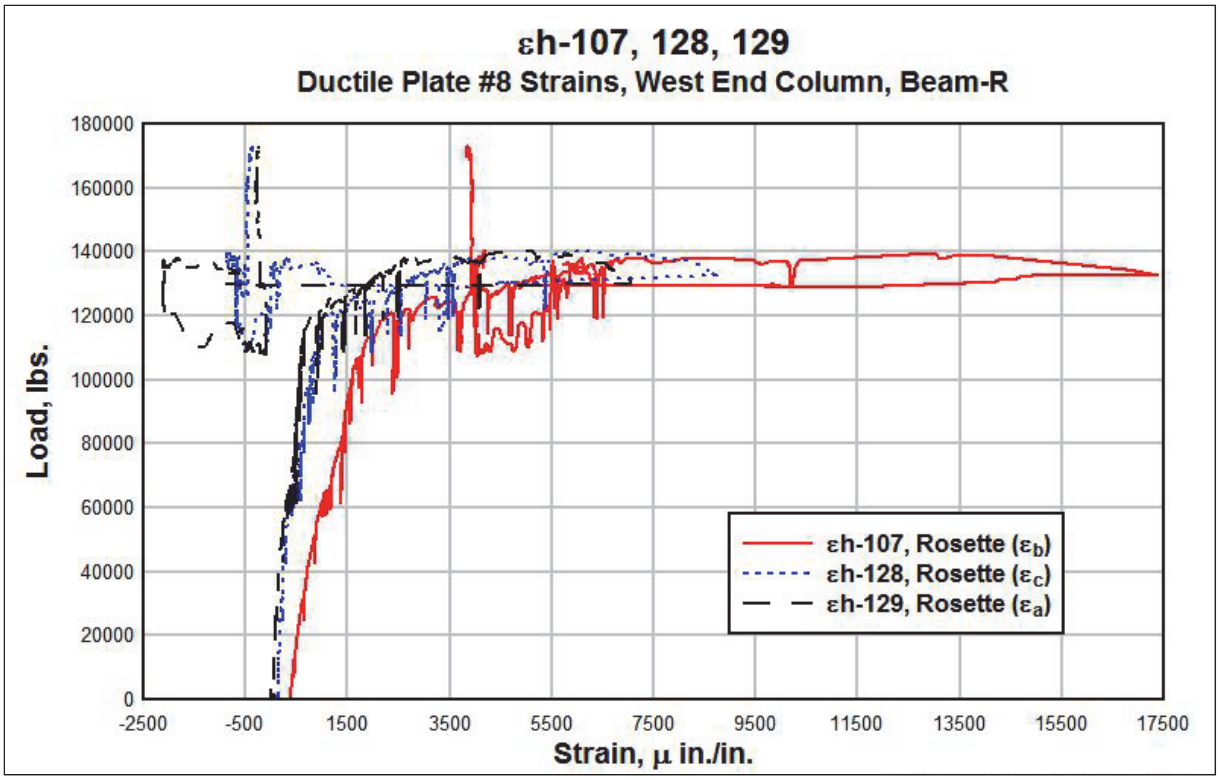

Figure 81. Strains in top lateral steel brace beam.

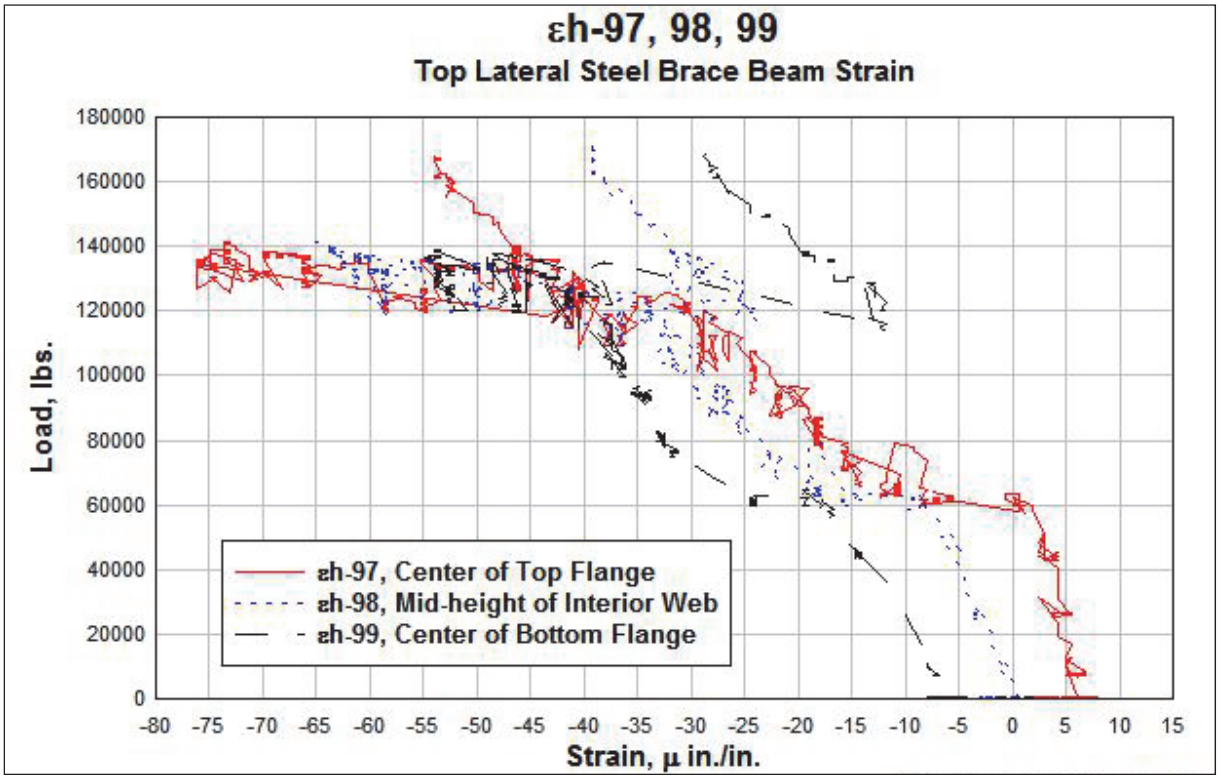

Figure 82. Layout of the orientation and numbering for the strain rosettes.

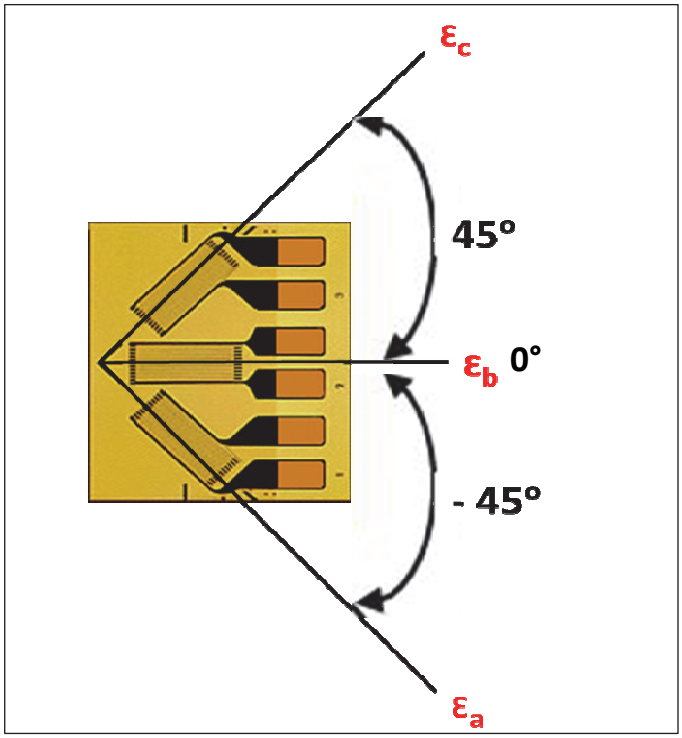

Table 4. Principal strains and orientation for ductile connection plate #1.

Location 1 - Ductile Connection Plate #1					
Rosette	Strain @ 210-min.			Principal Strains & Orientation	
ε_c	Ch-109	-8900μ in./in.		ε_1	2202μ in./in.
ε_b	Ch-66	-20400μ in./in.		ε_2	-20402μ in./in.
ε_a	Ch-110	-9300μ in./in.		ϕ_p	-0.78°

The principal strains were calculated using the configuration shown in Figure 82; (ε_1 = 2202 μ in./in.) (ε_2 = -20402 μ in./in.) at (ϕ_p = -0.78 deg.). The strain measurements in this connection plate exceed the nominal yield strain of A36 (0.12% or 1240 μ in./in.), indicating that the plate had significant plastic deformation, but no fracture. The orientation of the principal strains also validates the clockwise rotation on connection plate #1 due to the severe deflection.

Table 5 shows the principal strain (ε_1 and ε_2) and its orientation (ϕ_p) recorded on the ductile connection plate #2, at location #2. The tabulated data were taken from the peak values captured during the test. In this case the ductile connection plate #1 peak values were taken when the test

reached the 141-kip mark at 180 min of test. These values could be also linked to the system continuing out-of-plane behavior due to the failure of the M8 embedded plate on the top left end column, at 186 min of test. The principal strains on connection plate #2 are: (ε_1 = 15011 μ in./in.), (ε_2 = -211 μ in./in.), at (ϕ_p = 0.76 deg). The strain measurements in this connection plate also exceeded the nominal yield strain of A36, indicating that the plate had significant plastic deformation, but no fracture. The orientation of the principal strains also validates the counter-clockwise rotation on connection plate #2 due to the severe deflection.

Table 5. Principal strains and orientation for ductile connection plate #2.

Location 2 - Ductile Connection Plate #2					
Rosette	Strain @ 180-min.			Principal Strains & Orientation	
ε_c	εh-112	7800μ in./in.		ε_1	15011μ in./in.
ε_b	εh-113	15000μ in./in.		ε_2	-211μ in./in.
ε_a	εh-114	7000μ in./in.		ϕ_p	0.76°

Table 6 shows the principal strain (ε_1 and ε_2) and its orientation (ϕ_p) recorded on the ductile connection plate #3, at location #3. The principal strains on connection plate #3 are: (ε_1 = 4801 μ in./in.), (ε_2 = -18501 μ in./in.), at (ϕ_p = 78 deg) for the top rosette; and (ε_1 = 7430 μ in./in.), (ε_2 = -12930 μ in./in.), at (ϕ_p = 0.57 deg) for the bottom gauge. The strain measurements in this connection plate also exceed the nominal yield strain of A36, indicating that the plate had significant plastic deformation, but no fracture. The orientation of the principal strains also validates the counter-clockwise rotation on connection plate #3 due to the severe deflection.

Table 6. Principal strains and orientation for ductile connection plate #3.

Location 3 - Ductile Connection Plate #3					
Rosettes	Strain @ 216-min.			Principal Strains & Orientation	
ε_c	εh-116	-7000μ in./in.		ε_1	4801μ in./in.
ε_b	εh-117	-18500μ in./in.		ε_2	-18501μ in./in.
ε_a	εh-118	-6700μ in./in.		ϕ_p	0.78°
ε_c	εh-119	-7000μ in./in.		ε_1	7430μ in./in.
ε_b	εh-120	-12000μ in./in.		ε_2	-12930μ in./in.
ε_a	εh-121	1500μ in./in.		ϕ_p	0.57°

Table 7 shows the principal strain (ε_1 and ε_2) and its orientation (ϕ_p) recorded on the ductile connection plate #5, at location #5. The principal strains on connection plate #5 are: (ε_1 = 2956 μ in./in.), (ε_2 = -10656 μ in./in.), at (ϕ_p = -0.65 deg). These values could be linked to the system's continuous out-of-plane behavior due to the brittle failure of the M7 anchor bars and the failure of the M8 connection on the left beam. The strain measurements in this connection plate also exceeded the nominal yield strain of A36, indicating that the plate had significant plastic deformation, but no fracture. The orientation of the principal strains also validates the clockwise rotation on connection plate #5 due to the severe deflection and the rotation of the specimen toward the right end column.

Table 7. Principal strains and orientation for ductile connection plate #5.

Location 5 - Ductile Connection Plate #5					
Rosette	Strain @ 216-min.			Principal Strains & Orientation	
ε_c	εh-122	-2000μ in./in.		ε_1	2956μ in./in.
ε_b	εh-76	-10400μ in./in.		ε_2	-10656μ in./in.
ε_a	εh-123	-5700μ in./in.		ϕ_p	-0.65°

Table 8 shows the principal strain (ε_1 and ε_2) and its orientation (ϕ_p) recorded on the ductile connection plate #6, at location #6. The principal strains on connection plate #6 are: (ε_1 = 2765 μ in./in.), (ε_2 = -6165 μ in./in.), at (ϕ_p = -0.71 deg). These values could also be linked to the system continuing out-of-plane behavior due to the brittle failure of the M7 anchor bars and the failure of the M8 connection on the left beam. The strain measurements in this connection plate also exceed the nominal yield strain of A36, indicating that the plate had significant plastic deformation, but no fracture. The orientation of the principal strains validates the clockwise rotation on connection plate #6 due to the severe deflection.

Table 8. Principal strains and orientation for ductile connection plate #6.

Location 6 - Ductile Connection Plate #6					
Rosette	Strain @ 216-min.			Principal Strains & Orientation	
ε_c	εh-124	-1000μ in./in.		ε_1	2765μ in./in.
ε_b	εh-79	-6110μ in./in.		ε_2	-6165μ in./in.
ε_a	εh-125	-2400μ in./in.		ϕ_p	-0.71°

Table 9 shows the principal strains (ε_1 and ε_2) and its orientation (ϕ_p) recorded on the ductile connection plate #7, at location #7. The principal strains on connection plate #7 are: (ε_1 = 16201 μ in./in.), (ε_2 = -401 μ in./in.), at (ϕ_p = 0.78 deg). The strain measurements in this connection plate also exceeded the nominal yield strain of A36, indicating that the plate had significant plastic deformation, but no fracture. The counter-clockwise orientation on connection plate #7 could be result of the moment reaction at the support preventing the system to rotate toward the center stud due to the high magnitude bending moments.

Table 9. Principal strains and orientation for ductile connection plate #7.

Location 7 - Ductile Connection Plate #7					
Rosette	Strain @ 158-min.			Principal Strains & Orientation	
ε_c	εh-126	8000μ in./in.		ε_1	16201μ in./in.
ε_b	εh-104	16200μ in./in.		ε_2	-401μ in./in.
ε_a	εh-127	7800μ in./in.		ϕ_p	0.78°

Table 10 shows the principal strain (ε_1 and ε_2) and its orientation (ϕ_p) recorded on the ductile connection plate #8, at location #8. The principal strains on connection plate #8 are: (ε_1 = 17542 μ in./in.), (ε_2 = -1742 μ in./in.), at (ϕ_p = 0.74 deg). The strain measurements in this connection plate also exceeded the nominal yield strain of A36, indicating that the plate had significant plastic deformation, but no fracture. The counter-clockwise orientation on connection plate #8 could also be result of the moment reaction at the support preventing the system to rotate toward the center stud due to the high magnitude bending moments.

Table 10. Principal strains and orientation for ductile connection plate #8.

Location 8 - Ductile Connection Plate #8					
Rosette	Strain @ 175-min.			Principal Strains & Orientation	
ε_c	εh-128	8800μ in./in.		ε_1	17542μ in./in.
ε_b	εh-107	17500μ in./in.		ε_2	-1742μ in./in.
ε_a	εh-129	7000μ in./in.		ϕ_p	0.74°

4.4.4 Torsion load cells

Figure 83 shows the recorded tension loads on the torsion rods located at the bottom center beam-column connection, shown in Figure 32. The red load curve show the change in tension force on the bottom-left torsion rod

(T1), and the blue curve the bottom-right torsion rod (T2). Figure 83 depicts a difference between the measurements on these two gauges. The maximum tension force measured by the load cells on the torsion bars were 7.3 kip (T1) and 53.5 kip (T2). The difference between these measurements can be explained by two major factors. First, the system configuration, the two loads track qualitatively well during the initial response phase; however, a misalignment between the beam-column connections could have potentially generated tension forces on the torsion bars during the end of the first-quarter of the testing time. Second, failure of M7 bars, due to the fact that the bottom M7, Figure 10, bars in the left beam failed during the second and third quarters of the test, it could have possibly caused the system to release of energy on the torsion cell (T1), contrary to (T2), which absorbed all the torsion forces on the system soon after M7 failed.

Figure 83. Load cells on torsion rods bottom center column.

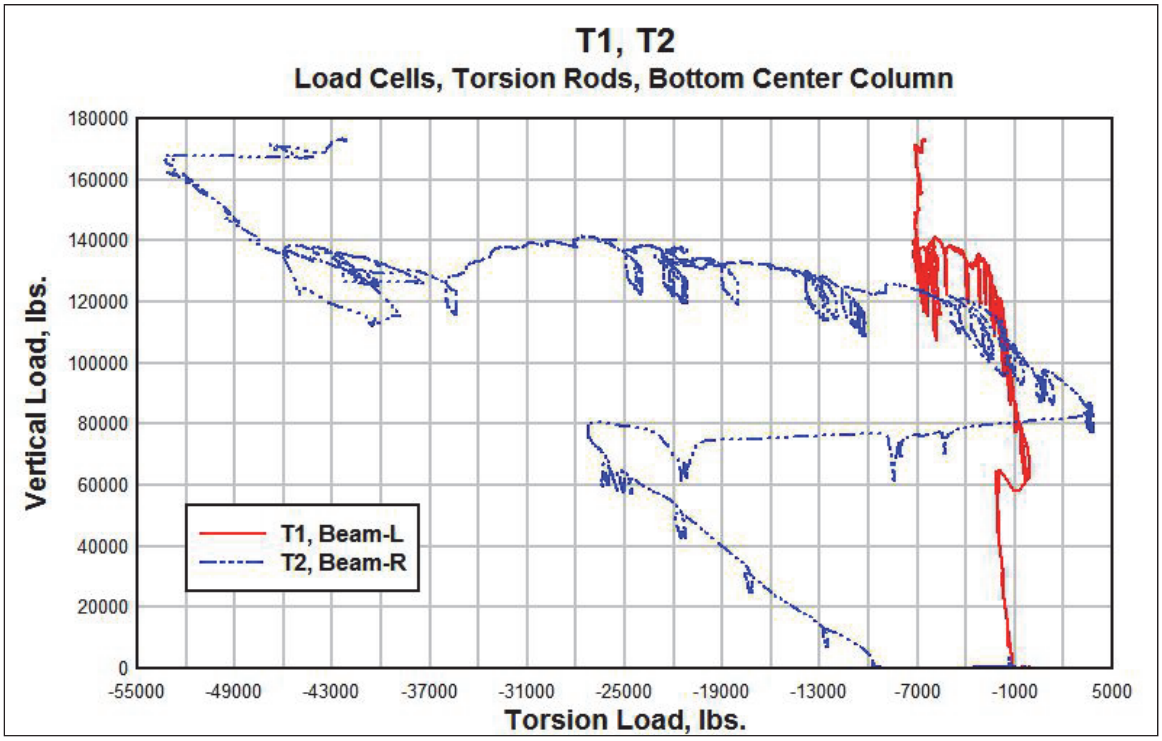

4.5 High-frequency response data

The structural cracks produced during loading generated propagating stress waves that were detectable as surface waves by the acoustic emission (AE) sensors. The AE behave like high frequency accelerometers that responded to stress waves originating from stimuli in the test beam (theoretically resulting from internal damage such as cracking) reaching the surface or boundaries where the AE sensors are located. These sensors generally have

a crystal that responds to energy in a non-linear fashion, with bandwidths from 60 to 1000 KHz, as shown in Figure 84. The acoustic events described in this section are defined as transient time histories with an amplitude measured in volts that exceed an arbitrary set level. Therefore the high frequency data were recorded as a set of discrete time events.

The red load curve in Figure 85 (pseudo-static response data L-95A) shows a sharp 135,000-lb loading drop at 216.3 min. This point, previously defined as “event IV", in Figure 39, will now be identified in this section as the primary failure of the beam “event 194", "216.3 min". This corresponds to the large acoustic emission response shown Figures 86 and 87.

Figure 88 shows the load data compared with data from two rebar strain gauges and three connecting plate strain gauges that were dual recorded, i.e., at 40 Hz and 2 MHz. Figure 89 shows the strain data recorded at 2 MHz at the primary failure. In this case, structural deformation is evident in both sets of data recorded at the high sample rate, 2 MHz, and the low sample rate, 40 Hz, since the event energy was high enough to cause deformation in this short duration of 50 ms. Specifically, εH–45 shows a transient strain variation of (15,500 μ in./in.) and a permanent deformation of (2000 μ in./in.). As can be seen in Table 11, the only other strain response events evident from the high-sample rate data were events 191 (Figures 90 and 91), 195 (Figure 92), and 197 (Figure 93). These were much smaller transient variations at (12 to 2500 μ in./in.), and permanent deformations were not observed.

Figure 84. Score Dunegan SE900-MWB calibration curve (Score Atlanta Inc. 2011).

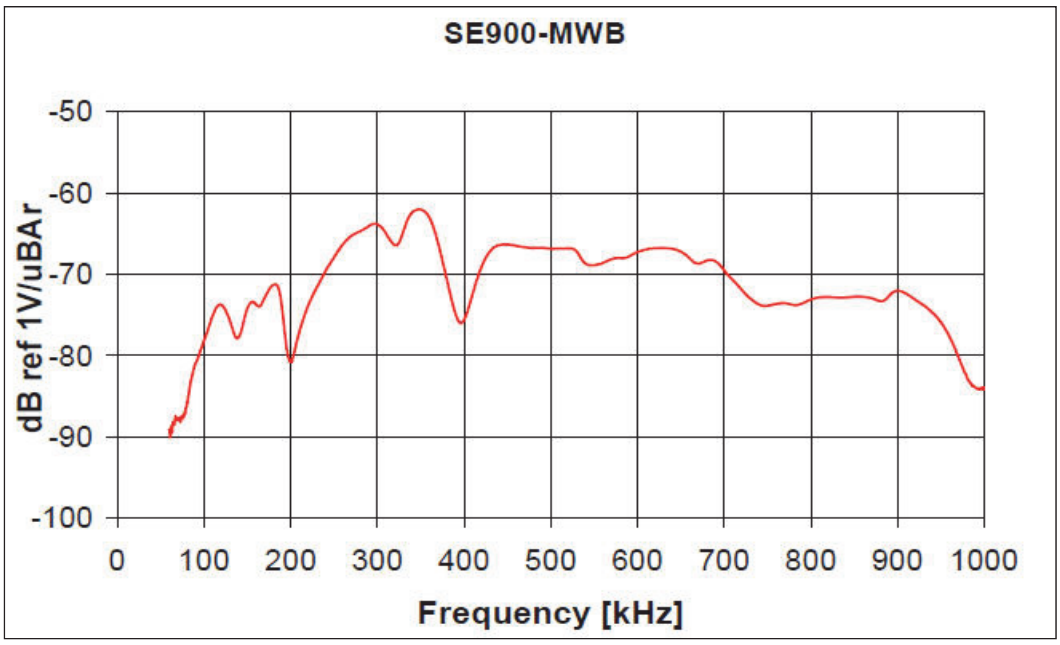

Figure 85. Load and displacements vs. time (40 Hz).

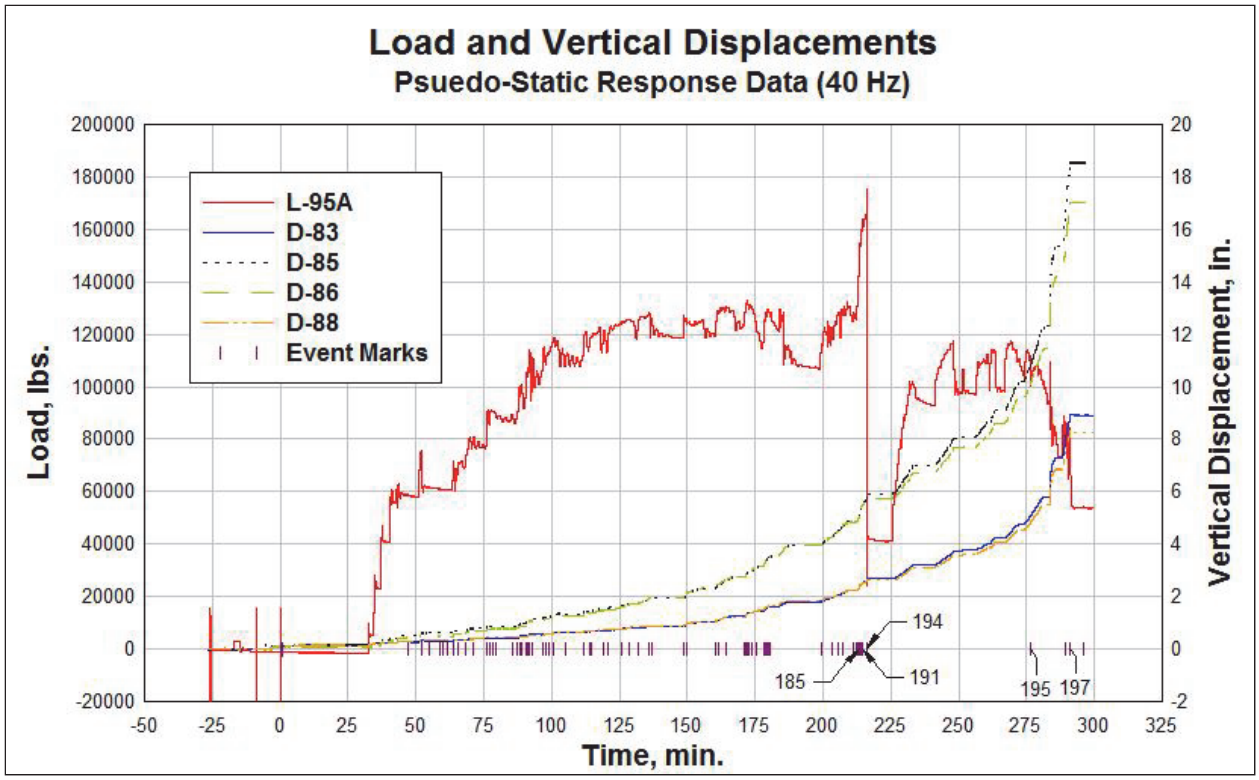

Figure 86. Load and acoustic emission for transient event 194 vs. time (2 MHz).

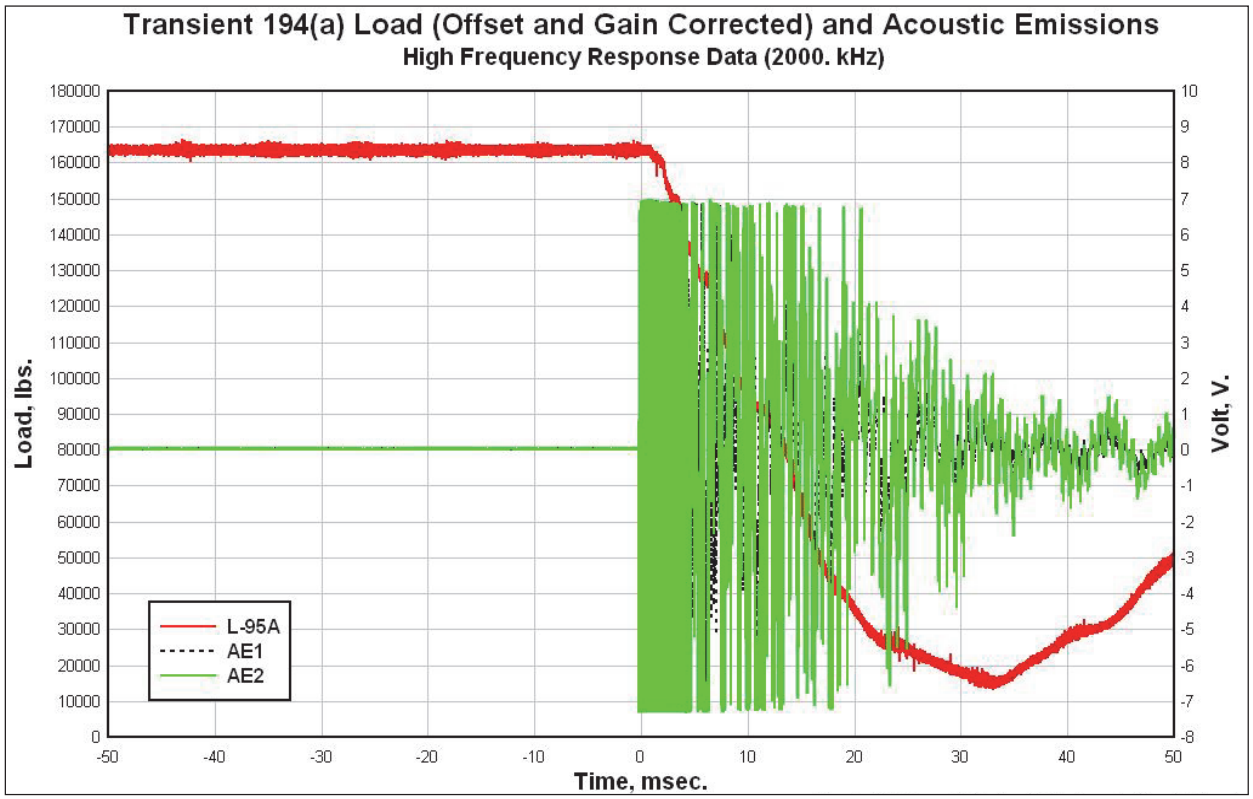

Figure 87. Load and acoustic emission for transient event 194(b) vs. time (2 MHz) for (a) 100 ms and (b) 50 ms.

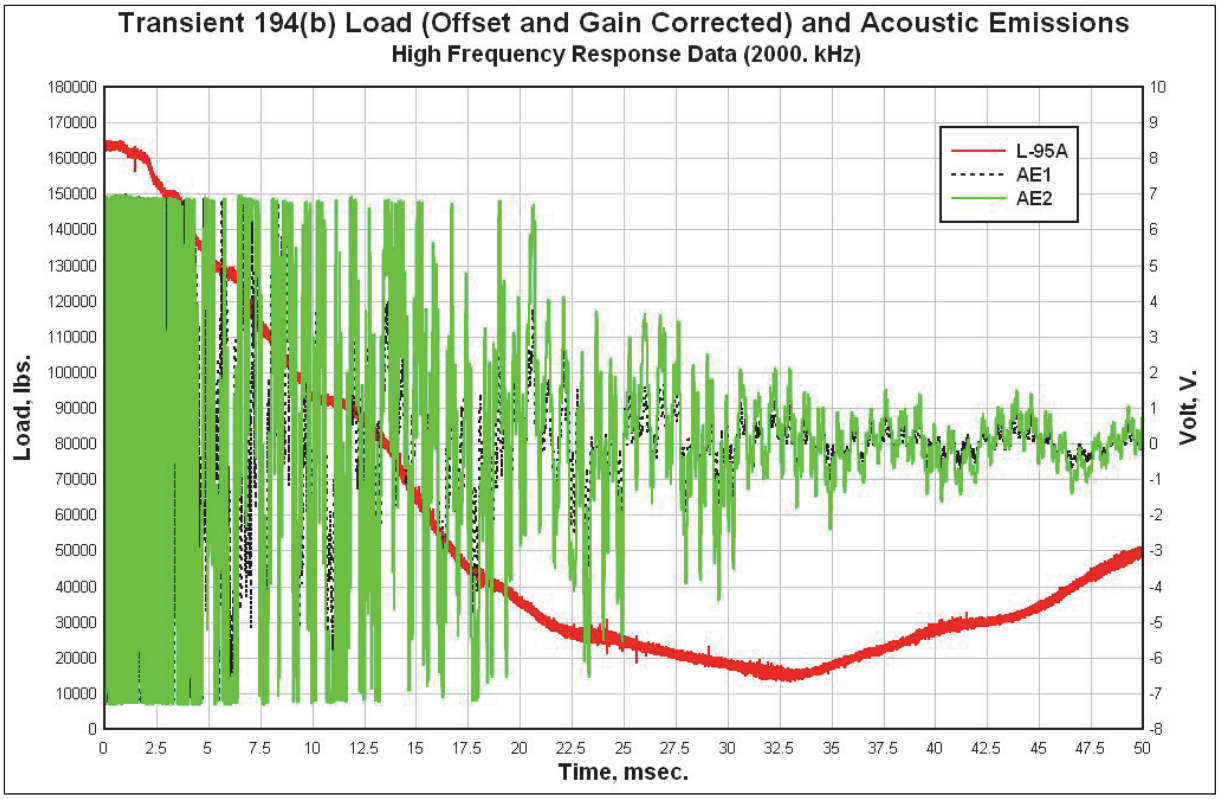

Figure 88. Load and strain vs. time (40 Hz).

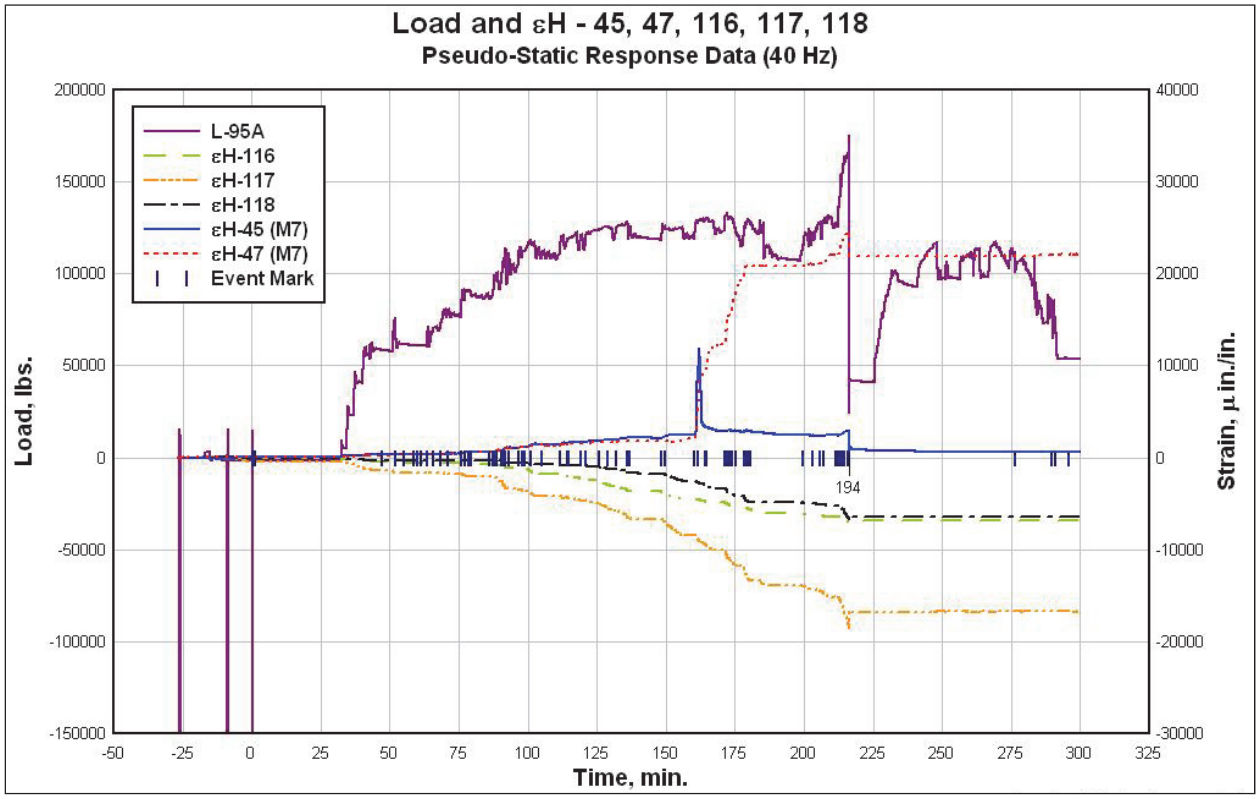

Figure 89. Strain vs. time (2 MHz) at transient event 194.

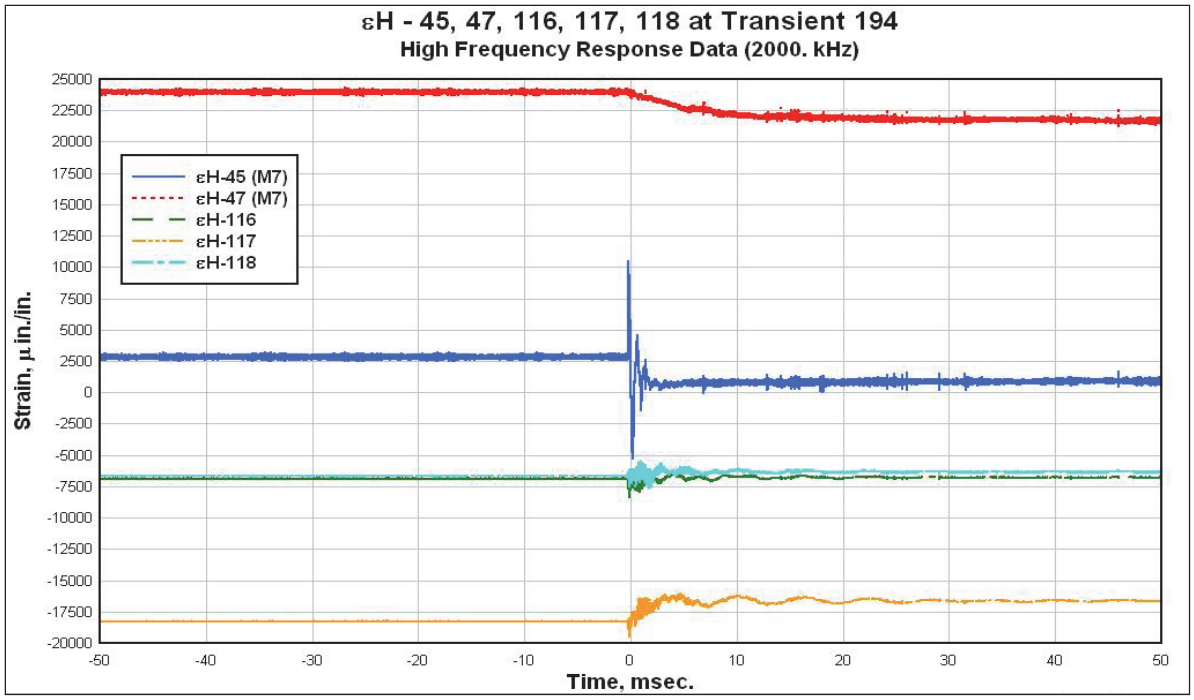

Table 11. Transient events activity.

Transient Event No.	Acoustic Emission Activity	Accelerometer Activity	Strain Activity	Load Activity	Zero-Time, Minutes
161	X				161.50
162	X				161.60
163	X				164.18
164	X				164.49
171	X				178.21
172	X				178.86
175	X				180.00
176	X				180.50
183	X				212.49
185	X	X			213.20
188	X				213.92
189	X	X			214.18
190	X				214.43
191	X	X	X	X	214.66
192	X	X			216.09
193	X	X			216.24
194	X	X	X	X	216.32
195	X	X	X	X	276.54
196	X	X			289.49
197	X	X	X	X	291.02

Figure 90. Strain vs. time (2 MHz) at transient event 191.

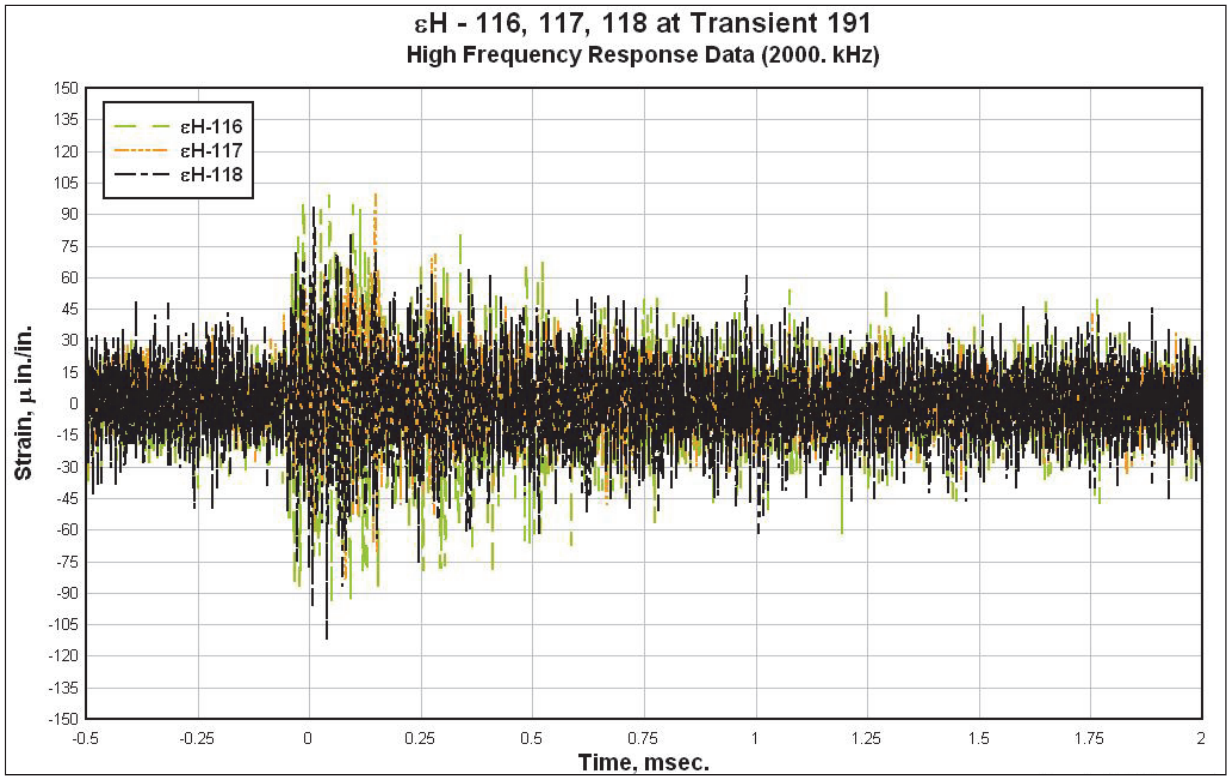

Figure 91. Strain vs. time (2MHz) at transient event 191 (εH–116, 117, and 118, Mean Subtracted), vs. Time, (2 MHz), replotted of Figure 90 from -0.25 to 0.5 msec.

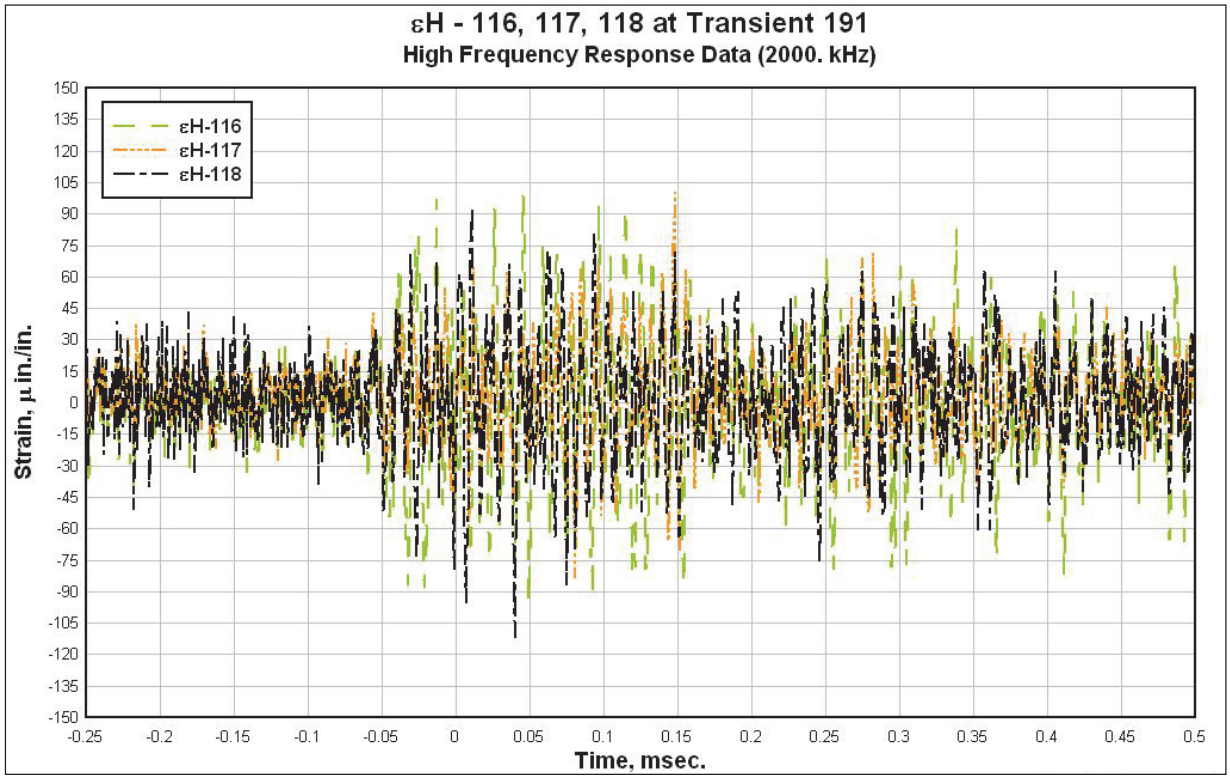

Figure 92. Strain vs. time (2 MHz) at transient event 195.

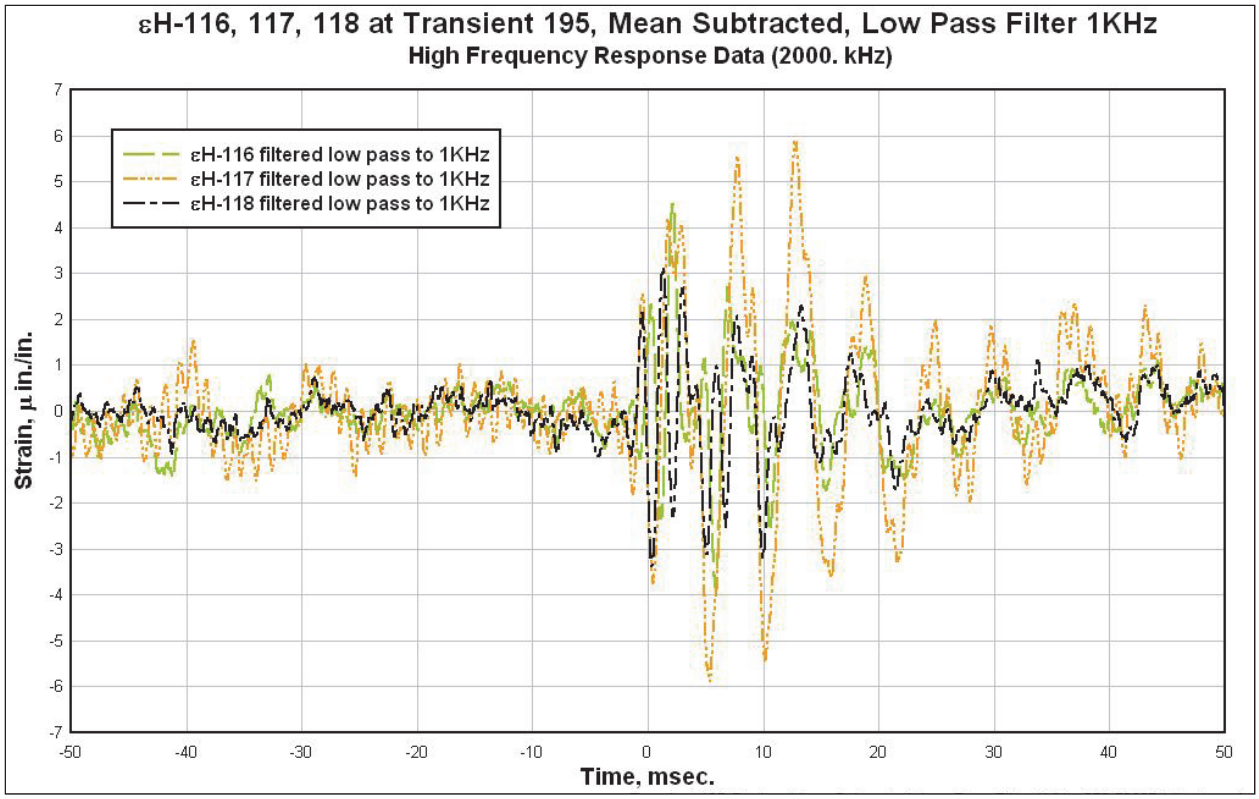

Figure 93. Offset strains vs. time (2MHz) at transient event 197.

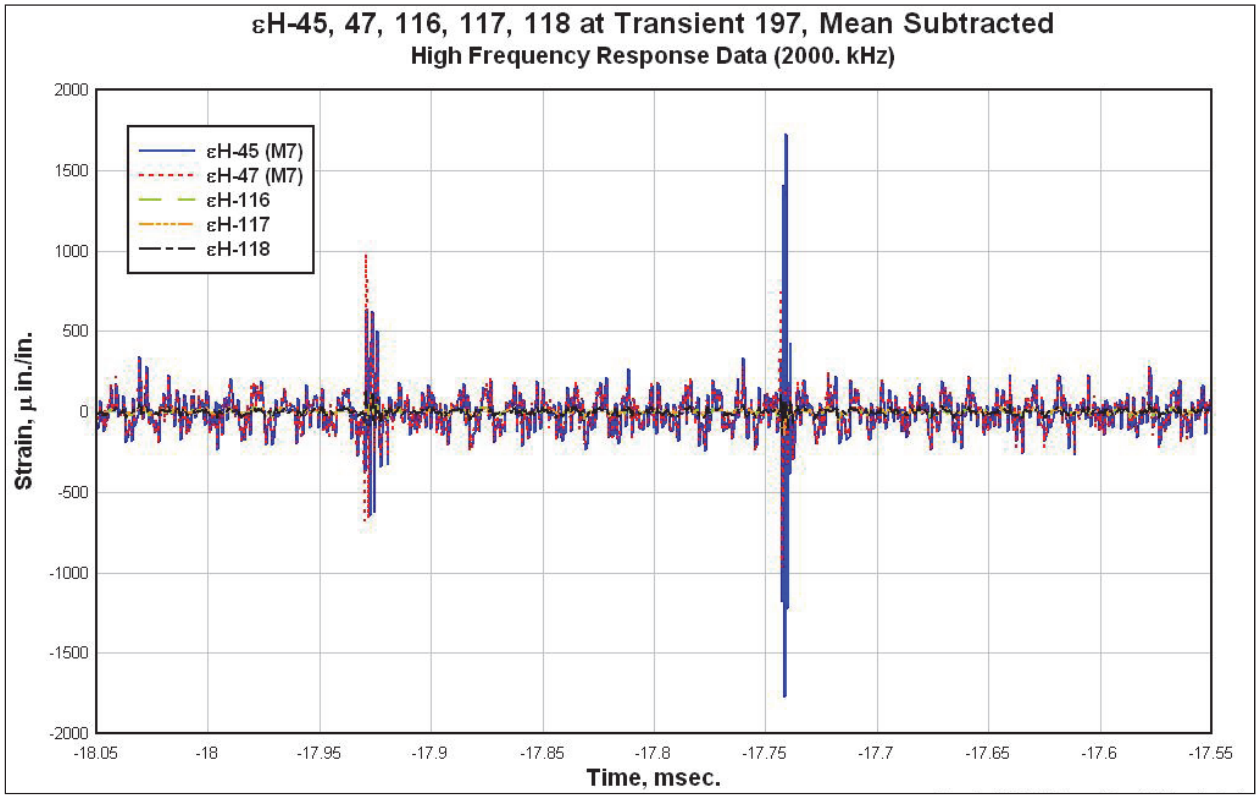

The accelerometer data recorded at 2 MHz generally complimented the recorded highest amplitude level acoustic emission signals. Figure 94 shows an example of an accelerometer peak-to-peak signal of approximately 1000 g's where an AE event was observed on transient 194 with amplitude of about 14 V.

Figure 94. Acceleration data (2MHz) at transient event 194.

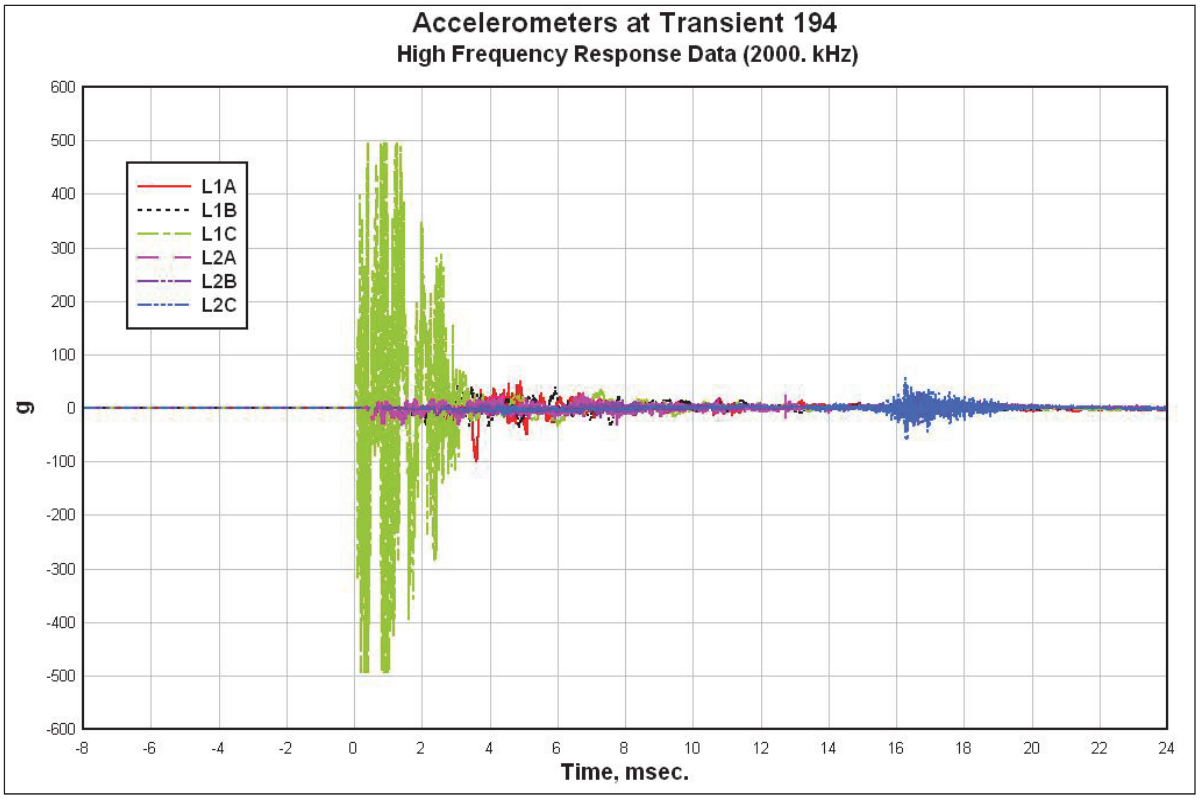

Likewise, Figures 95 and 96 show low level complementary acoustic emission and peak-to-peak accelerometer signals of 0.3 V and 2.6-g transient acceleration variations, respectively. Acoustic emission channels AE1 and AE2 produced activity on almost all of the events. Each of these events were triggered either by a manual trigger, a discriminator trigger on AE1 set at various levels, or a system restart.

For the events included in this report, Table 11 lists which high-speed sensors showed activity. In 19 of these 20 events, the following base-10 logarithmic data presentation shows that the count of peak amplitude levels in a certain amplitude range, or bin values (Figure 97), of the acoustic emission reading will trend higher for the upper-range bins as the structure approaches failure.

Figure 95. Low-level acoustic emission signals at transient event 185.

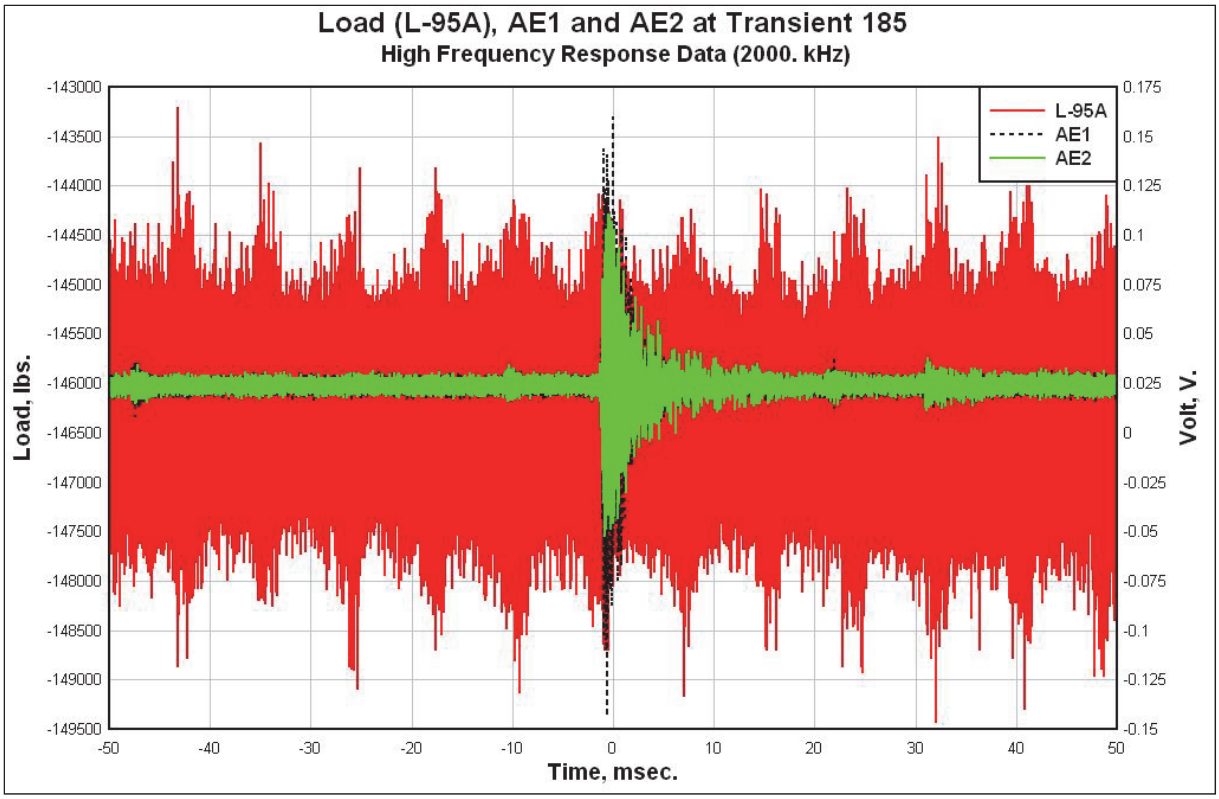

Figure 96. Low-level accelerometer signals at transient event 185.

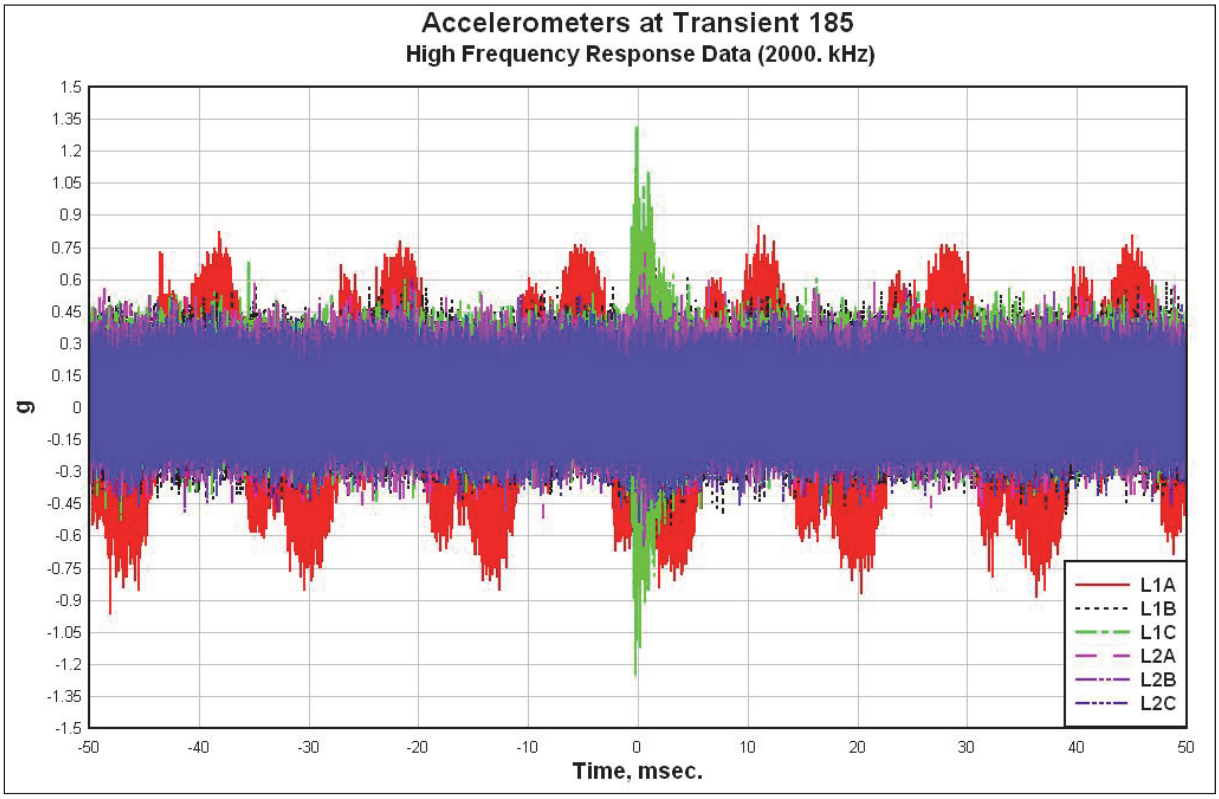

Figure 97. Acoustic bin values.

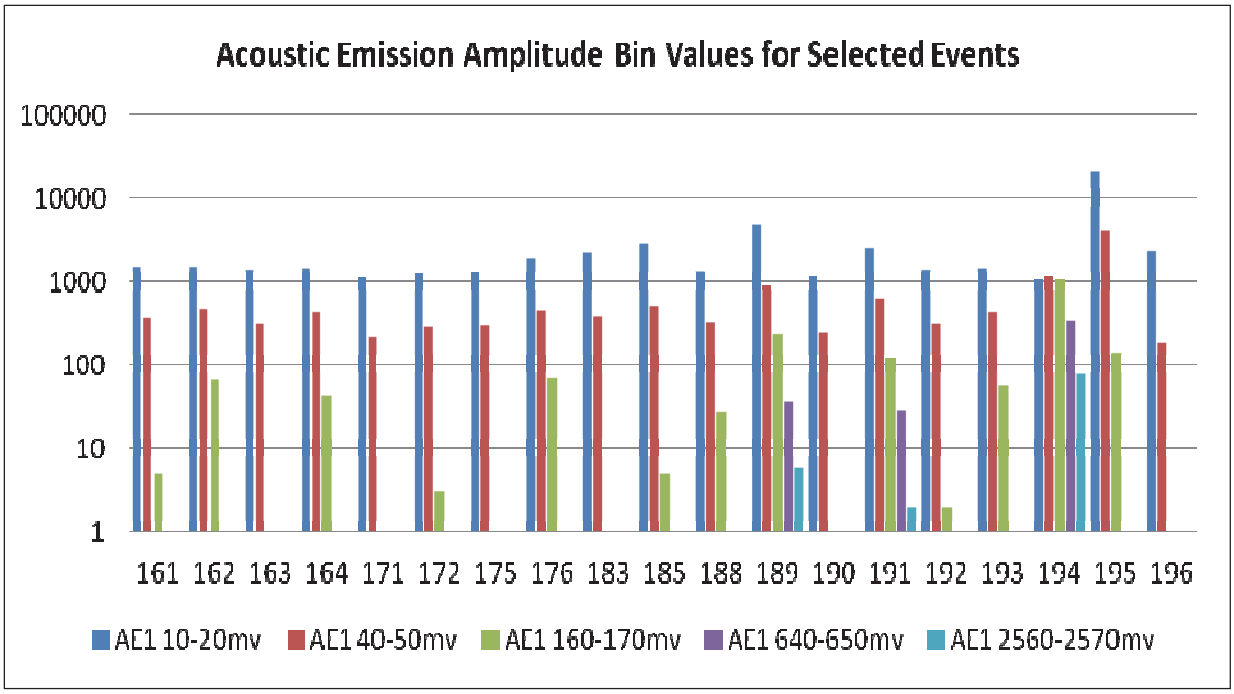

Figure 98 shows a base-10 logarithmic relationship for each of the 20 events. The maximum values for each of the acoustic emission, accelerometer, and strain sensors are compared with the load curve.

The comparison of data shown in Figure 98 could be helpful in assessing real-time structural health. Fast Fourier Transform (FFT) analysis (Appendix D: Selected Data Scans Recorded at 2 MHz, High-Sample Rate) shows variations in the frequency content of the acoustic emissions. For instance, events 183 and 185, as well as all events after and including the primary failure at 194, show lower than nominal frequency content. This frequency content on the surface does not seem to indicate predictive behavior but is noticeably different after failure. The frequency content may be of more use in separating the in-plane and out-of-plane stress wave content to eliminate external structure stimuli. Once those are eliminated, the in-plane progressive causes of the beam failure could be more readily assessed in real time. Figure 99 shows this in a bin format and is the result of differential bandpass filtering of the maximum filtered absolute values of AE2. Note here that after and including the primary failure, the amplitude of the lower-frequency bandpass events (20 KHz to 70 KHz) exceed the higher frequency bandpass events (100 KHz to 1000 KHz) at events 194, 195, and 196. Before the primary failure, the opposite is true for most events except events 164, 175, and 185. To further examine this behavior, smaller

laboratory tests could be conducted with more optimal placement of the acoustic emission sensors to detect in-plane waves and the use of test specimens designed to fail at specific points.

Figure 98. Load event marks for AE1, LC1, and εH-117

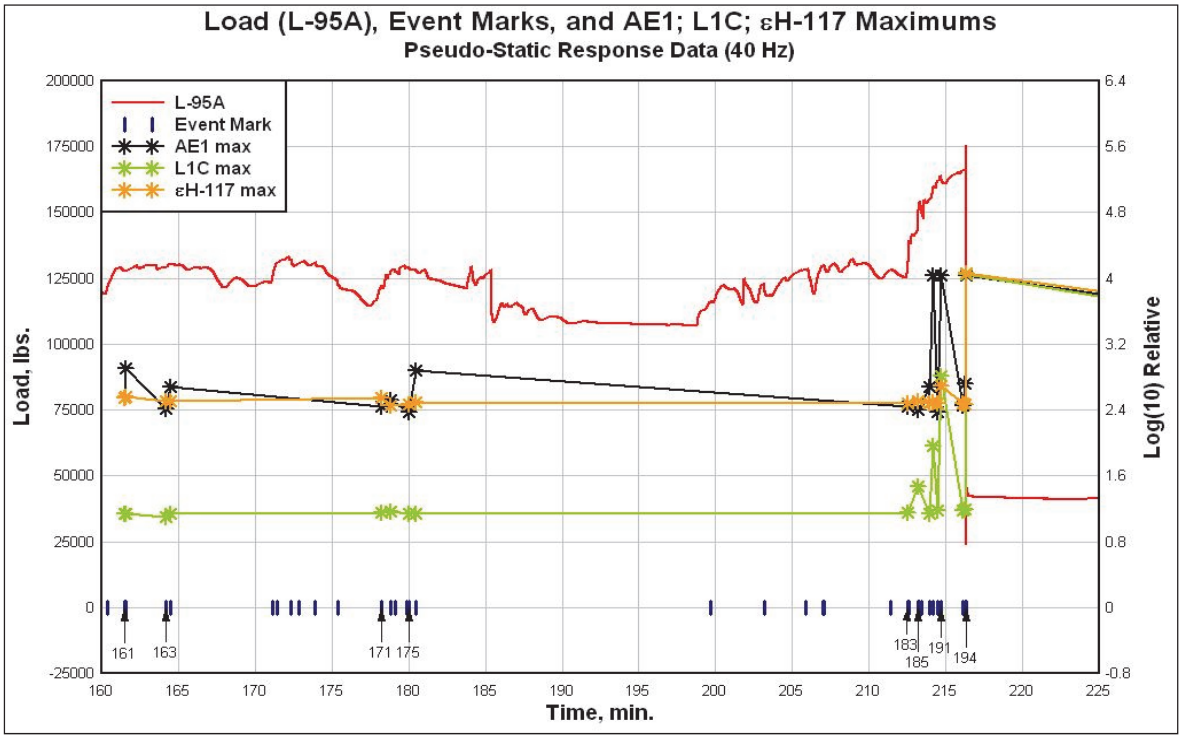

Figure 99. Filtered maximums AE2 absolute values.

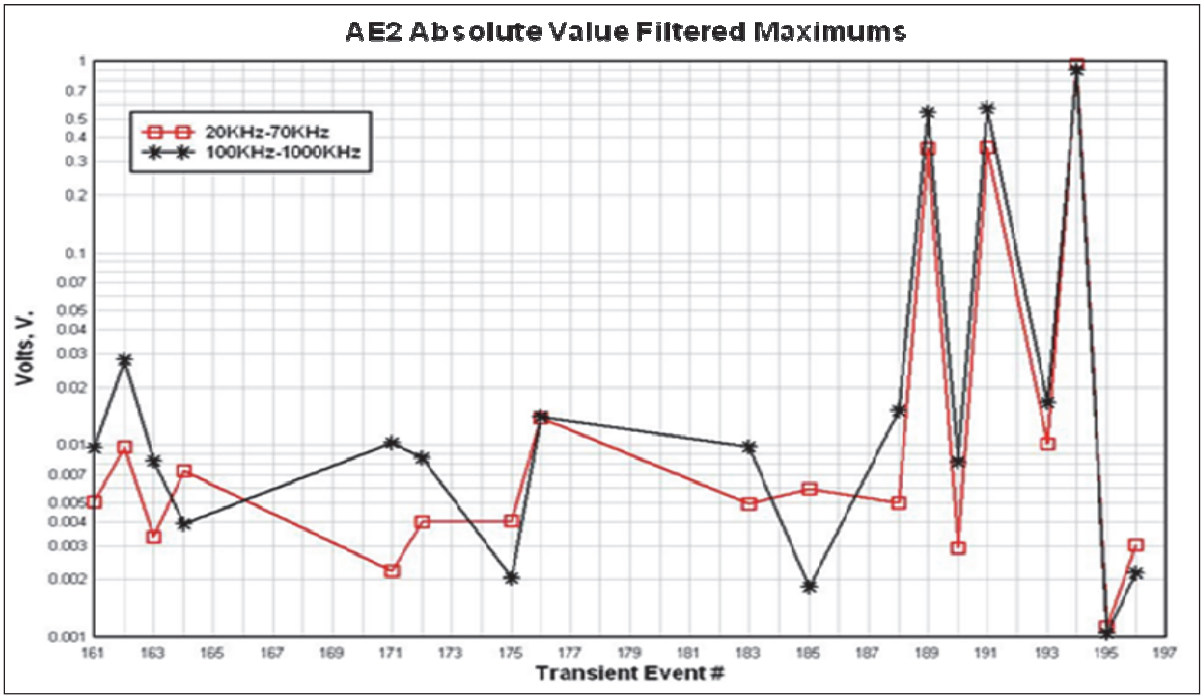

5 Conclusions and Recommendations

This report presented an experimental study of a precast concrete beam-column connection system, consisting of three columns and two deep beams. The beam-column system represents a portion of the structural components of a 10-story office building with a rectangular plan. This building was designed for Seismic Design Category B (SDC-B). The specimens were subjected to monotonically increasing vertical displacement of the unsupported center column/stub to observe their behavior under a simulated column removal scenario, including the development of catenary action in the beams. The vertical displacement of the center column/stub was increased until the vertical load-carrying capacity was considered inadequate.

The data of the overall behavior of the beam-column assembly was recorded using two different data acquisition systems, at different sampling rates, (61) channels recorded at 40 Hz and (12) channels recorded at 2 MHz. The data from the acoustic emission sensors were recorded at 2 MHz showed trends useful for developing a prediction methodology to identify imminent progressive or disproportionate collapse in precast concrete structures. In general, the first observed failure event corresponded to the brittle fracture of the main #10 steel reinforcing bars. The second observed failure event corresponded to the connection failure of the top (M8) embedded plate on the left (east) end column. These two observed events significantly reduced the capacity of the system.

Based on the study reported herein, the following actions are recommended for future testing and analytical research:

1. Re-design the (M6 and M7) connections. The weld between the anchor bars and the angles should be re-designed to a mechanical connection in order to eliminate the potential “heat affected zone” on the bars due to the welding process. Subsequently increasing the capacity of the system.
2. Record all sensors not recorded at a sampling rate of 2 MHz or faster at no less than 1 kHz.
3. There remains hypothesis testing to evaluate the statistical significance of the correlation of the data from the selected and recorded AE events with the data from all sensors.

4. Conduct a series tests on 1/4-scale test specimens and use a statistical design of experiment approach to evaluate the significance of parameters useful for identifying imminent collapse.
5. Include more AE sensors on the end columns.
6. It's recommended to conduct further analysis of the rate of observed acoustic emission events prior to and after each the failure of the second M7 bar and the M8 embedded plate.

These test results are promising but limited. Much smaller repeatable tests could be conducted to focus on specific areas of this large test and examine this technique for monitoring structural health over time.

References

ASTM A36. 2008. Standard specification for carbon structural steel. http://www.astm.org/Standards/A36.htm.

ASTM A615. 2009. Standard specification for deformed and plain carbon-steel bars for concrete reinforcement. http://www.astm.org/Standards/A615.htm.

ASTM A706. 2009. Standard specification for deformed and plain low-alloy steel bars for concrete reinforcement. http://www.astm.org/Standards/A706.htm.

Sadek, F., J. A. Main, H. S. Lew, S. D. Robert, V.P. Chiarito, S. El-Tawil. 2010. *An experimental and computational study of steel moment connections under a column removal scenario*. Technical Note 1669. Gaithersburg, MD: National Institute of Standards and Technology.

Score Atlanta Inc. 2011. Score dunegan SE 900-MWB datasheet. https://score-atlanta.com/products/pdf/SE900-MWB%20Datasheet.pdf>.

Shankar Nair, R. 2004. Progressive collapse basics. *North American Steel Construction Conference*. Long Beach, CA: Modern Steel Construction.

UFC 4-023-03. 2005. Unified Facilities Criteria (UFC): Design of building to resist progressive collapse. NFEC/USACE/AFCESA.

Appendix A: SDC-B Instrumentation Drawings

Figure A1. Overview of instrumentation layout of SDC-B.

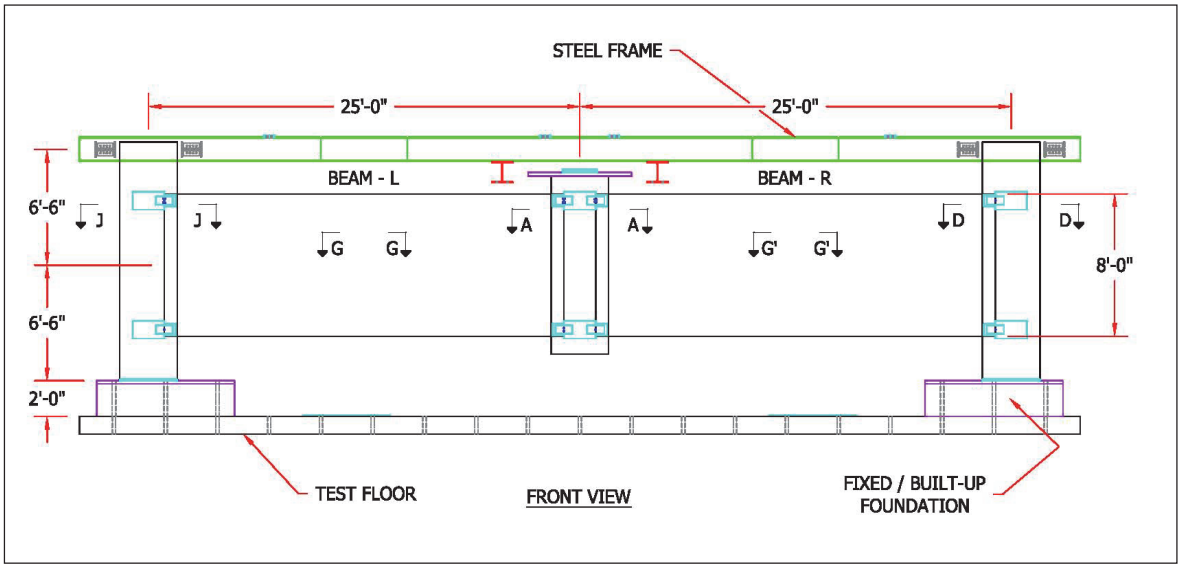

Figure A2. Section A-A of SDC-B overview layout.

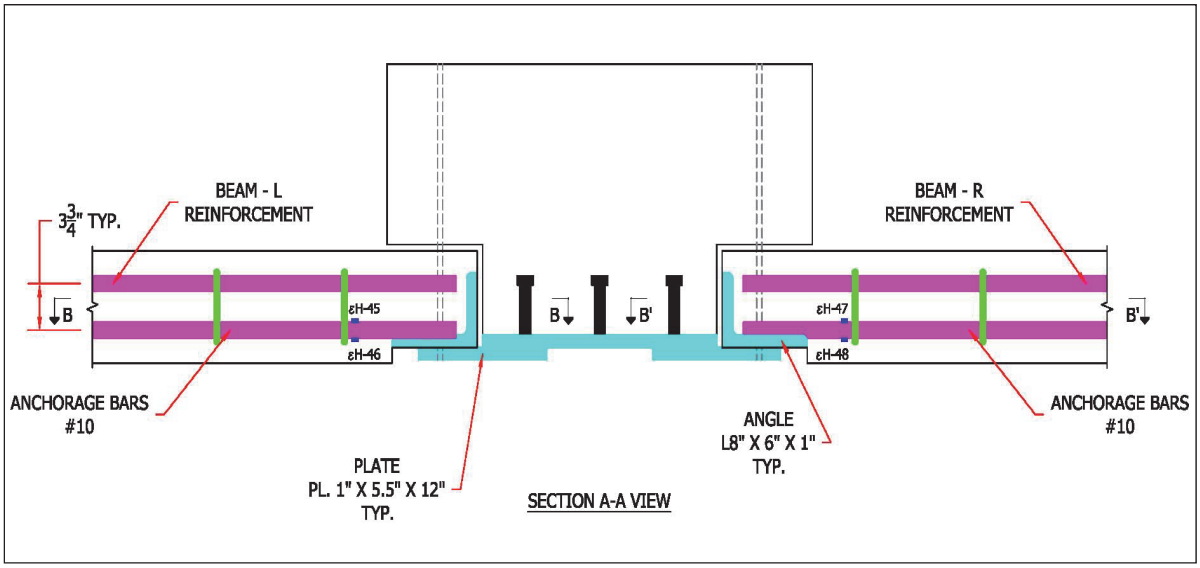

Figure A3. Section B-B of SDC-B overview layout.

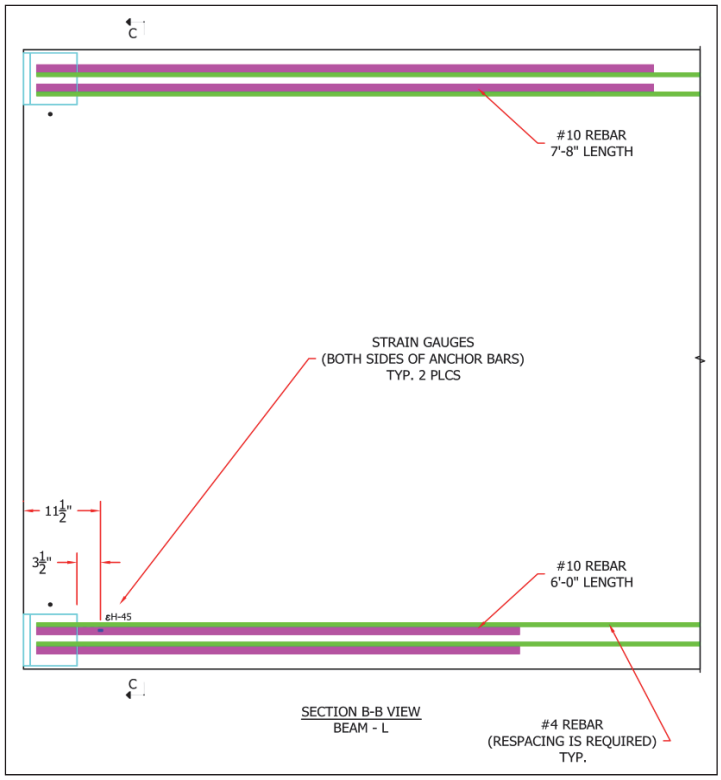

Figure A4. Section B'-B' of SDC-B overview layout.

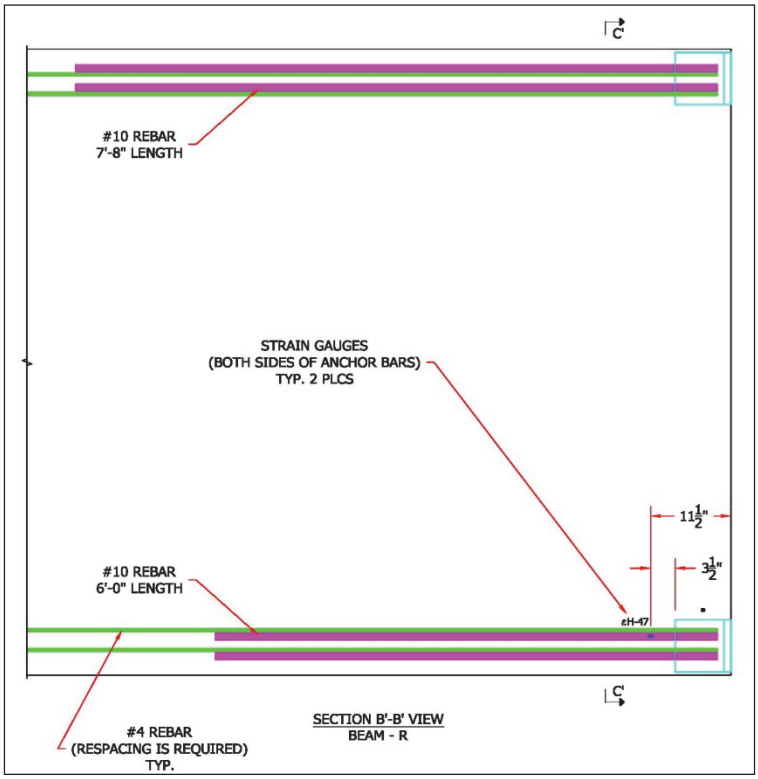

Figure A5. Sections C-C and C'-C' of SDC-B overview layout.

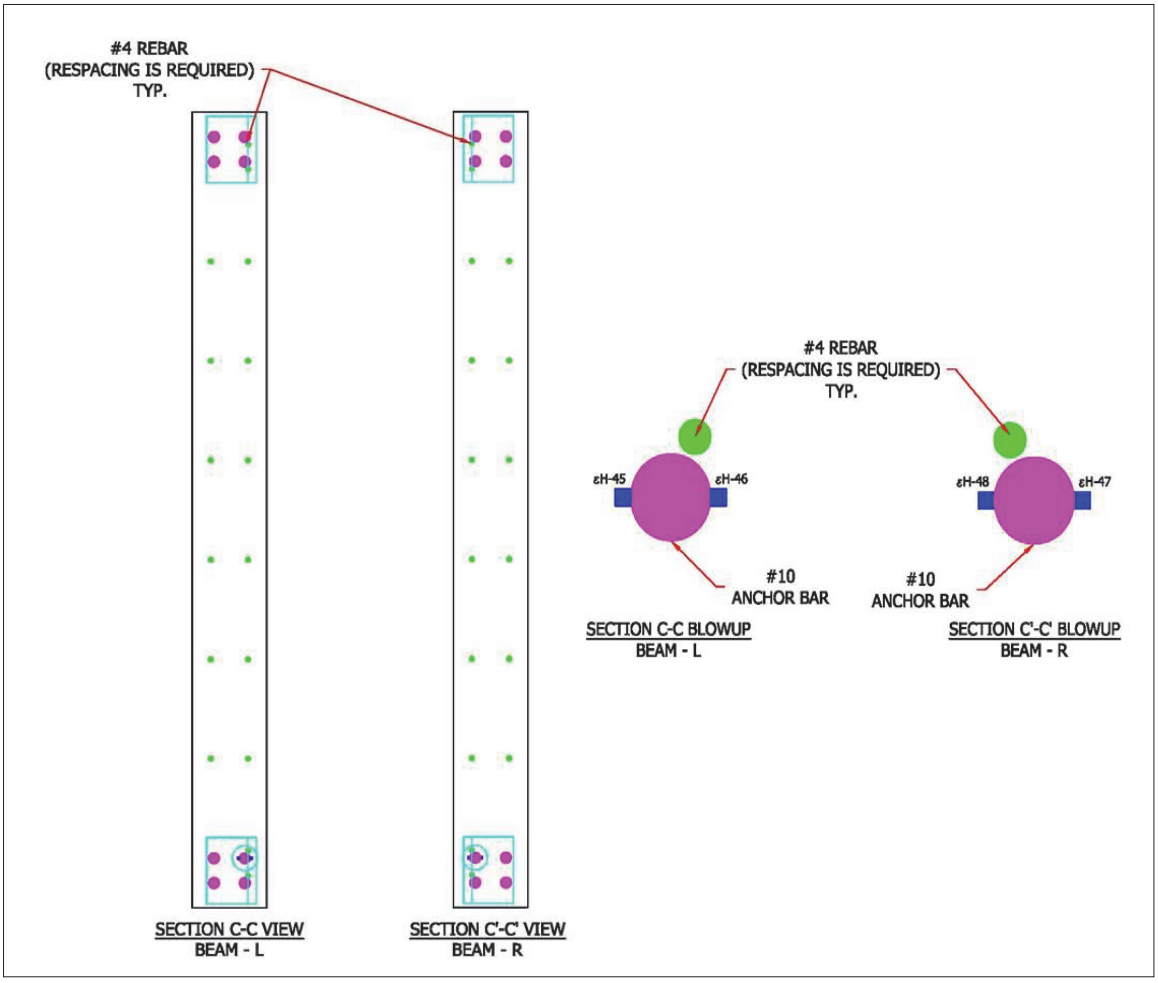

Figure A6. Section D-D of SCD-B overview layout.

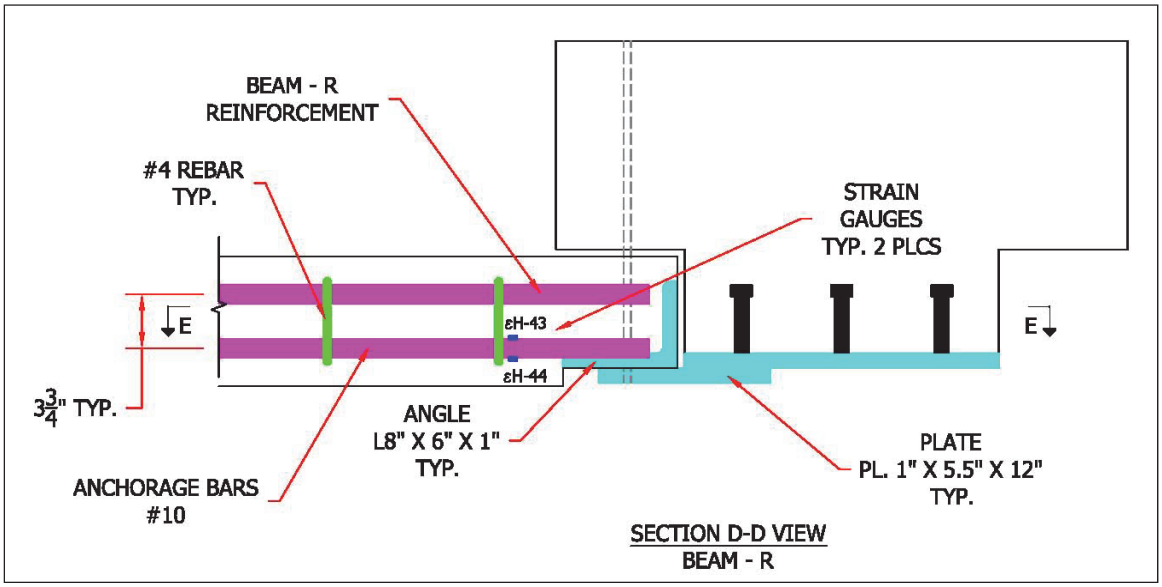

Figure A7. Section E-E of SDC-B overview layout.

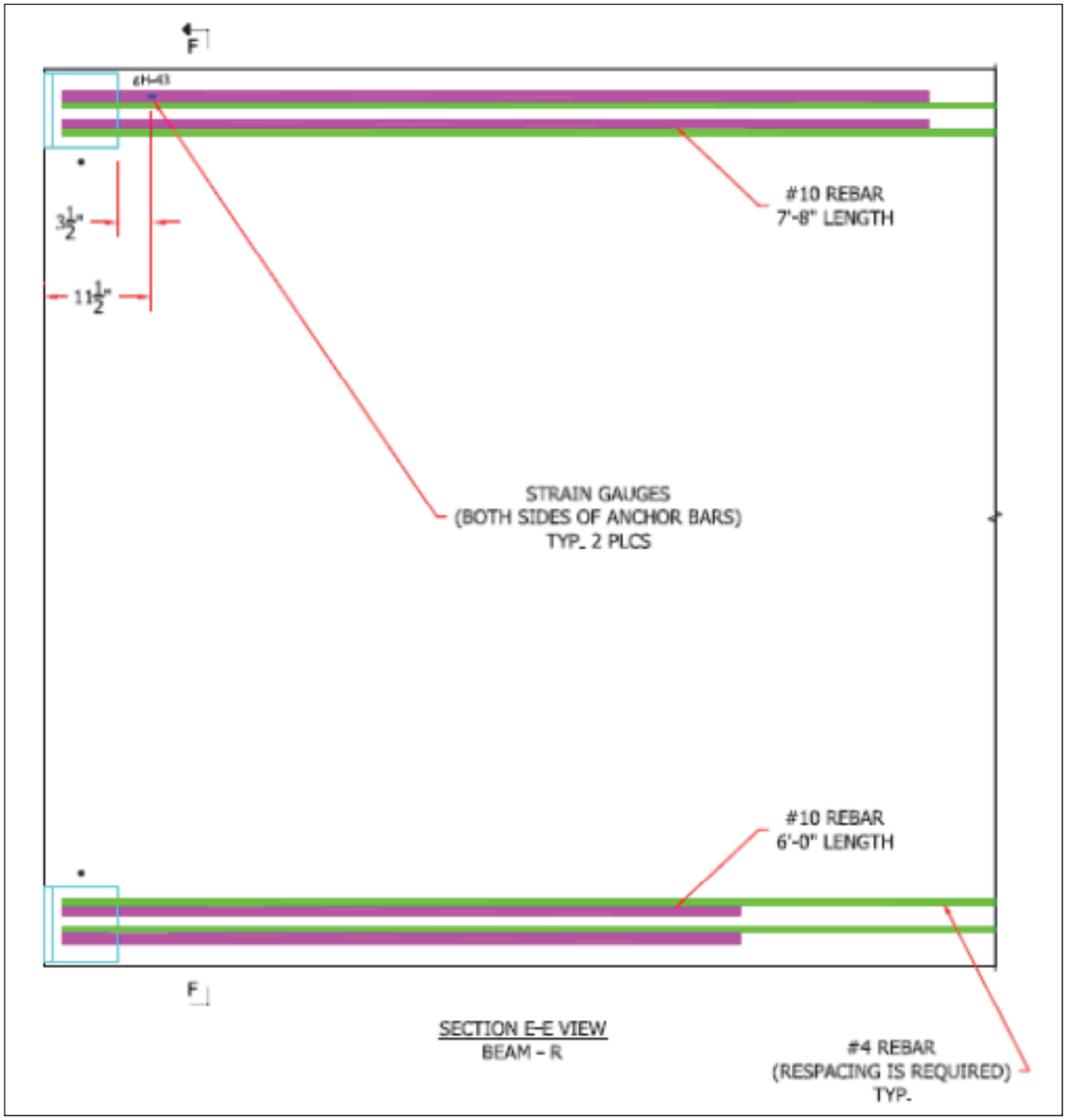

Figure A8. Section F-F of SDC-B overview layout.

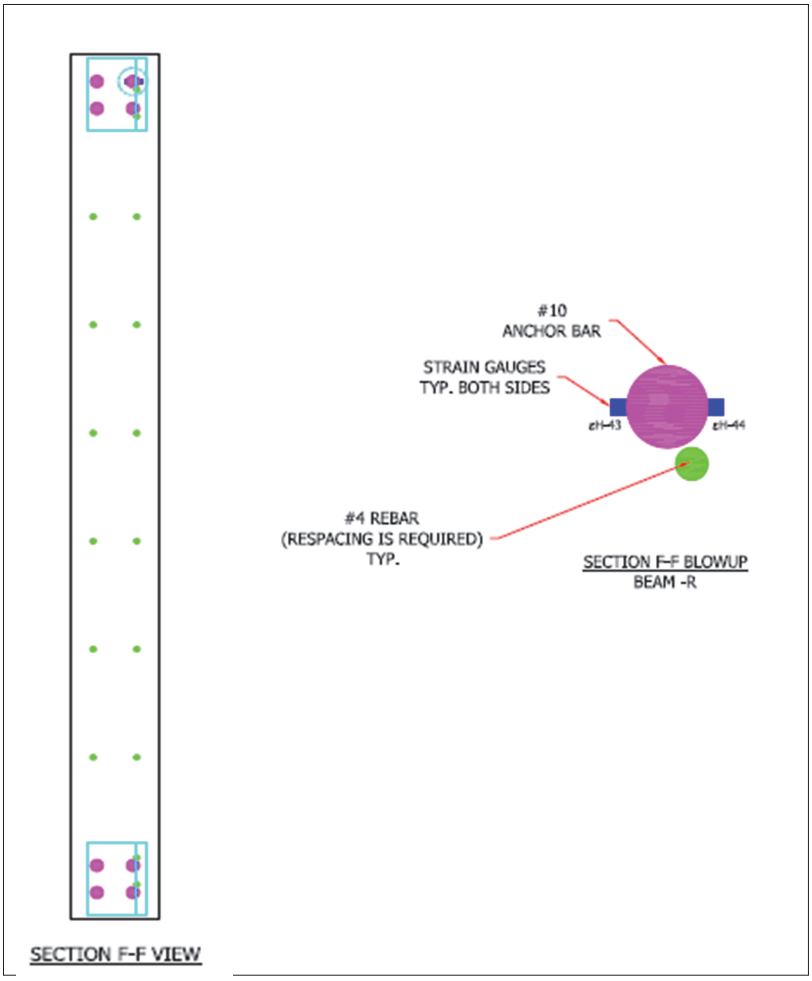

Figure A9. Section G-G of SDC-B overview layout.

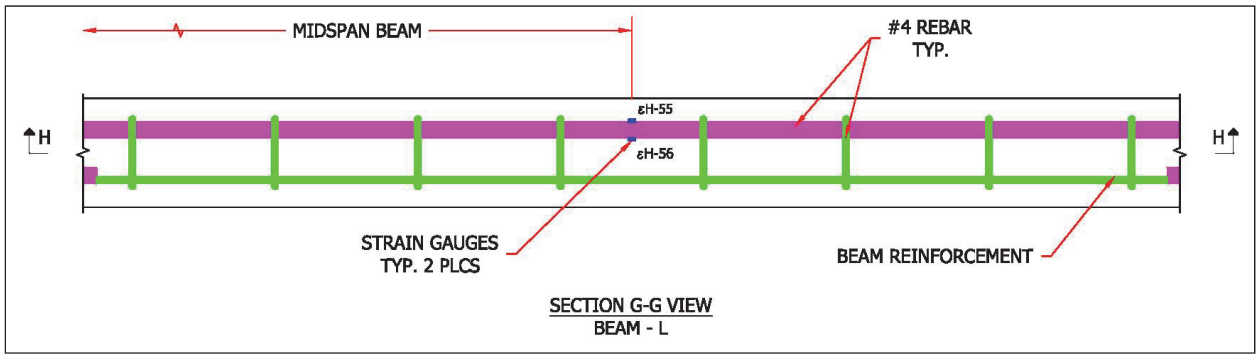

Figure A10. Section H-H of SDC-B overview layout.

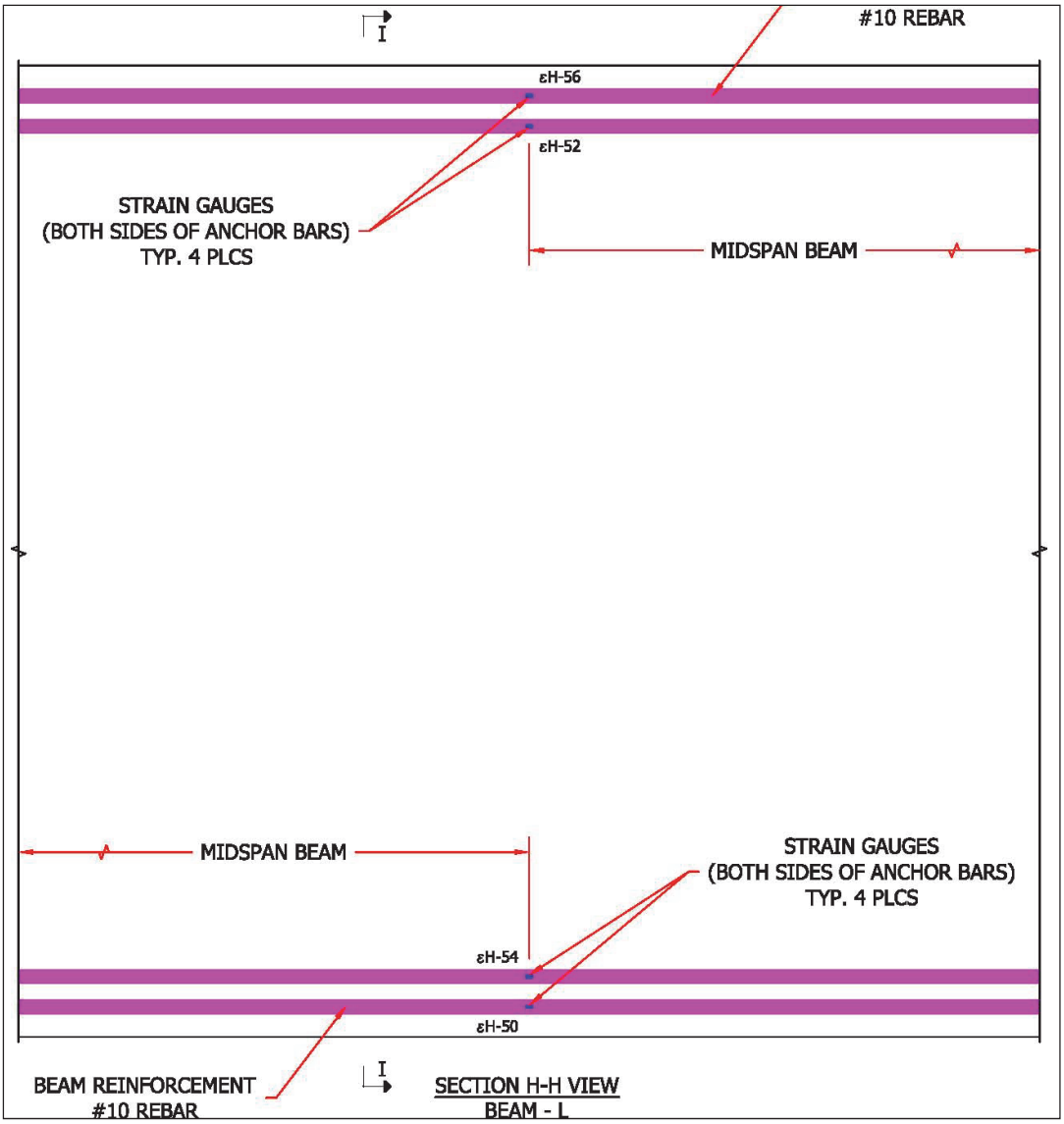

Figure A11. Section G'-G' of SDC-B overview layout.

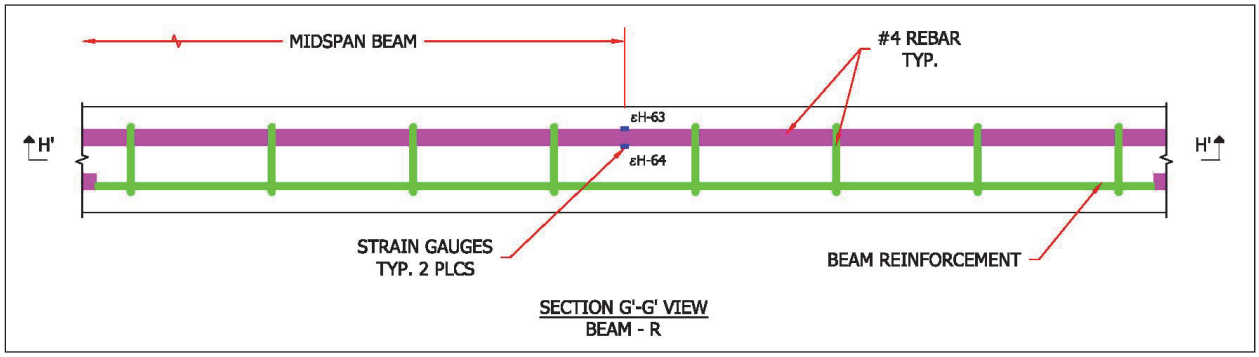

Figure A12. Section H'-H' of SDC-B overview layout.

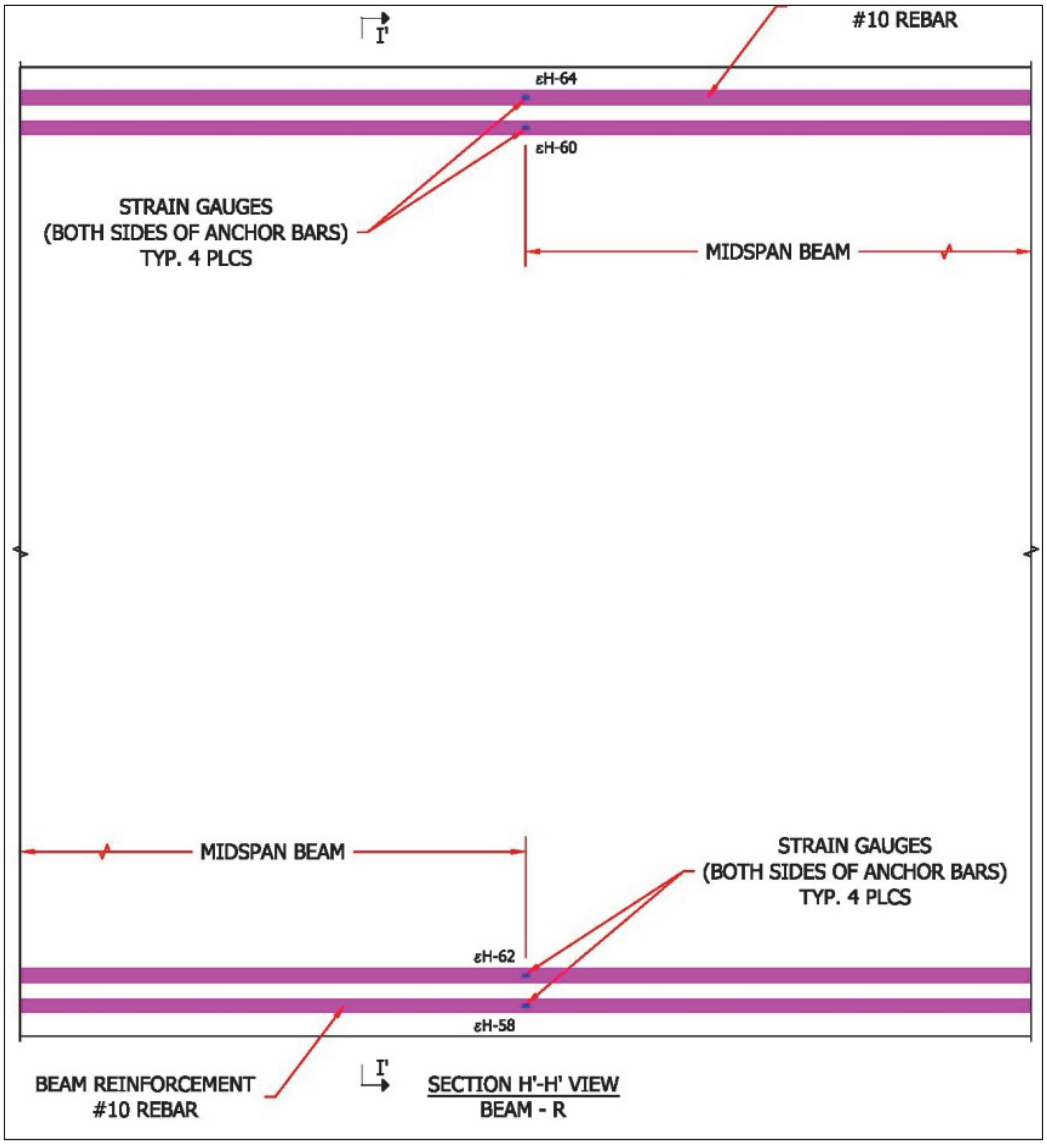

Figure A13. Section I-I of SDC-B overview layout.

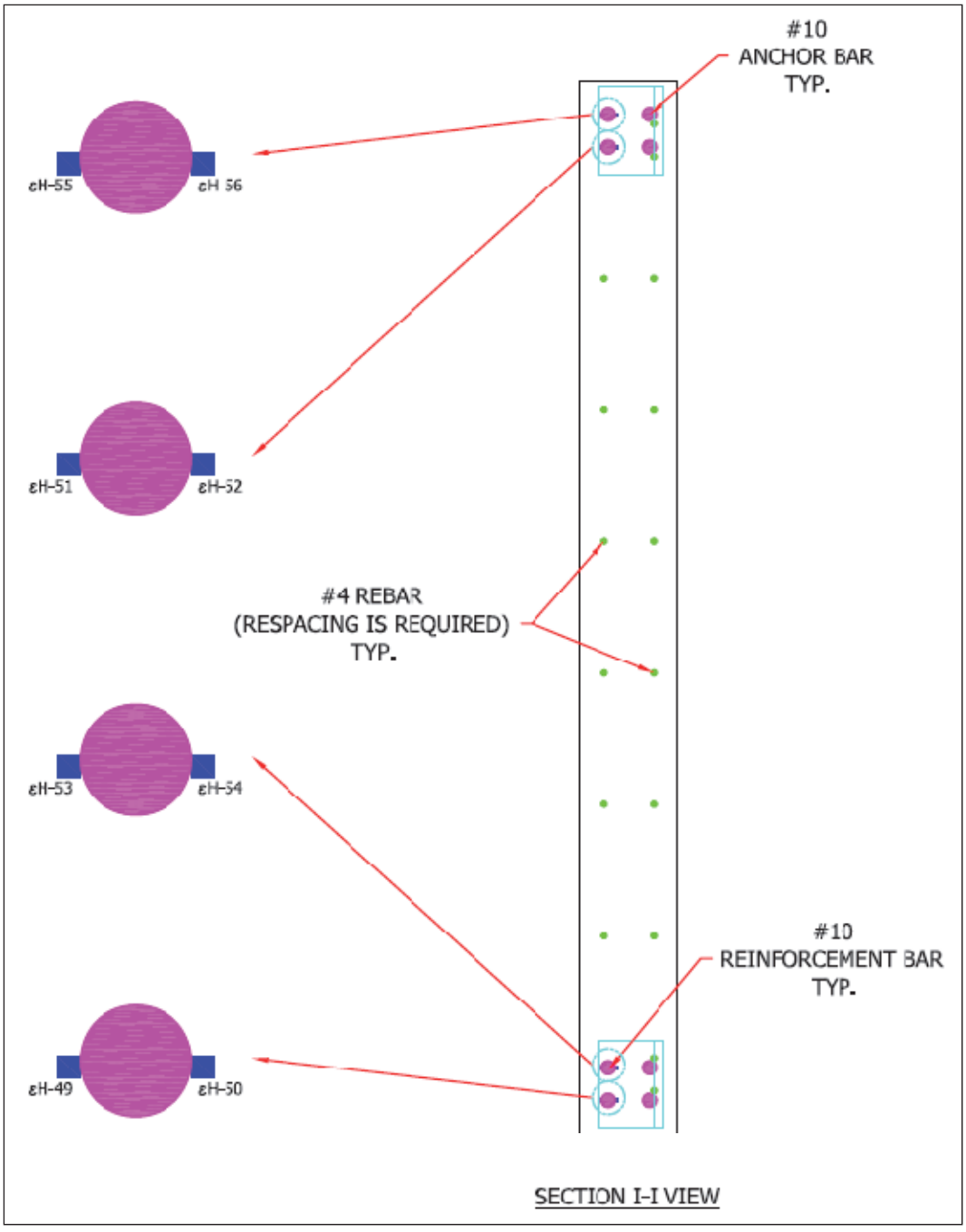

Figure A14. Section I-I' of SDC-B overview layout.

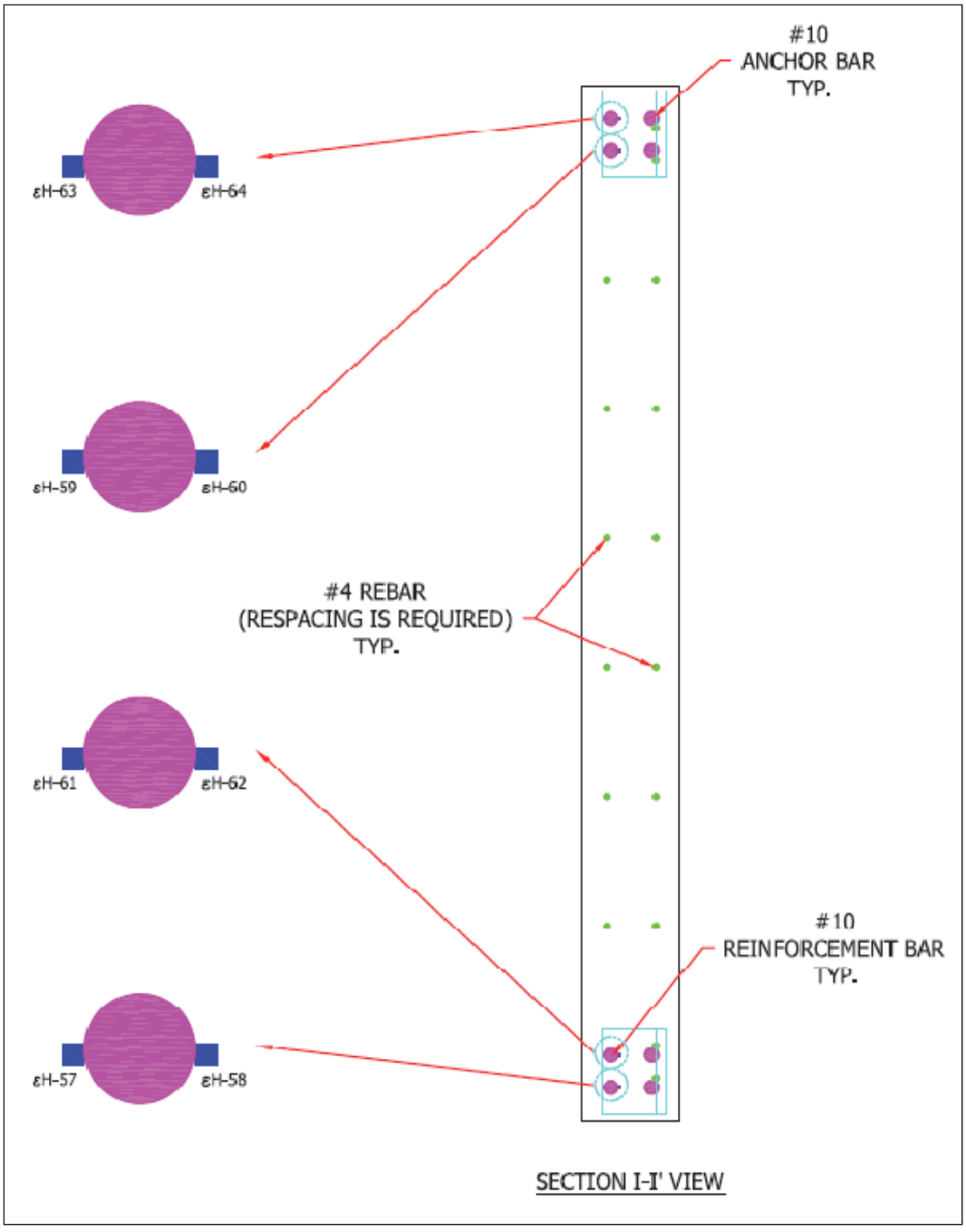

Figure A15. Section J-J of SDC-B overview layout.

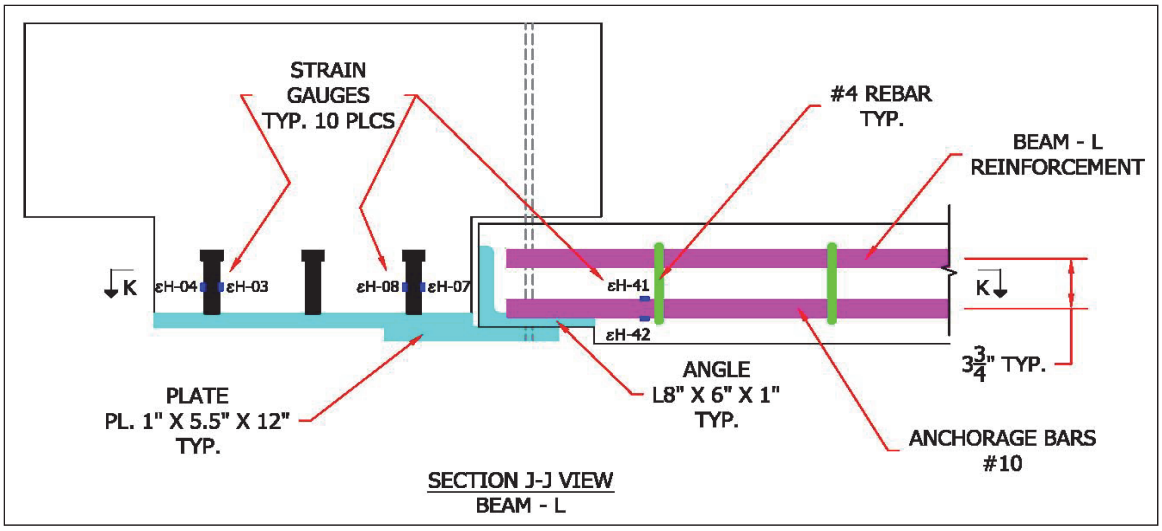

Figure A16. Section K-K of SDC-B overview layout.

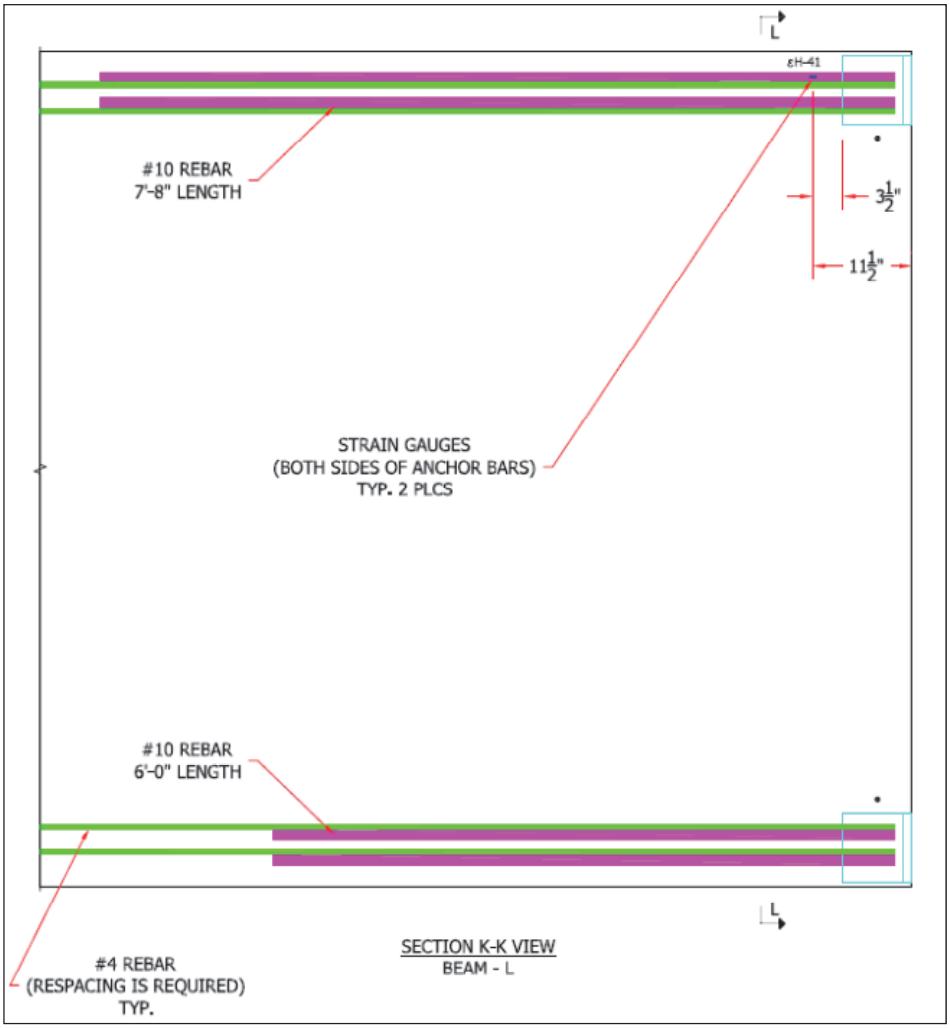

Appendix B: Experiment Procedure

Brittle Failure
Precast Concrete Beam-Column Connection
Seismic Design Category-B

Experimental Testing Procedure

1. Place spacers between top loading plate and ram.
2. Place plywood over the windows of the instrumentation building that is located in front of the reaction frame.
3. Move all nonessential personnel from the testing floor before starting the test.
4. Begin recording of instrumentation data and digital video.
5. Remove angle supports from bottom of stub column.
6. Remove all essential personnel from test floor.
7. Place people at each entrance to the test floor to prevent people from walking on test floor during the experiment. The people watching the doors will be out of the line of sight of the reaction frame and specimen.
8. Initiate hydraulic ram and load in displacement control mode at 0.5 in./min using displacement increments as described in the next page; *make pauses of 10 min between some increments until failure or the hydraulic ram runs out of stroke.
9. Unload the hydraulic ram.
10. Allow all nonessential personnel on test floor.
11. Obtain posttest measurements and photographs.
12. Secure test specimen and rope off area around reaction frame.

* During each pause, only authorized personnel will be obtaining data from the cracking patterns on the specimen. Once all the data are obtained, the Project Engineer will give the call to proceed loading.

SDC-B Increment Displacement Test Execution

Test Day: October 5, 2012
Test Time: 10:53 to 15:09
Displacement and Loading Increments:

Table B1. SDC-B Experiment Procedure.

Start Time (hr)	Center Ram Displacement (in.)	Load (kips)	Time Finished (hr)	Pause (min)
10:53	0.10	8	10:55	
10:57	0.20	25	10:59	02:00
11:02	0.30	43	11:05	03:00
11:08	0.40	61	11:12	03:00
11:15	0.50	60	11:18	03:00
11:19	0.70	76	11:21	01:00
11:31	0.80	86	11:37	10:00
11:40	0.90	96	11:42	03:00
11:46	1.00	106	11:50	04:00
11:52	1.20	101	11:56	02:00
11:58	1.40	124	12:03	02:00
12:13	1.60	127	12:21	10:00
12:22	1.80	131	12:31	01:00
12:33	2.00	121	12:39	02:00
12:49	2.40	128	13:00	10:00
13:02	2.80	123	13:09	02:00
13:12	3.20	127	13:18	03:00
13:20	3.60	129	13:23	02:00
13:25	4.00	117	13:30	02:00
13:40	5.00	127	13:52	10:00
13:54	5.84	47	13:59	02:00
14:07	7.00	100	14:15	08:00
14:22	8.00	100	14:31	07:00
14:32	9.00	105	14:46	01:00
14:48	10.00	112	14:54	02:00
14:56	12.00	106	15:03	02:00
15:04	15.00	71	15:08	01:00
15:09	18.25	53	15:13	01:00

Appendix C: Data Acquisition System

The transient data on this test were recorded at a sample rate of two million samples per second (2 MHz) on a Hi-Techniques Synergy8 Data Acquisition System, S/N SYG-0611-8503, at 2 ms/s with no filtering using four 2 MHz, 16-bit four channel ADC Modules with Universal Inputs. This system is shown in Figure C1.

Figure C1. Hi-Techniques Synergy8 data acquisition system.

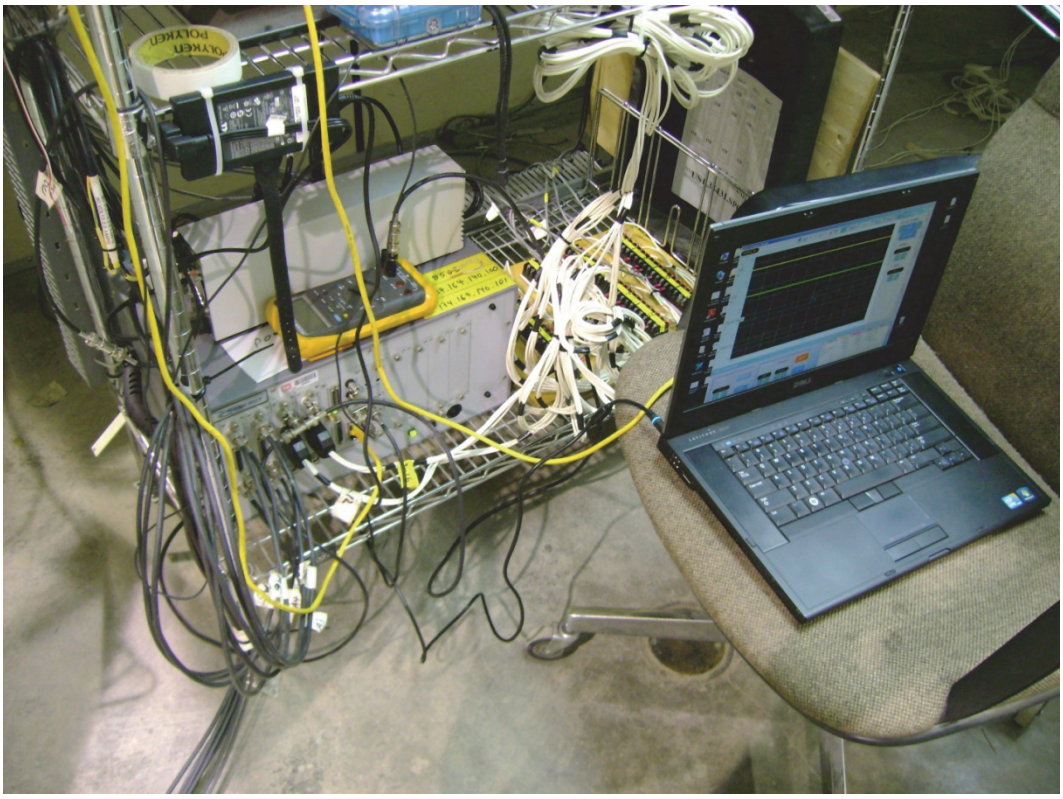

Each event was triggered either by a manual trigger, a discriminator trigger sourced from channel AE1 set at various levels duly noted, or a system restart. High-speed instrumentation specifications are in Table C1.

On the underside of the left and right beams were six accelerometers. Their locations with the Center Pillar center line reference (CL) were the following.

- L1A = CL - 23’ 4”
- L1B = CL - 12’ 6”

- L1C = CL - 6’ 8”
- L2A = CL + 23’ 4”
- L2B = CL + 12’ 6”
- L2C = CL + 6’ 8”

Table C1. High-speed instrumentation specifications.

Ch. No.	Channel Name	Sensor Type	Sensor Make	Sensor Model	Sensor Serial No.
1	L1A	Accelerometer	PCB	352B10	38494
2	L1B	Accelerometer	PCB	A353B17	9214
3	L1C	Accelerometer	PCB	A353B17	9212
4	L2A	Accelerometer	PCB	A353B17	9211
5	L2B	Accelerometer	PCB	A353B17	9210
6	L2C	Accelerometer	PCB	A353B17	9209
7	AE1	Acoustic Emission	Score-Dunegan	SE900-MWB	10/000001?
8	AE2	Acoustic Emission	Score-Dunegan	SE900-MWB	10/0000010
9	Load	Load Cell	Sensotec	41	172285
10	Trigger Out	System Output	Cable	N/A	N/A
11	M7-45(eh45)	Strain	Vishay/Micro-Measurements		N/A
12	M7-47(eh47)	Strain	Vishay/Micro-Measurements		N/A
13	T3-S1(eh116)	Strain	Vishay/Micro-Measurements		N/A
14	T3-S2(eh117)	Strain	Vishay/Micro-Measurements		N/A
15	T3-S3(eh118)	Strain	Vishay/Micro-Measurements		N/A
16	Manual Trigger	Wire	N/A	N/A	N/A

The location of:
Acoustic Emission:

- AE1 CL – 2 in. adjacent to tab 3.
- AE2 CL – 2 in. and 3 in. below AE1.

- M7-45(eh45) strain gauge on internal rebar left of tab 3.
- T3-S1, T3-S2, and T3-S3 strain gauges on tab 3.

The trigger-out channel is a BnC to co-axial cable output of the Synergy8 Timebase Module and was recorded on both the high-speed and low-speed systems. This trigger-out was only partially functional due to a software anomaly of the Synergy software and the 8-slot Synergy chassis. Because

of this anomaly, the recorded signal on the high-speed system did not show the falling edge of the trigger and therefore is of no use. The low-speed record of this channel is required to synchronize the low- and high-speed systems. The system should maintain a logic low (not triggered) on the trigger line until the trigger occurs generating a logic high, and then return to a logic low after the data scan is completed. Instead, the trigger line returns to a logic high (triggered) after data are saved to memory and remains there until another data scan is completed. To find the true zero time, we must use the return from a logic high to a logic low as the mark of the end of the data acquisition span and subtract the post trigger data time from that mark.

Strains M7-45(eh45), M7-47(eh47), T3-S1, T3-S2, and T3-S3 were hard wired from the instrumentation junction box to the main patch panel.

Appendix D: Selected Data Scans Recorded at 2 MHz, High-Sample Rate

Figure D1. Transient 161 at 161.49757 min of testing time.

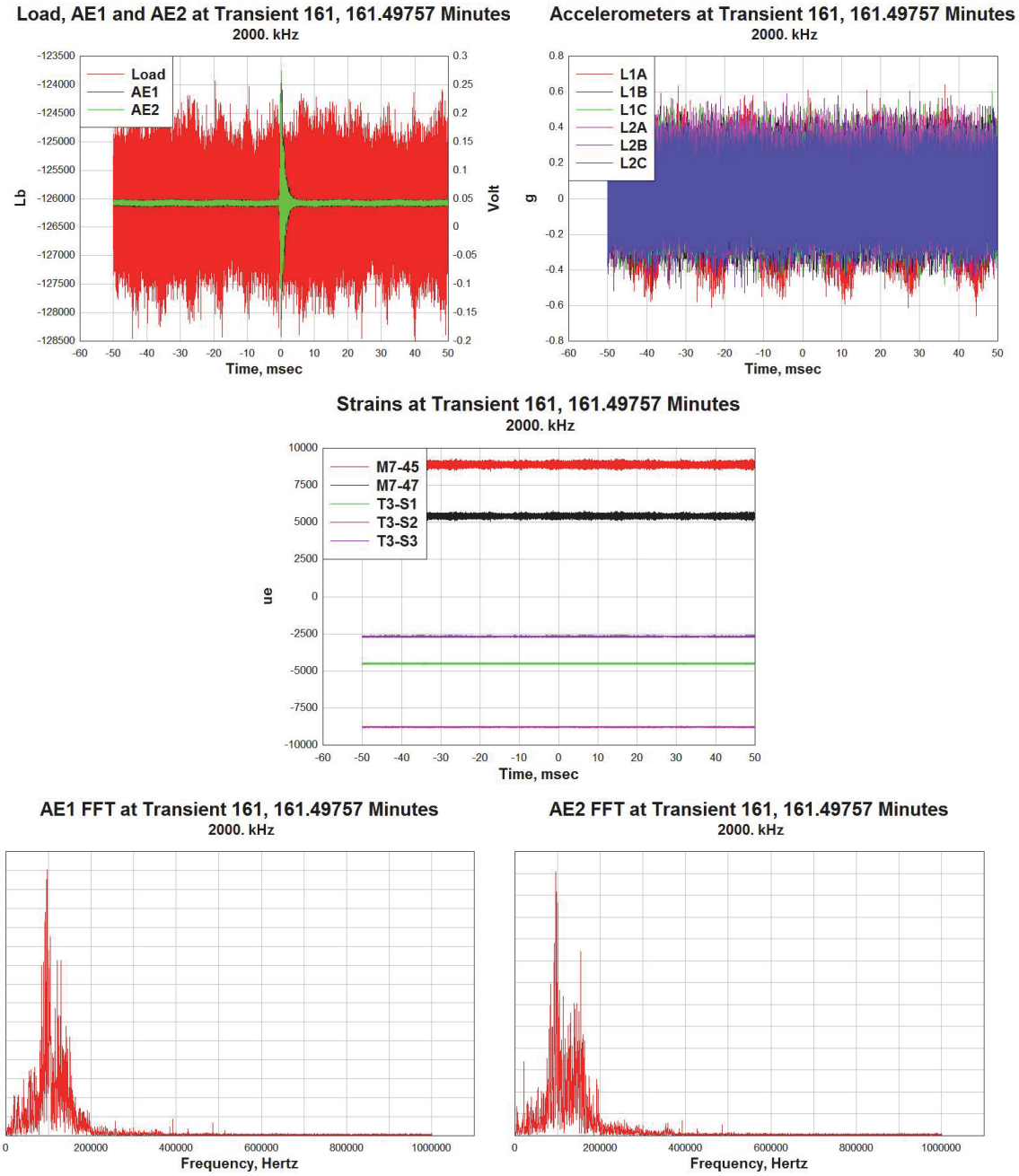

Figure D2. Transient 162 at 161.59777 min of testing time.

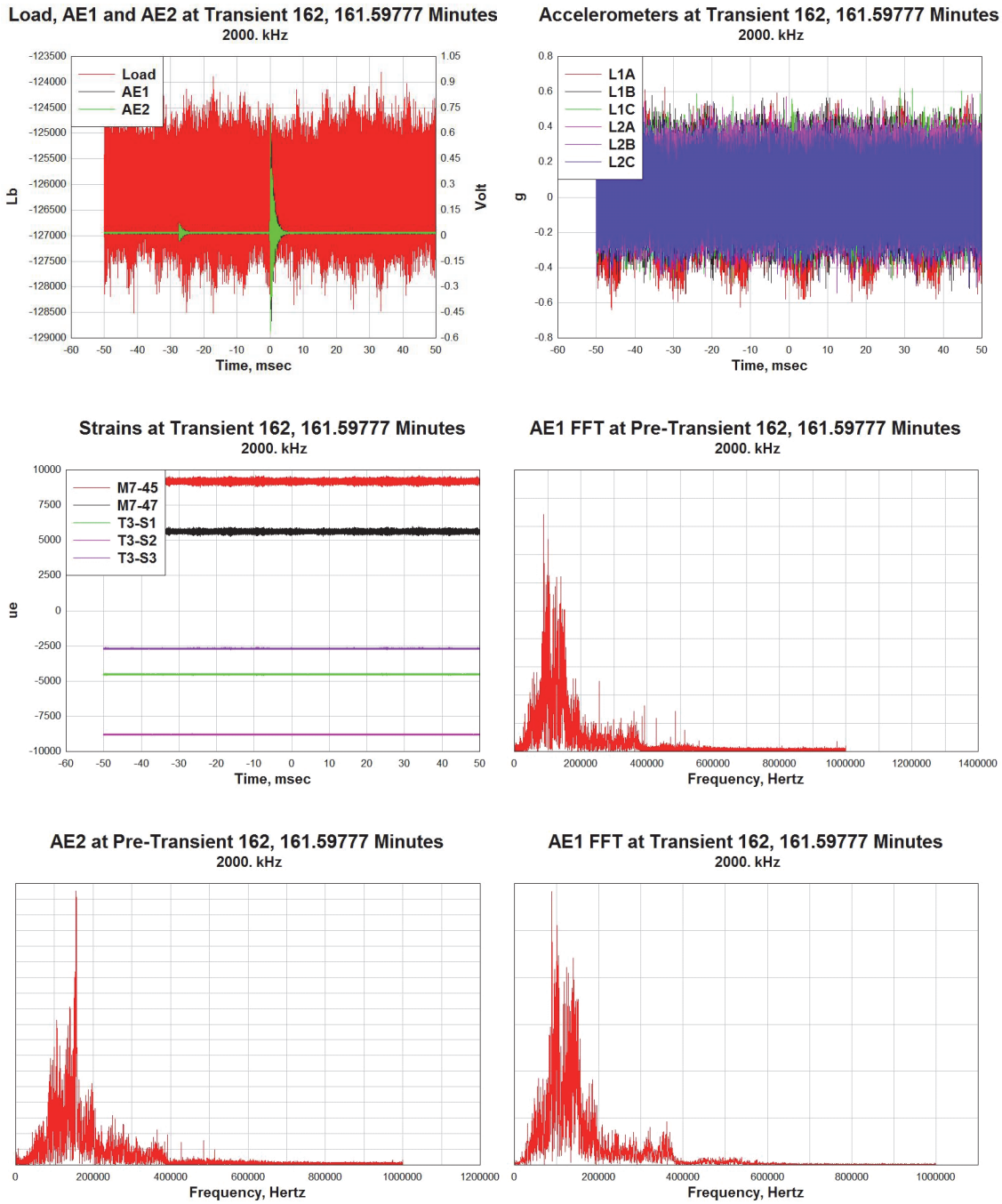

Figure D3. Transient 163 at 164.18237 min of testing time.

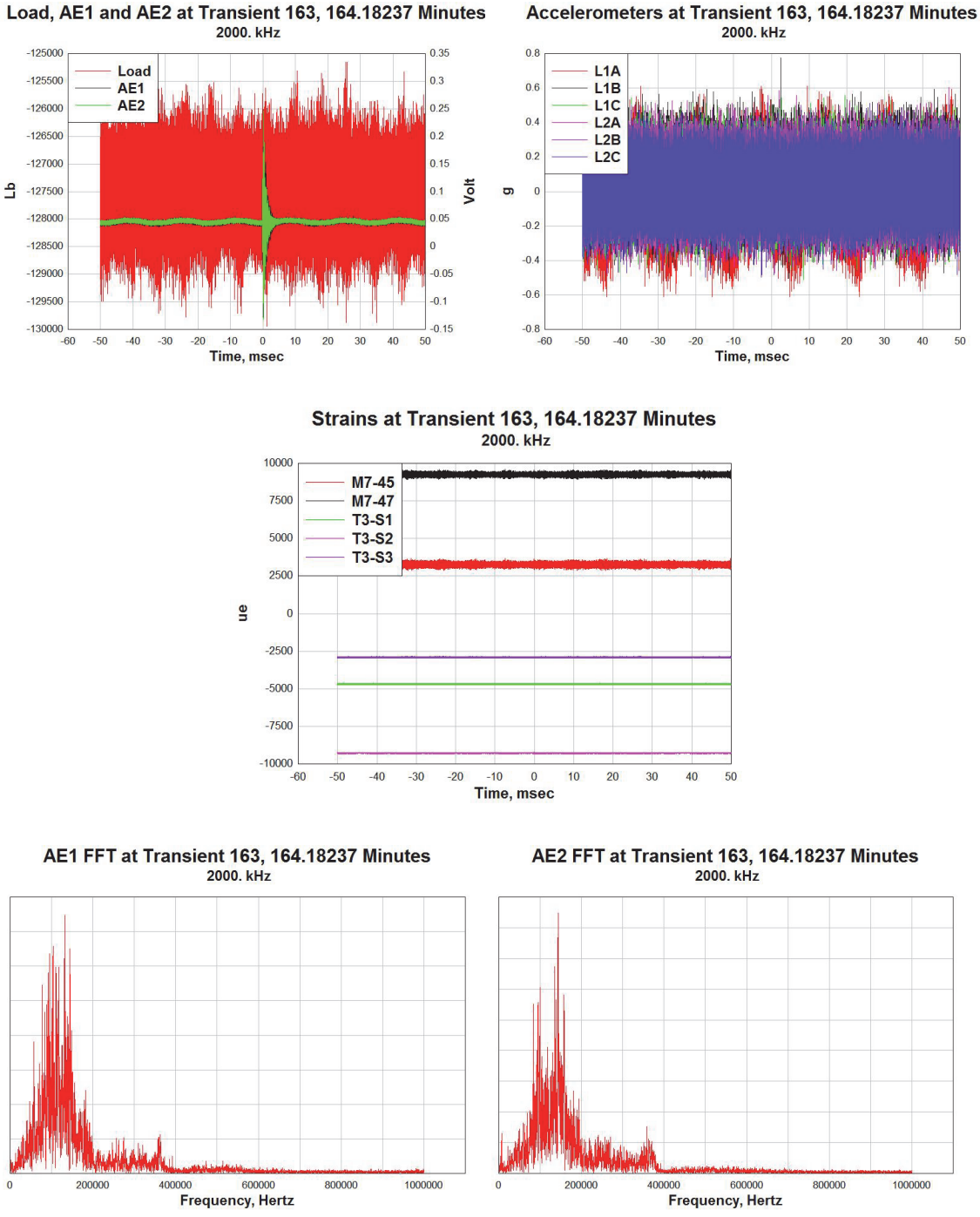

Figure D4. Transient 164 at 164.49407 min of testing time.

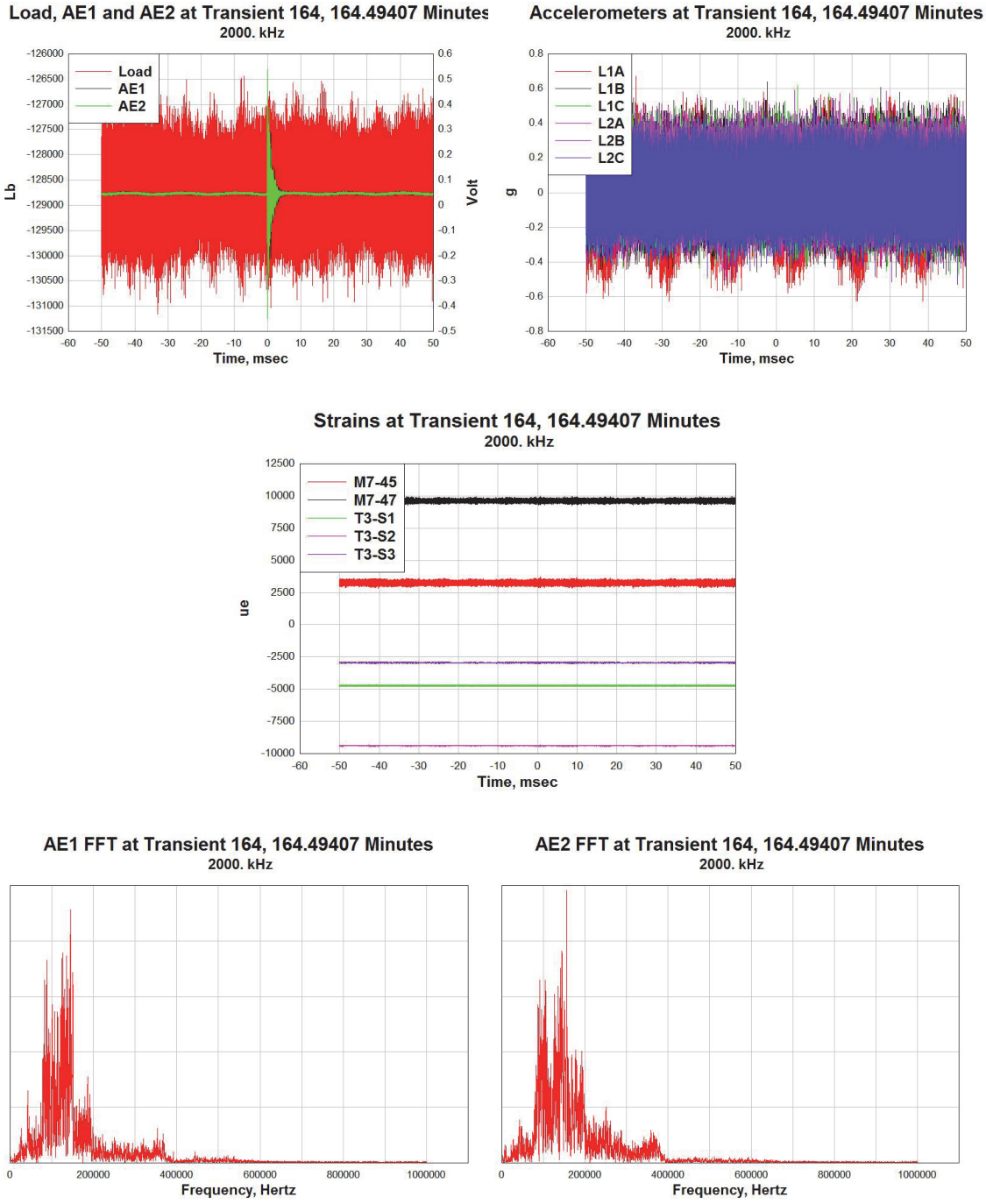

Figure D5. Transient 171 at 178.20737 min of testing time.

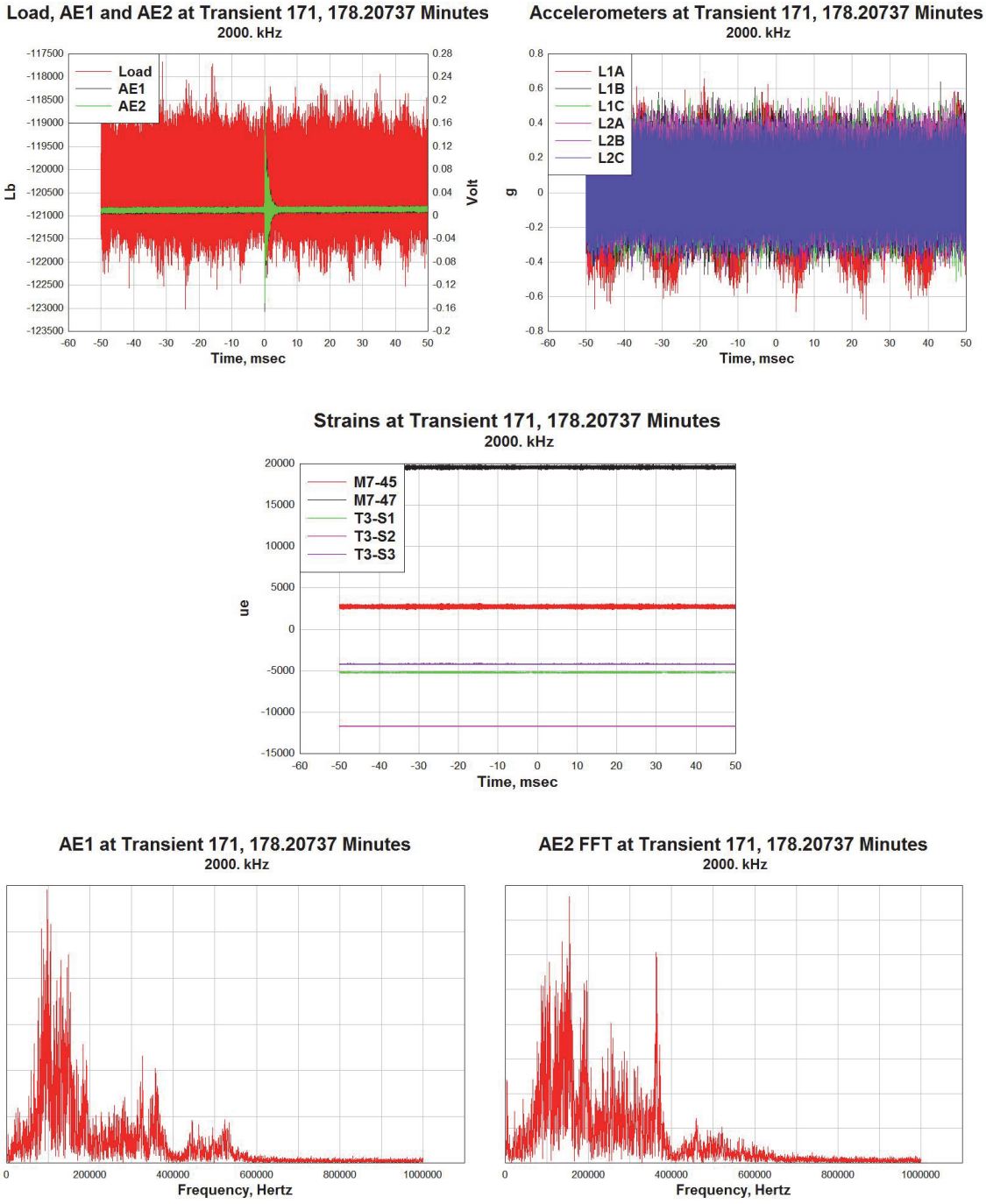

Figure D6. Transient 172 at 178.86057min of testing time.

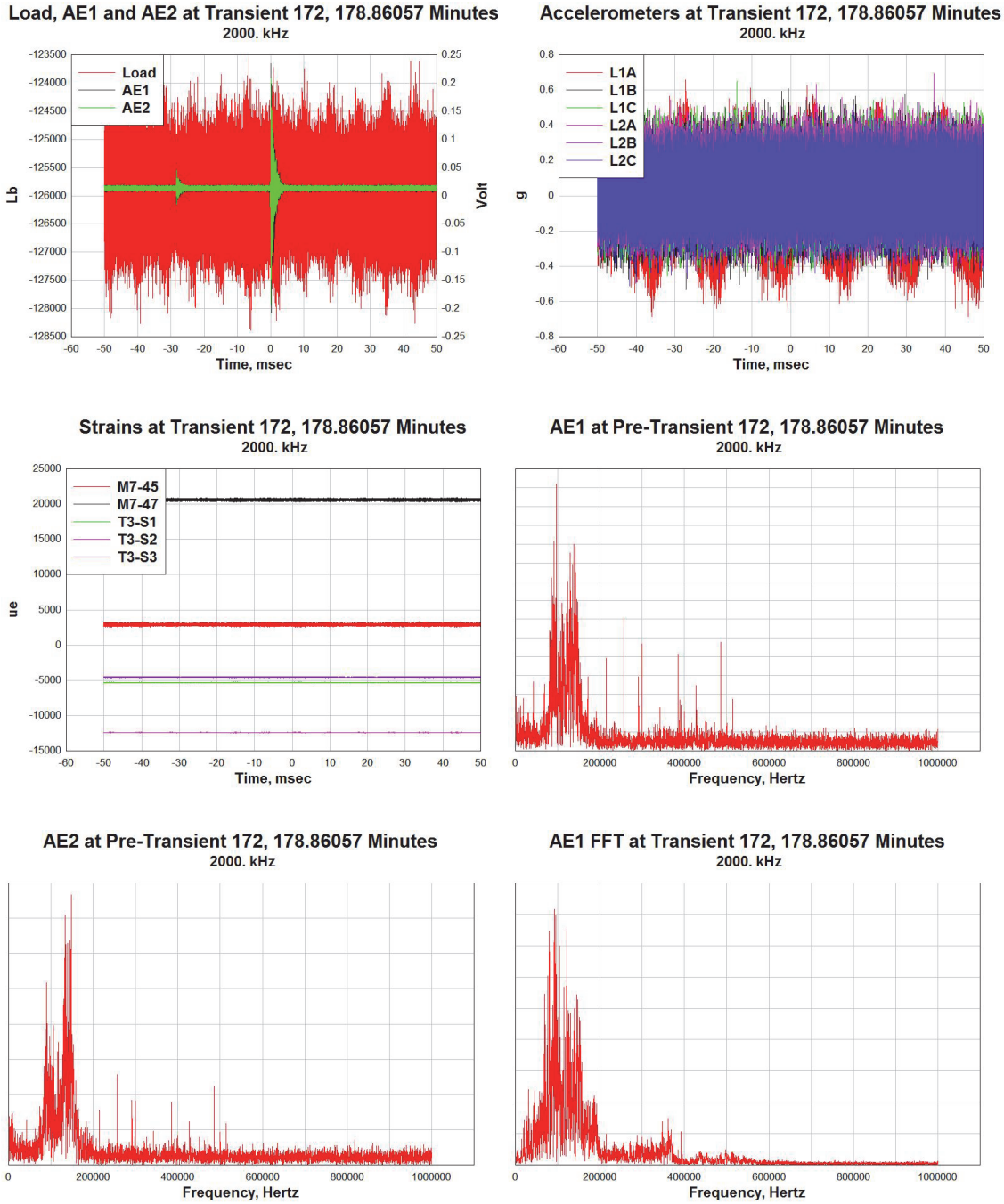

Figure D7. Transient 175 at 180.00937 min of testing time.

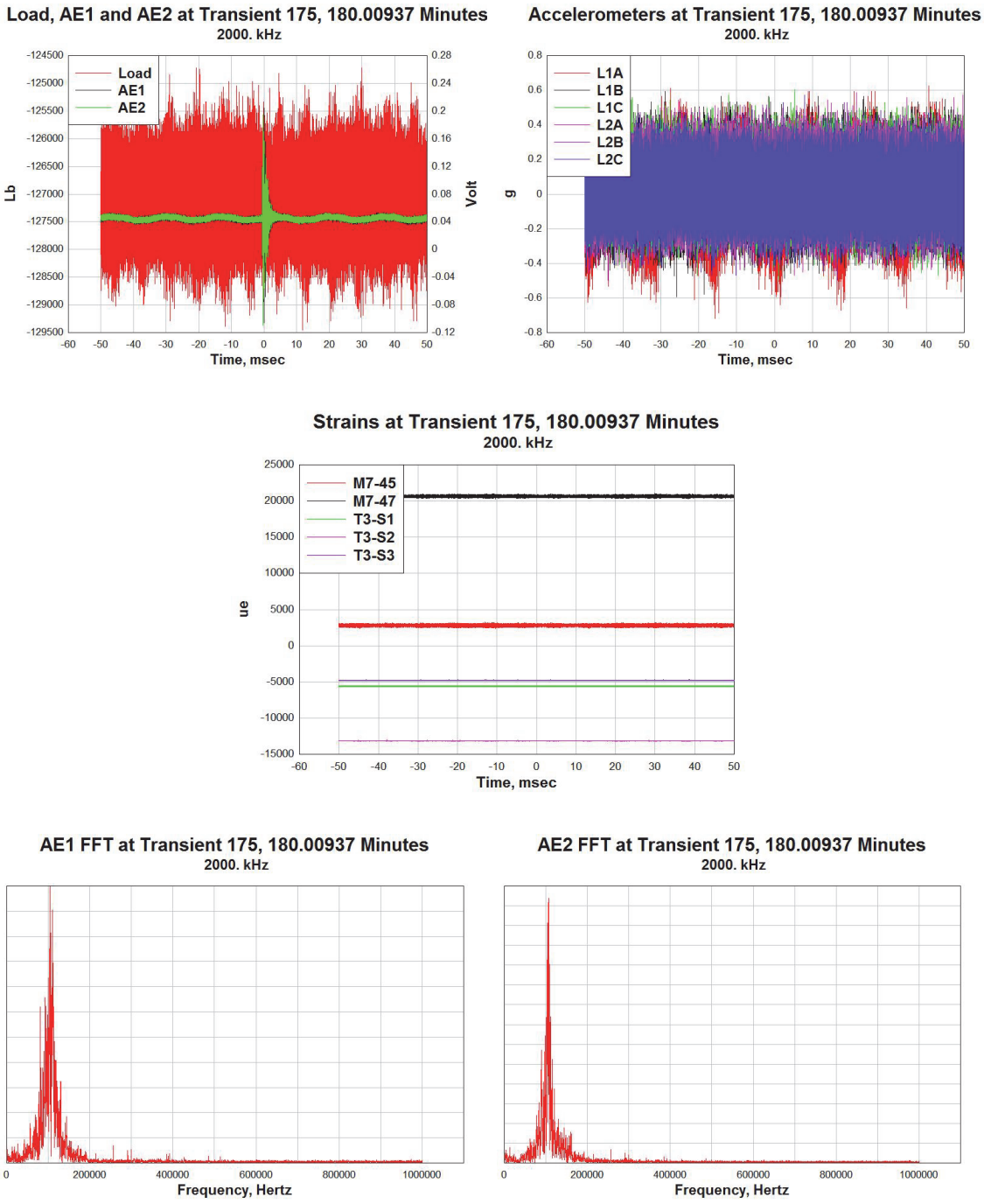

Figure D8. Transient 176 at 180.49957 min of testing time.

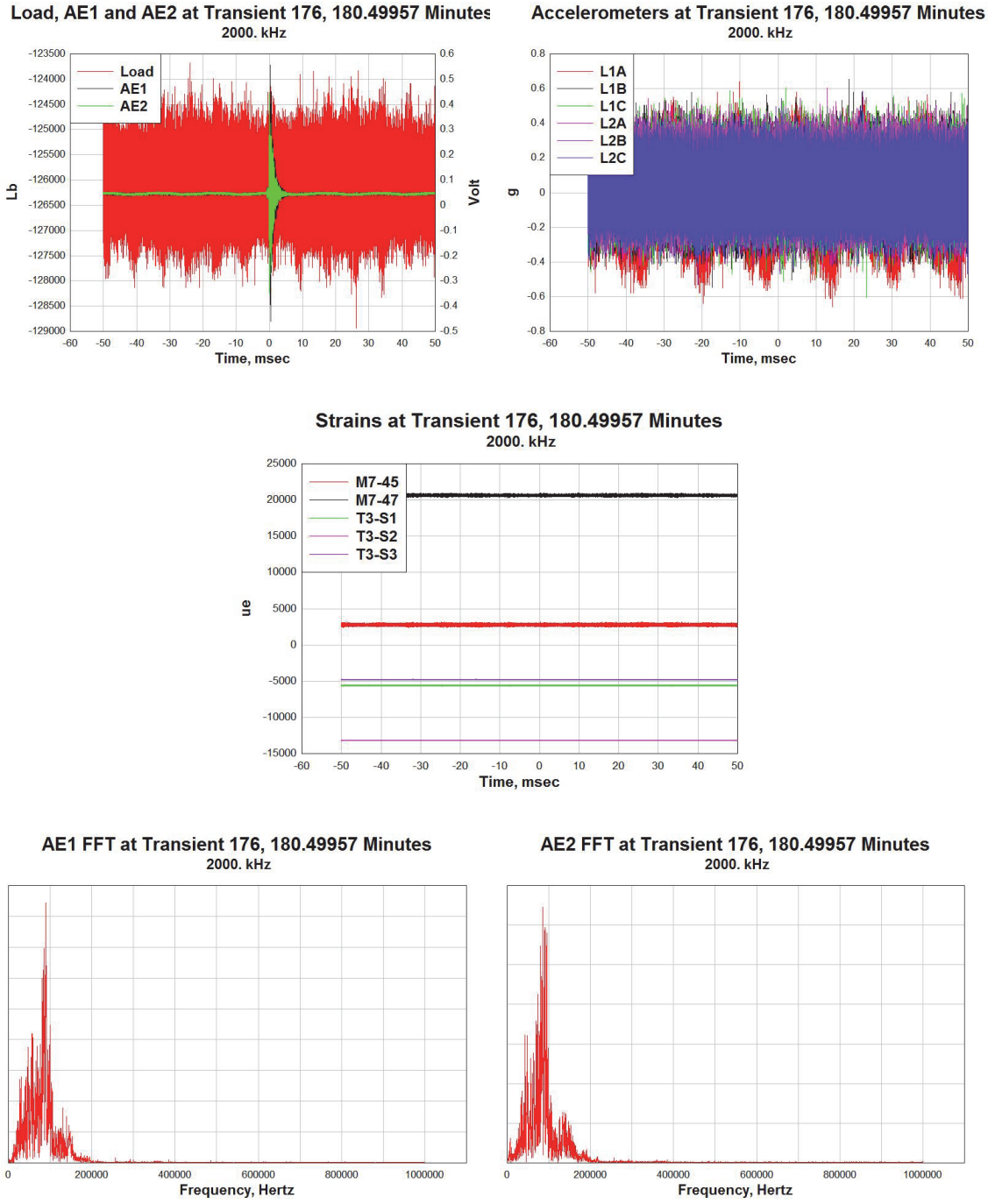

Figure D9. Transient 183 at 212.49307 min of testing time.

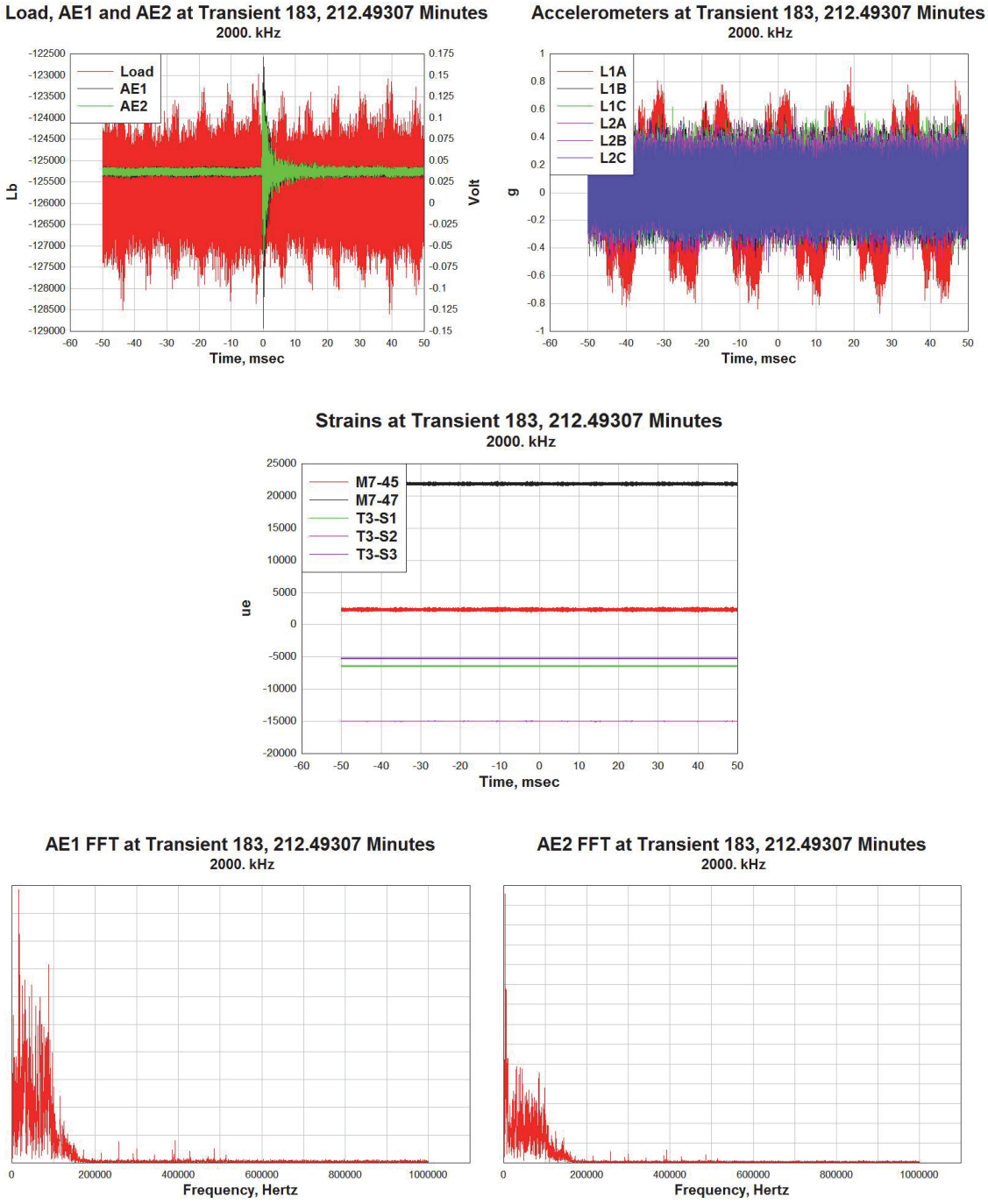

Figure D10. Transient 185 at 213.20287 min of testing time.

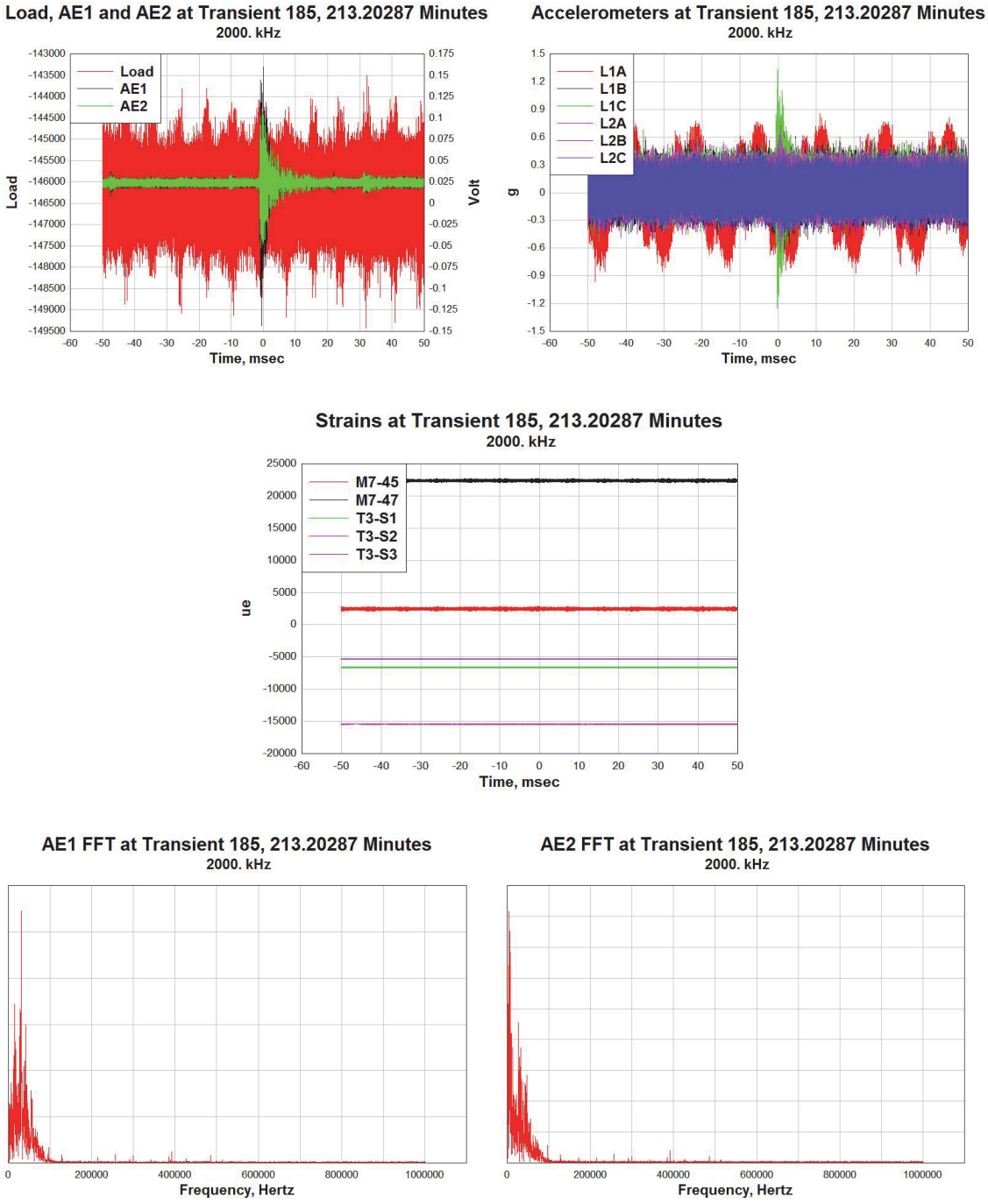

Figure D11. Transient 188 at 213.92347 min of testing time.

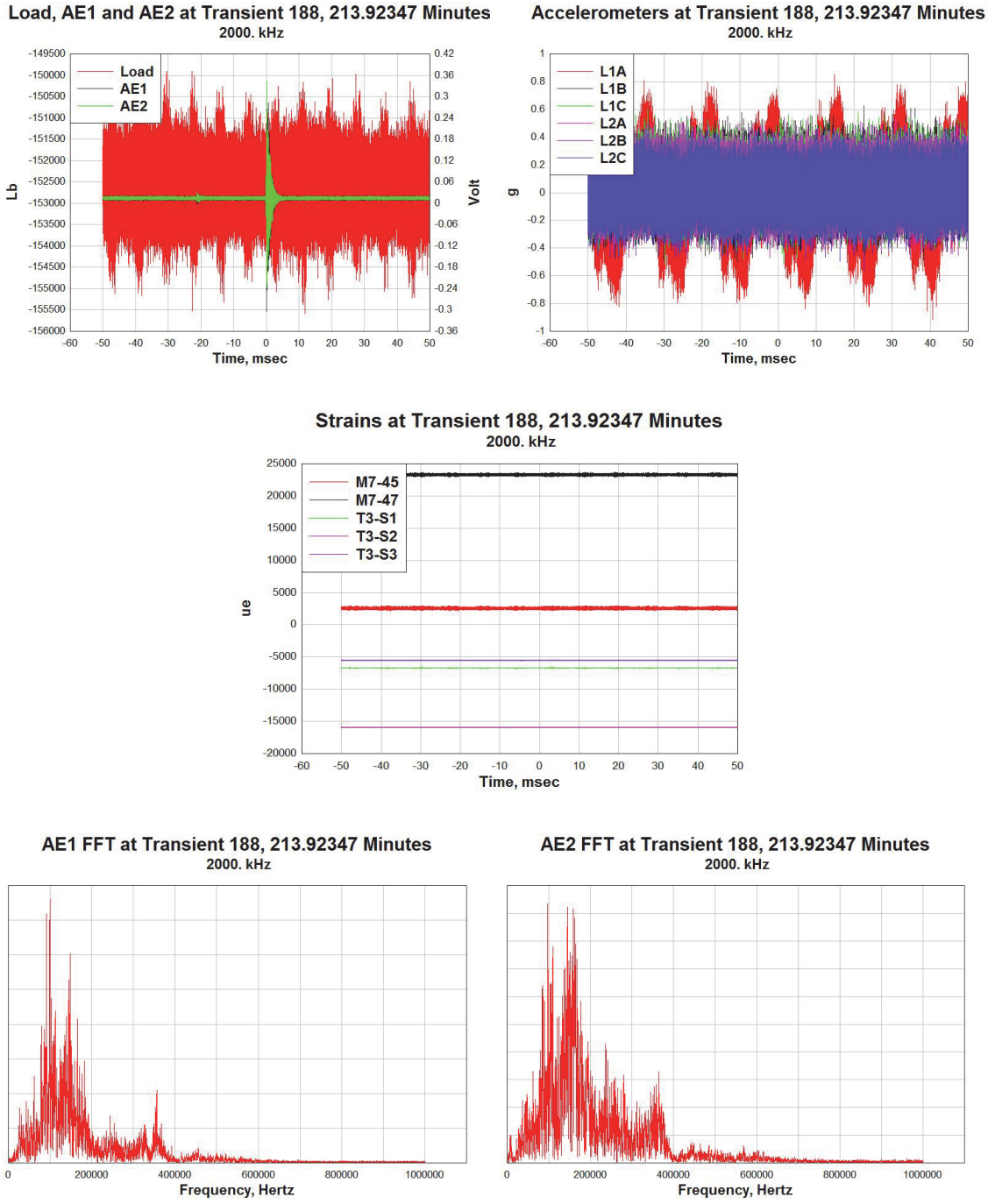

Figure D12. Transient 189 at 214.17967 min of testing time.

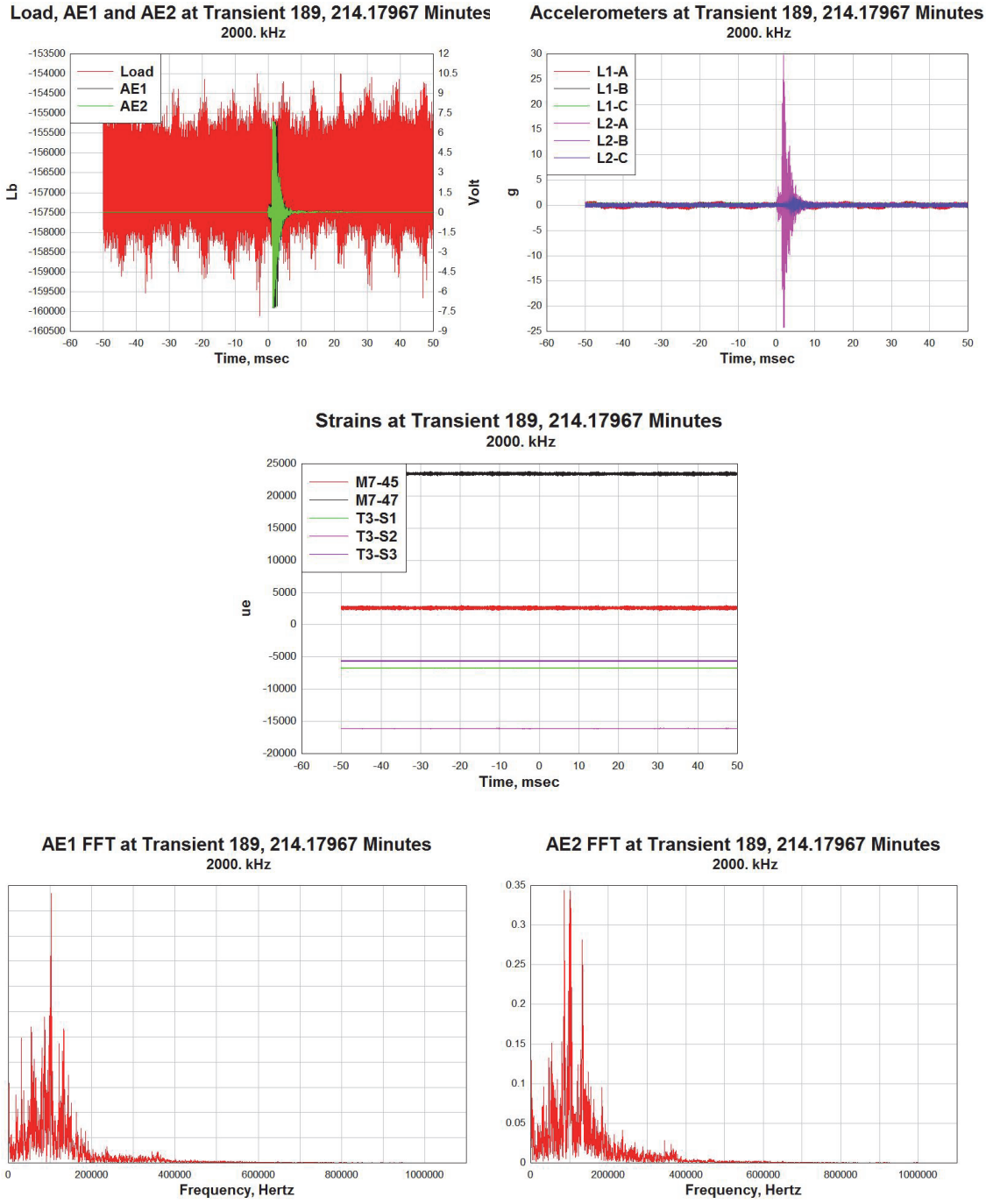

Figure D13. Transient 190 at 214.42847 min of testing time.

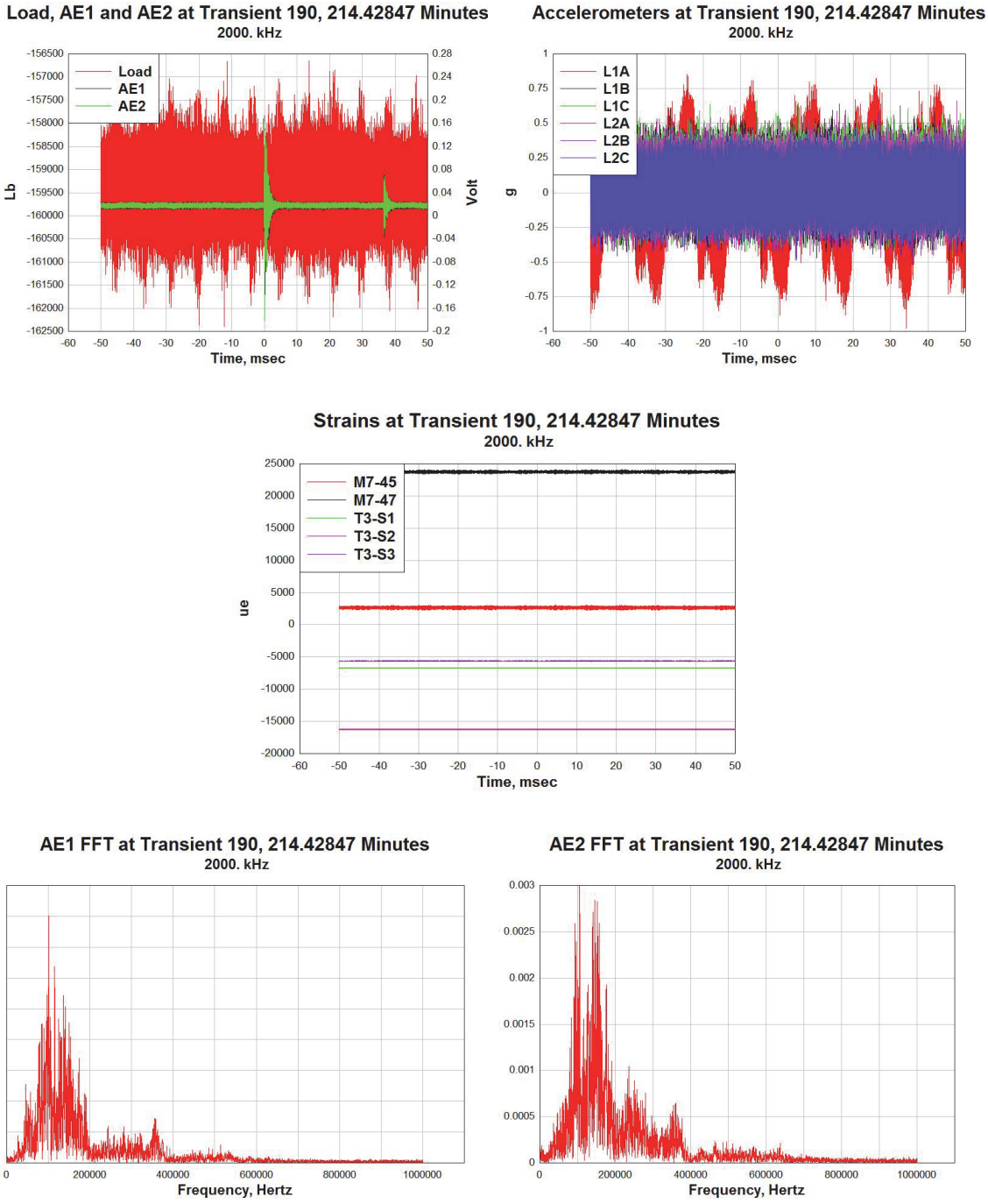

Figure D14. Transient 191 at 214.65727 min of testing time.

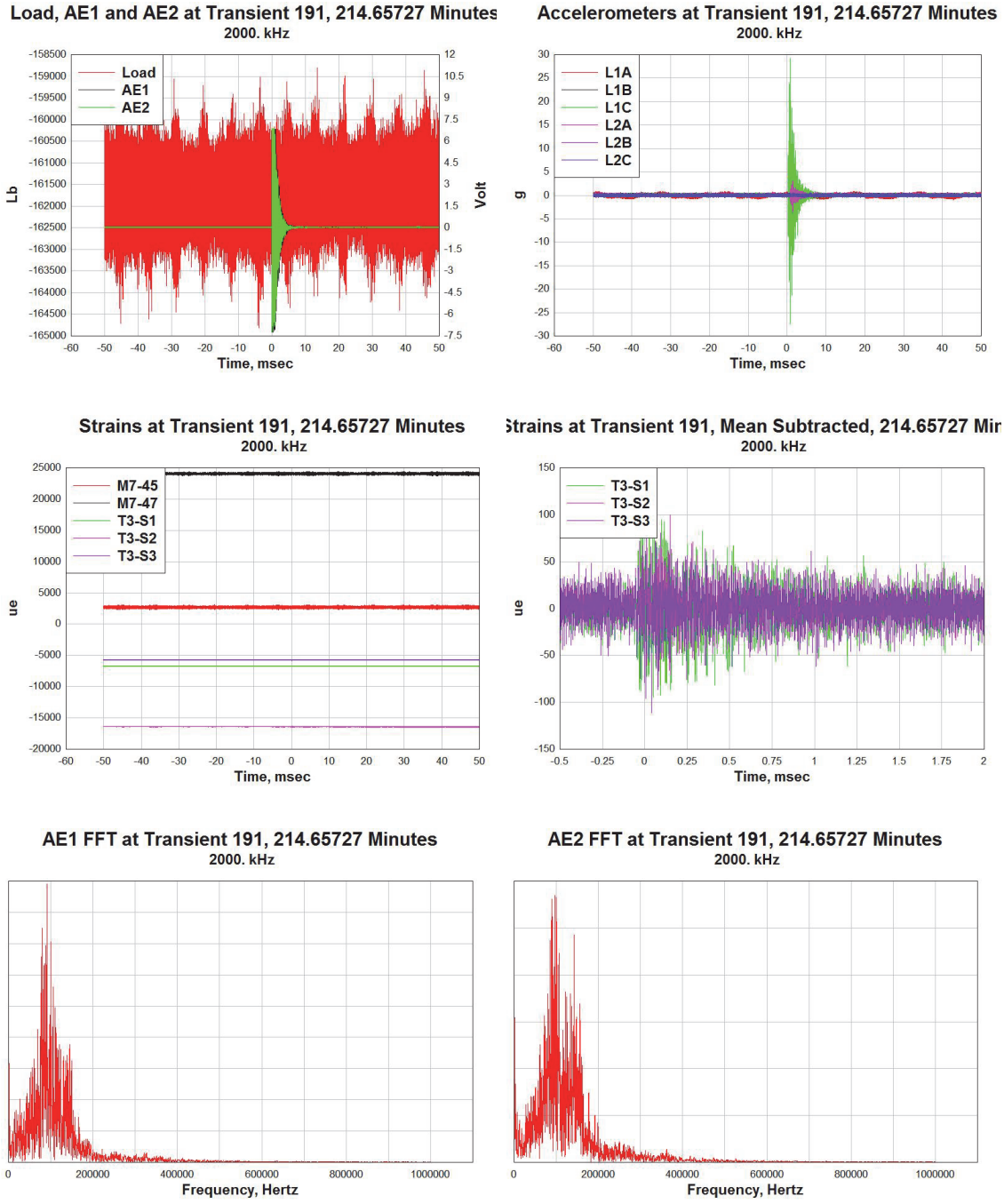

Figure D15. Transient 192 at 216.08777 min of testing time.

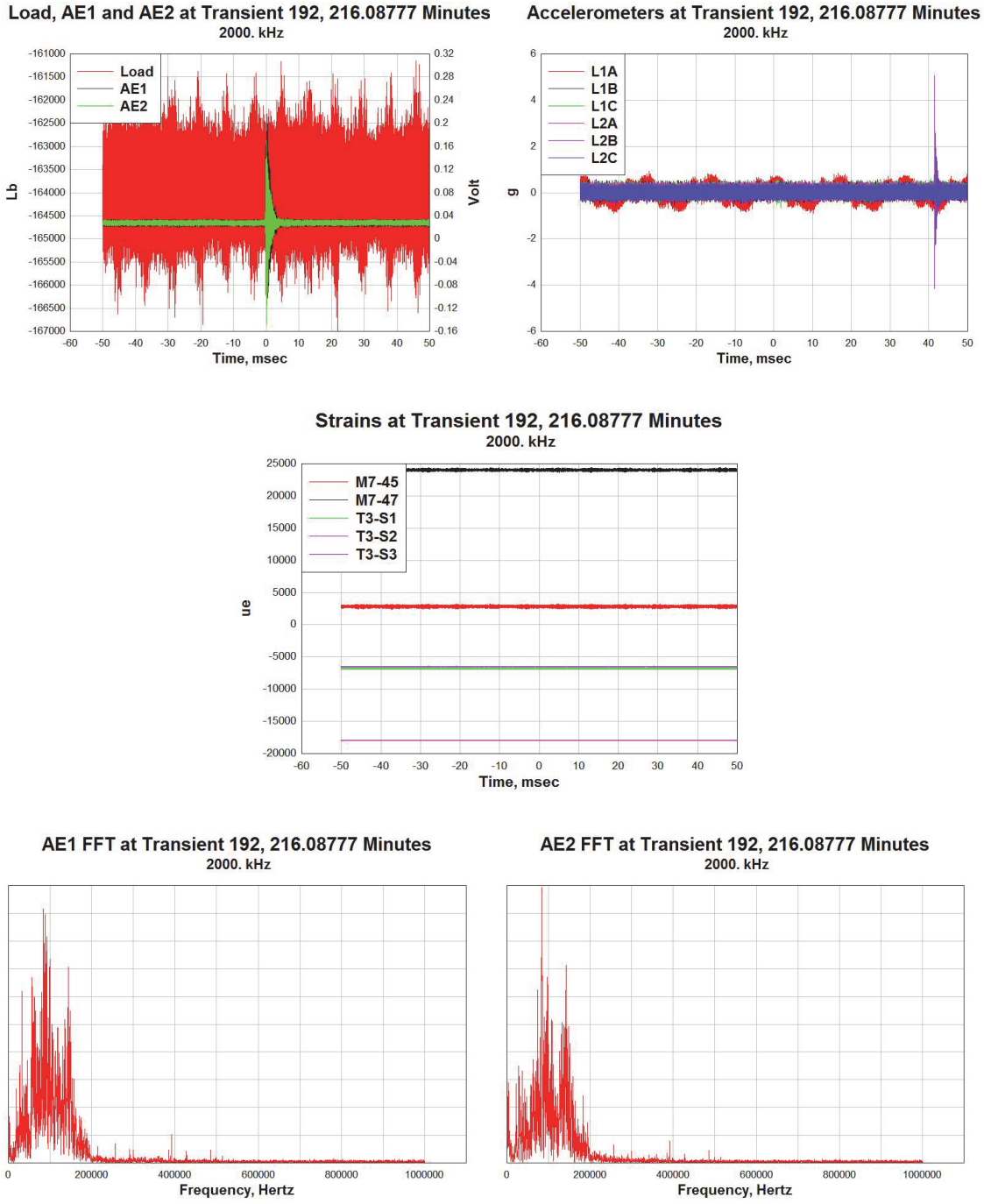

Figure D16. Transient 193 at 216.24227 min of testing time.

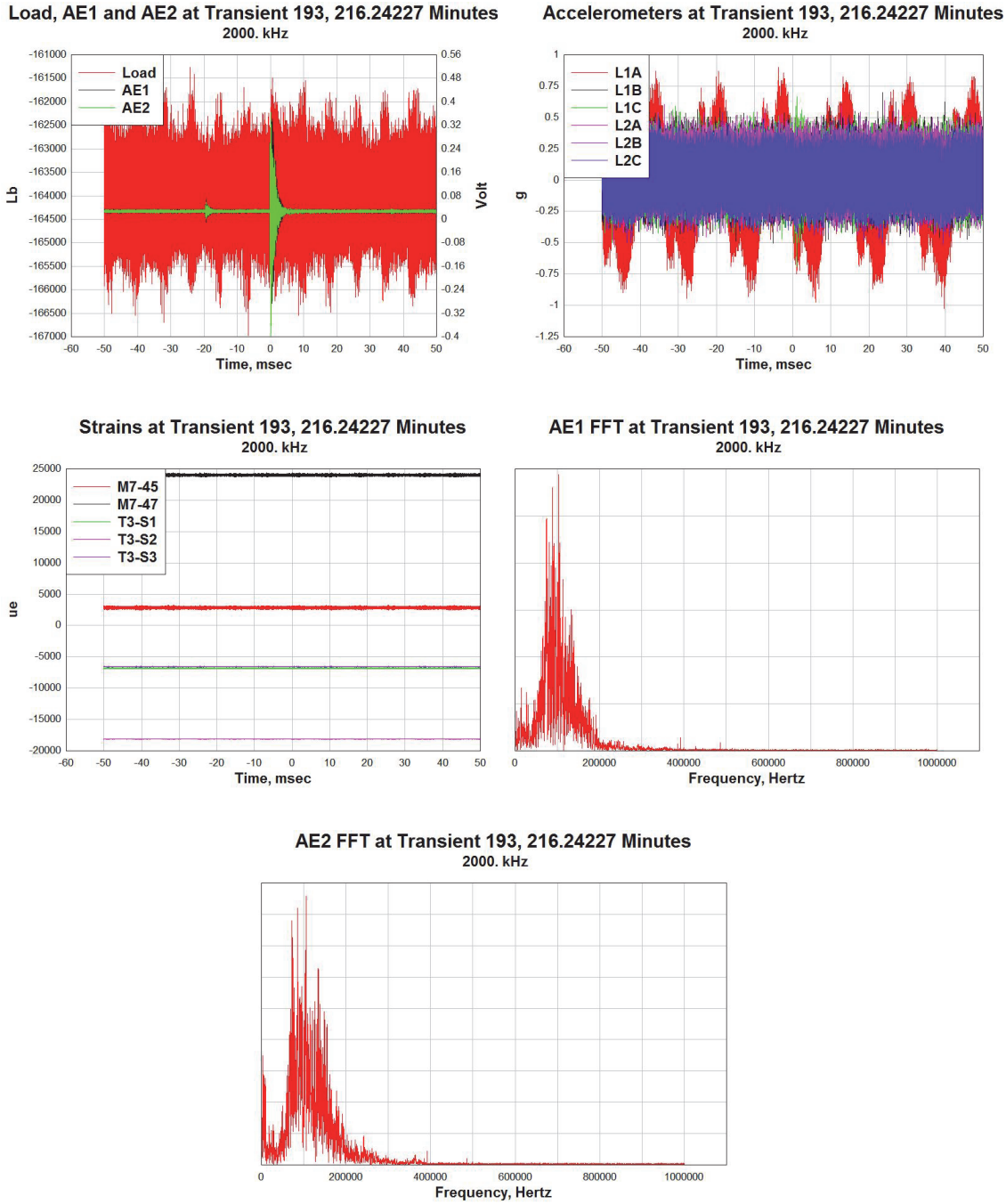

Figure D17. Transient 194 at 216.31747-min. of testing time.

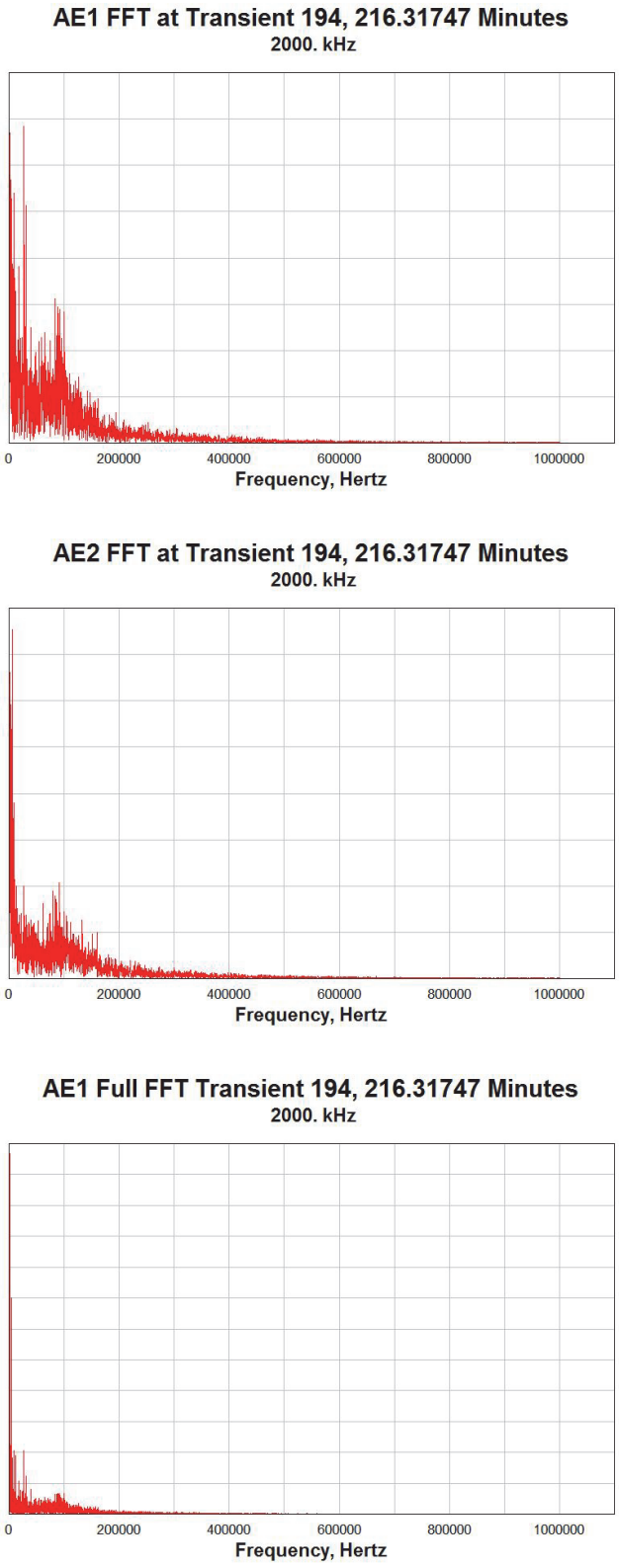

Figure D18. Transient 195 at 276.53837 min of testing time.

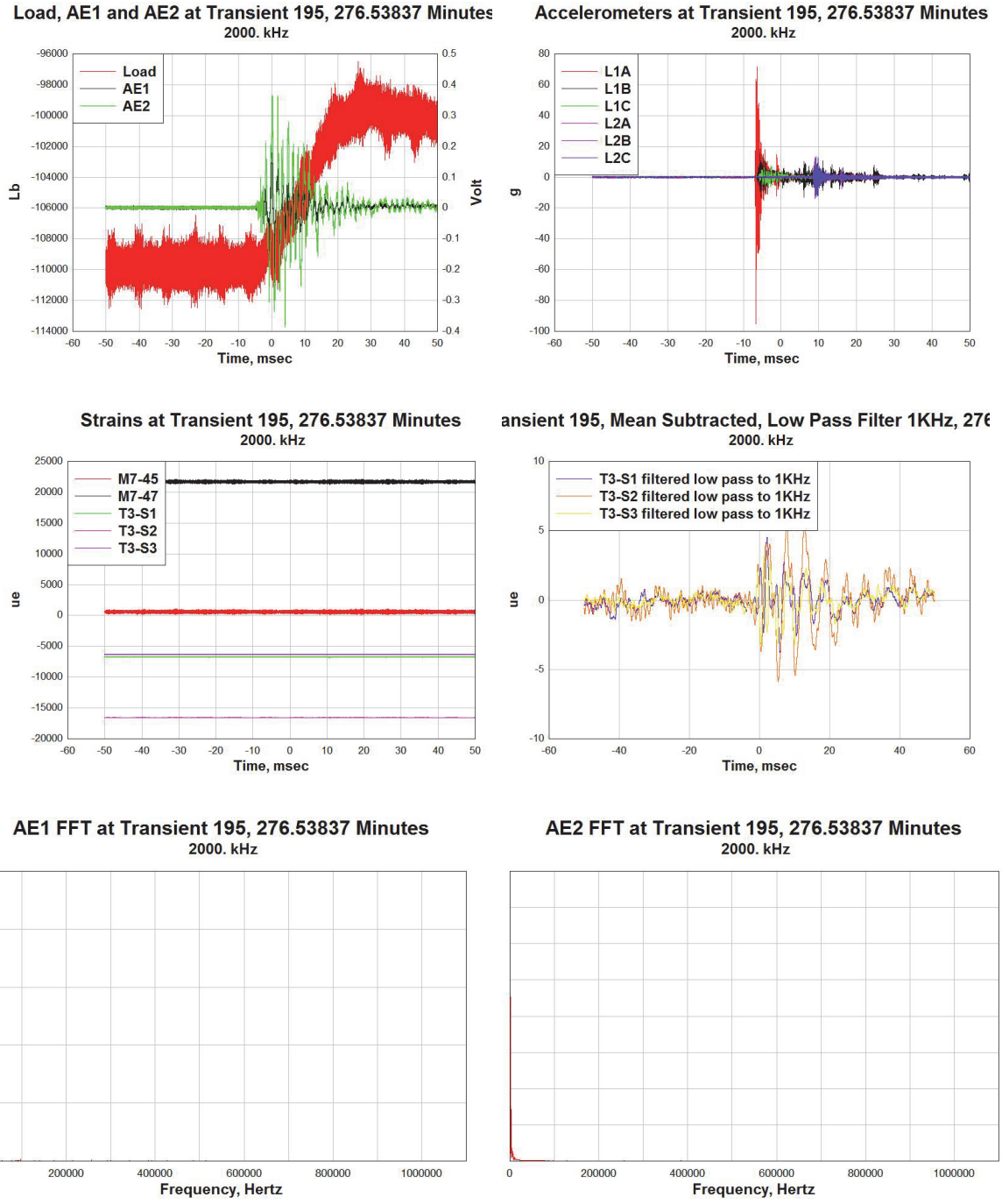

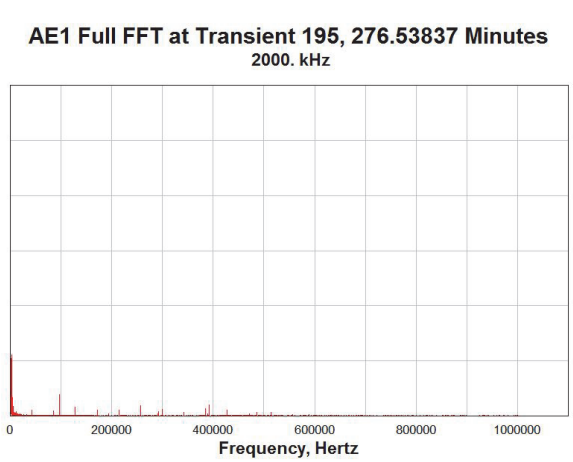
AE1 Full FFT at Transient 195, 276.53837 Minutes
2000. kHz
0
200000
400000
600000
800000
1000000
Frequency, Hertz

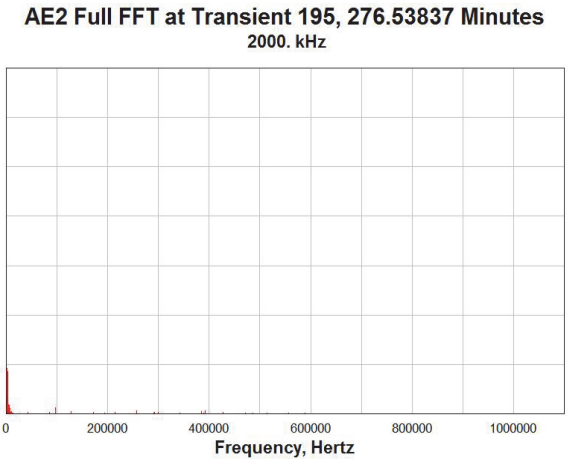
AE2 Full FFT at Transient 195, 276.53837 Minutes
2000. kHz
0
200000
400000
600000
800000
1000000
Frequency, Hertz

Figure D19. Transient 196 at 289.48657 min of testing time.

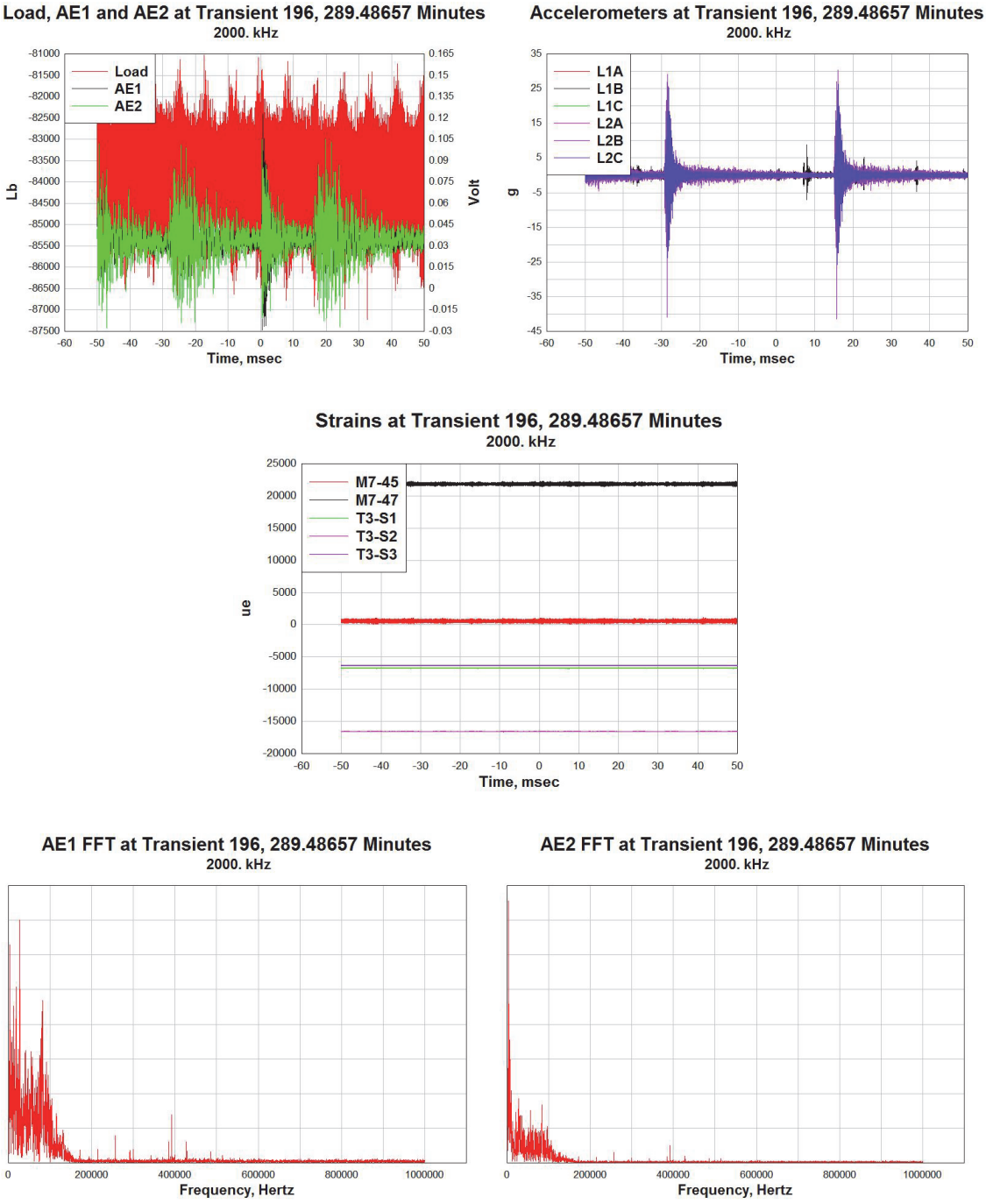

Figure D20. Transient 197 at 291.01937 min of testing time.

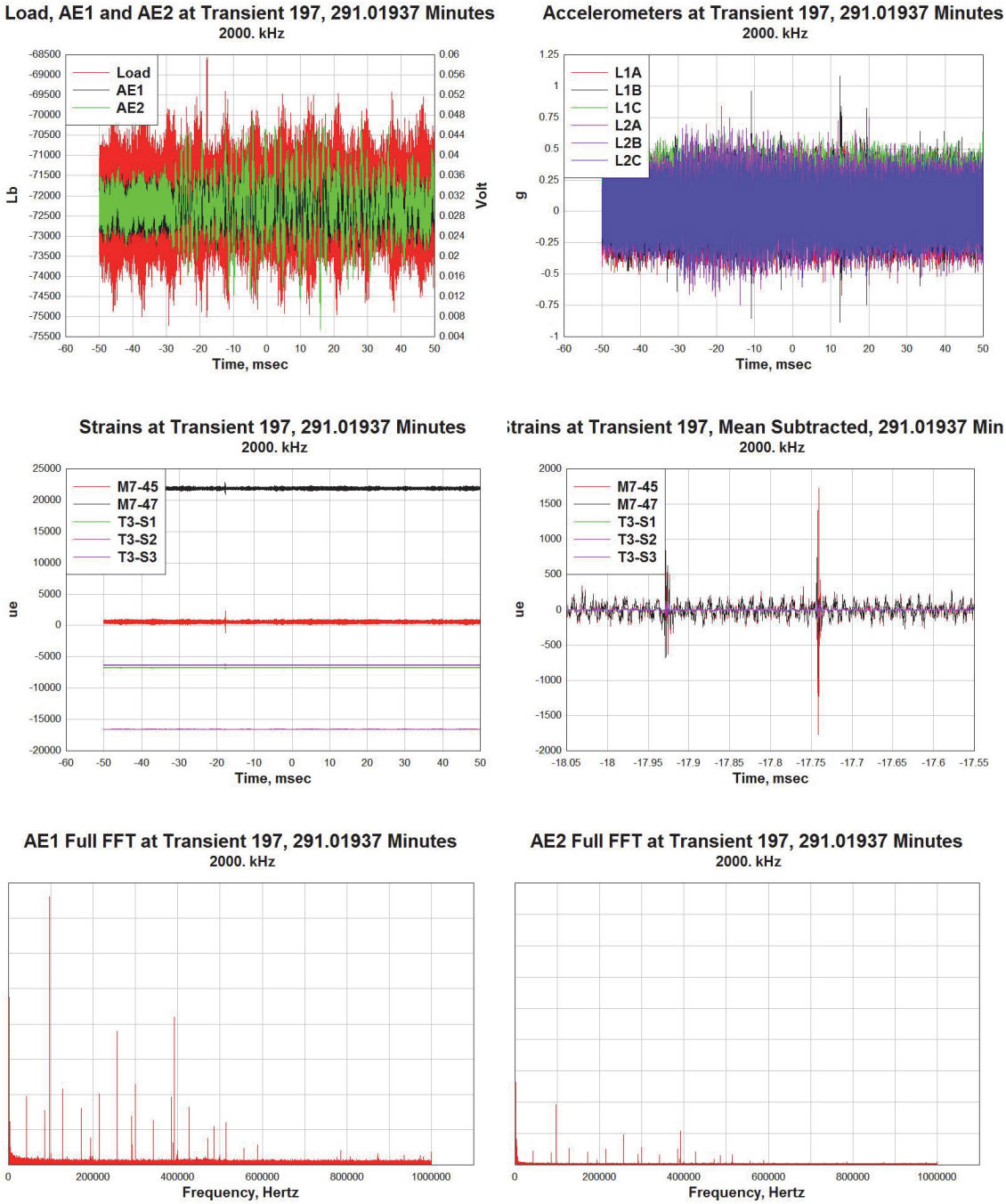

Appendix E: SDC-B Reinforcement A706 Samples Tensile Test Data

A total of (22) bars were sent to Bodycote for Tensile Test - ASTM E8. Table E1 show the ultimate strain recorded from the tensile test of (6) rebar samples. The SDC-B was design using the following bar sizes. Figure E1 to Figure E6 show the strain response of the tested A706 samples.

Table E1. List of rebar samples sent to Boycote for tensile test – ASTM E8.

Sample #	Bar Size	Symbol	Diameter	Label	εu (%)	εu_{avg} (%)
227	#10	V-32W4	1-1/4"	#B	17.80	18
228	#10	V-32W4	1-1/4"	#B	17.95	
231	#8	∞C25W4	15/16"	#D	17.75	18
232	#8	∞C25W4	15/16"	#D	18.16	
222	#4	∞C13W4	1/2"	#H	10.77	11
223	#4	∞C13W4	1/2"	#H	10.71	

Figure E1. Tensile test A706 - #10 bar, sample #227, strain vs. load graph.

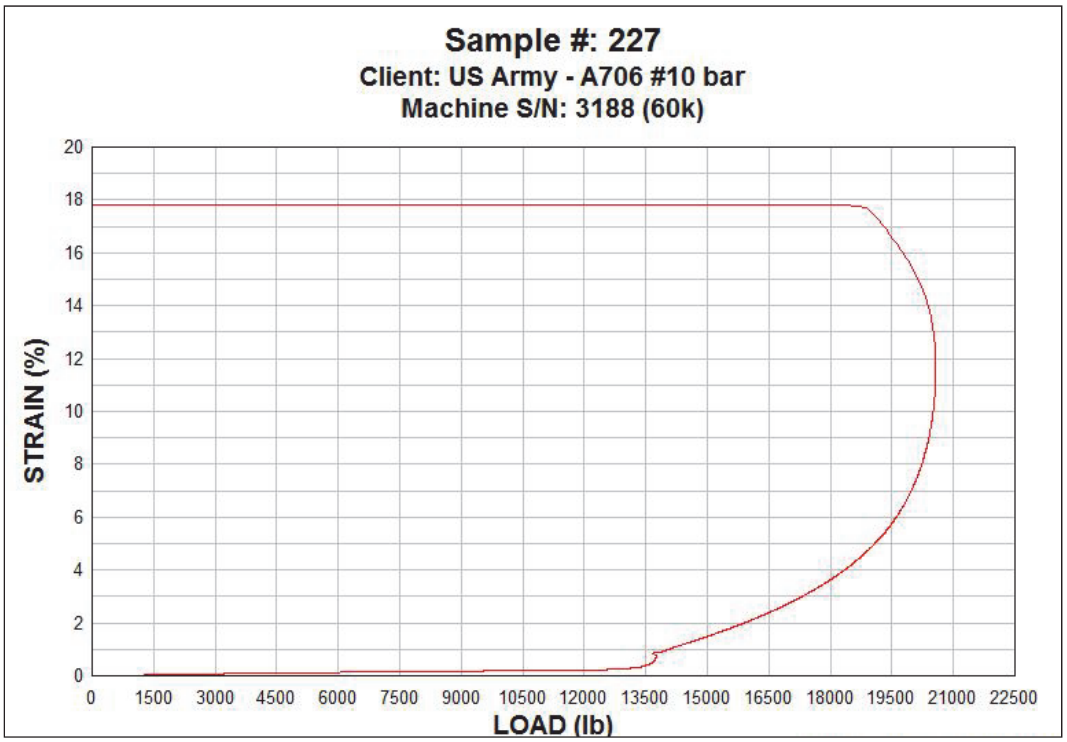

Figure E2. Tensile test A706 - #10 bar, sample #228, strain vs. load graph.

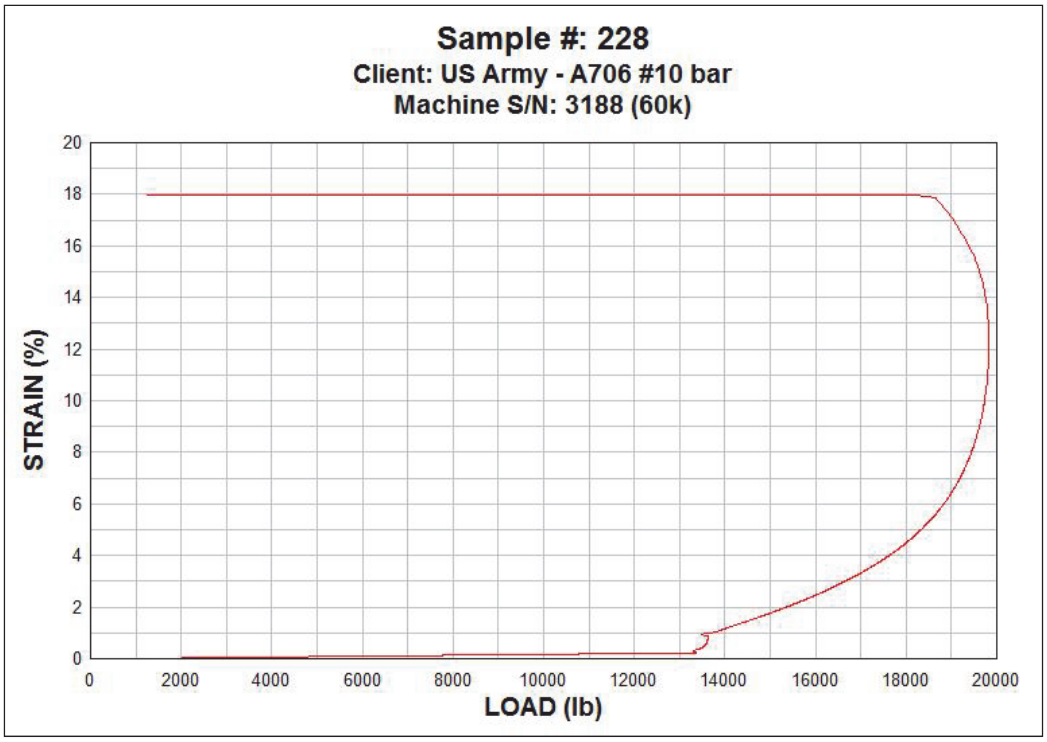

Figure E3. Tensile test A706 - #8 bar, sample #231, strain vs. load graph.

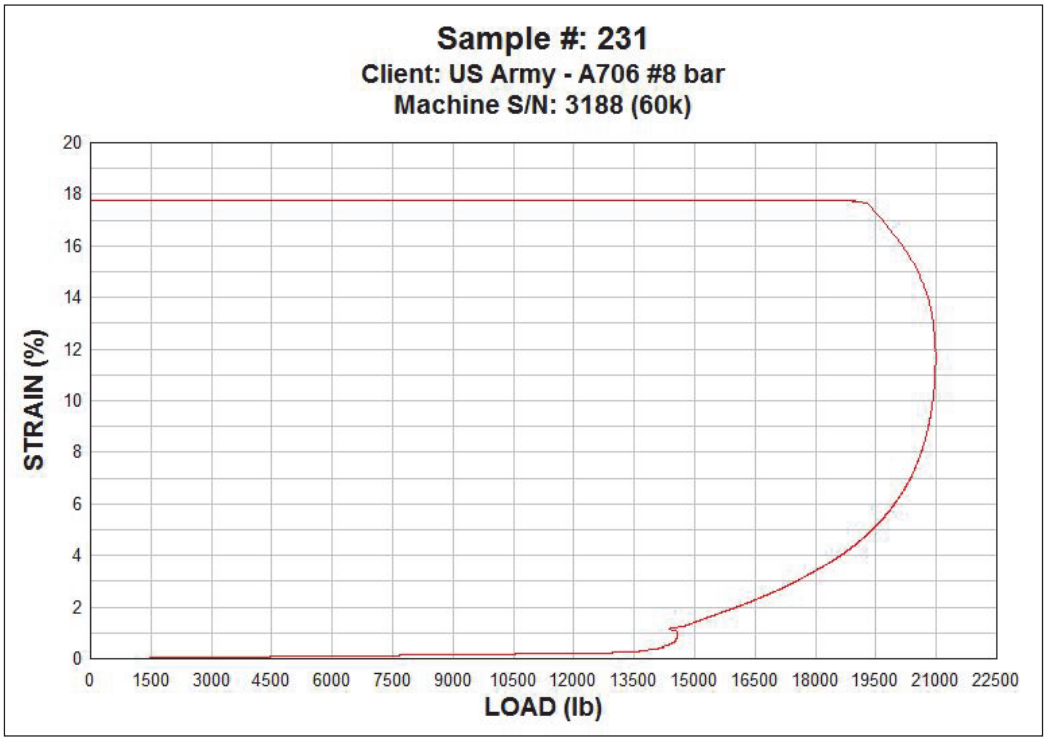

Figure E4. Tensile test A706 - #8 bar, sample #232, strain vs. load graph.

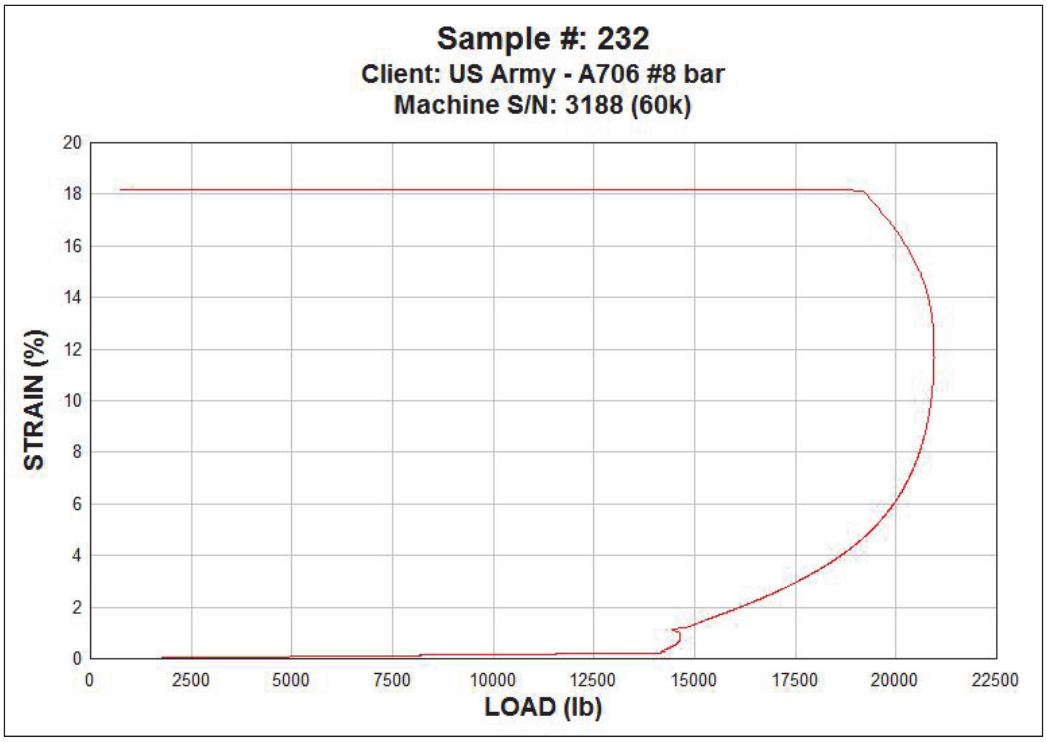

Figure E5. Tensile test A706 - #4 bar, sample #222, strain vs. load graph.

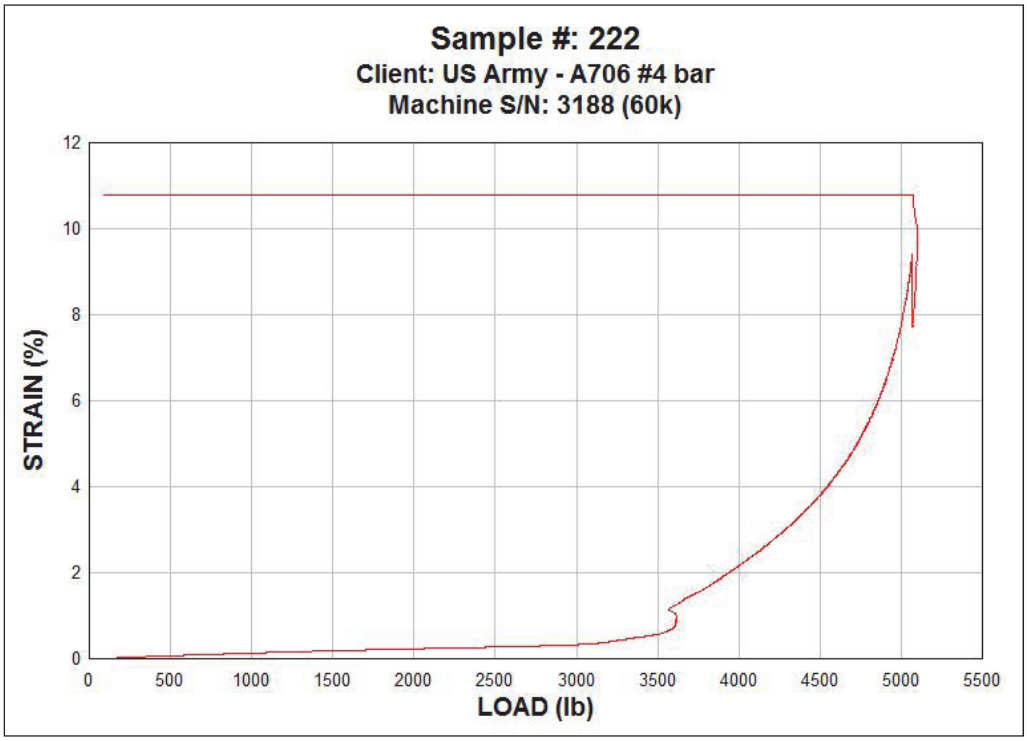

Figure E6. Tensile test A706 - #4 bar, sample #223, strain vs. load graph.

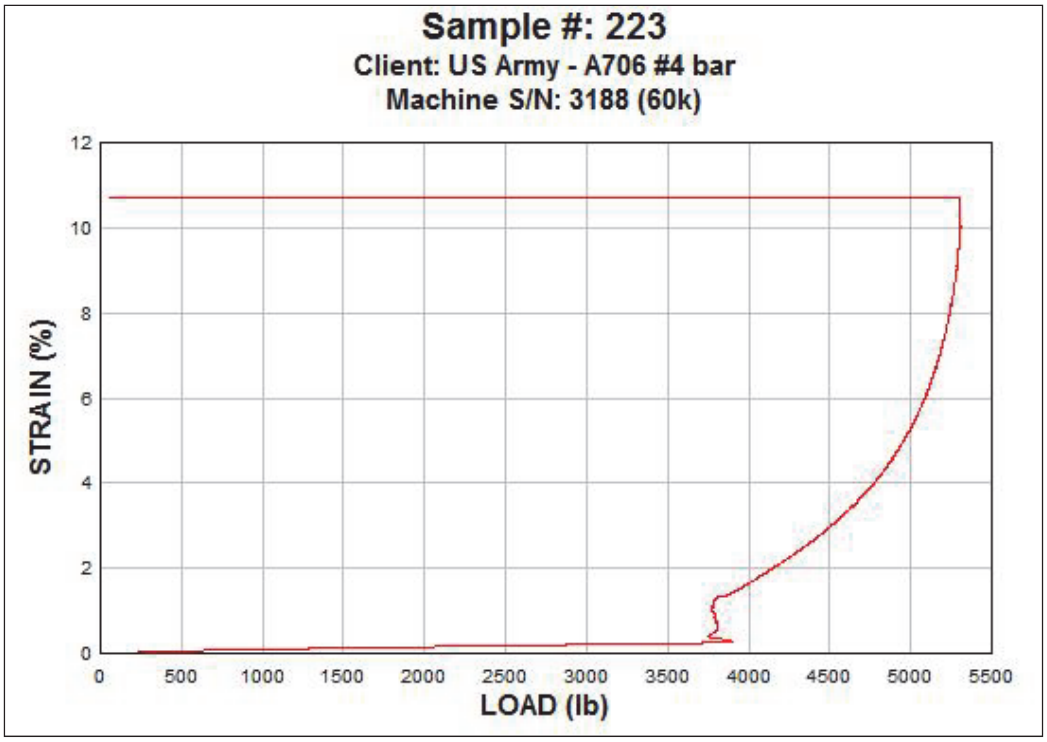

Appendix F: Experimental Safety Procedures

Brittle Failure
Precast Concrete Beam-Column Connection
Seismic Design Category - B

TEST SAFETY PROCEDURE

During the execution of the Brittle Failure Precast Concrete Beam-Column Connection Experiment (SDC-B), all personnel around the test frame and specimen must be wearing appropriate safety equipment such as hard hats, safety glasses, and steel toe shoes. **The yellow painted line on the test floor will serve as the boundary where safety equipment must be worn. Also, the yellow caution lines indicated the boundary where personnel access is allowed during the test. No personnel are allowed to cross the caution lines during the test.**

The static test will encompass applying a load to the top of the stub column using a hydraulic ram that is mounted overhead. The condition of the test specimen will be monitored while it is being loaded, and the testing will stop if the specimen reaches a point where loading it further would pose a safety concern. All employees occupying the upstairs offices and downstairs offices will be required to evacuate their offices 15 minutes before the test or stay in their offices. All employees on the lab floor must be evacuated 15 minutes before the test. The following procedures will be taken leading up to, during, and following the testing:

1. Move all nonessential personnel from the testing floor before starting the test.
2. Place people at each entrance to the test floor to prevent people from walking on test floor during the experiment. The people watching the doors will be out of the line of sight of the reaction frame and specimen.
3. Plywood will cover the windows of the instrumentation building that is located in front of the reaction frame.
4. Only the instrumentation personnel will have access to the inside of the instrumentation building.
5. The specimen will be loaded at increments of 25,000 lb, making a pause of 10-15 minutes between each increment until failure or the maximum

stroke of the hydraulic ram is reached. If the specimen has not reached failure, then a spacer will be placed between the specimen and the ram, and the test will continue until failure

6. Non-essential personnel are not allowed on the test floor until the project engineer on site gives the all clear after all testing has been done on the test specimen.
7. After the testing ends, personnel will be allow adjacent to the test specimen to examine the specimen, **but not inside the reaction frame**.
8. The load will removed from the stub column, and the specimen will be braced to keep it stable.

REPORT DOCUMENTATION PAGE

Form Approved
OMB No. 0704-0188

1. REPORT DATE *(DD-MM-YYYY)*	2. REPORT TYPE	3. DATES COVERED *(From - To)*
December 2014	Final	

4. TITLE AND SUBTITLE

Experimental Evaluation of the Failure of a Seismic Design Category – B Precast Concrete Beam-Column Connection System

5a. CONTRACT NUMBER

5b. GRANT NUMBER

5c. PROGRAM ELEMENT NUMBER

6. AUTHOR(S)

Jorge O. Torres-Alamo, Vincent P. Chiarito, and Henry L. Blake

5d. PROJECT NUMBER

5e. TASK NUMBER

5f. WORK UNIT NUMBER

7. PERFORMING ORGANIZATION NAME(S) AND ADDRESS(ES)

Geotechnical and Structures Laboratory
U.S. Army Engineer Research and Development Center
3909 Halls Ferry Road
Vicksburg, MS 39180-6199

8. PERFORMING ORGANIZATION REPORT NUMBER

ERDC TR-14-12

9. SPONSORING / MONITORING AGENCY NAME(S) AND ADDRESS(ES)

Department of Homeland Security
Washington, DC 20528

10. SPONSOR/MONITOR'S ACRONYM(S)

DHS

11. SPONSOR/MONITOR'S REPORT NUMBER(S)

12. DISTRIBUTION / AVAILABILITY STATEMENT

Approved for public release; distribution is unlimited.

13. SUPPLEMENTARY NOTES

14. ABSTRACT

Modern cities across the United States choose to use multistory buildings in an attempt to optimize the available construction space. These structures are required by governing building codes to be designed for regional or site-specific seismic hazards that affect the resulting loads on moment resisting beam-column connections. These seismically designed connections and seismic structural systems provide resistance to shear and moment forces resulting from the seismic loads. But little is known about predicting their capacity in a brittle manner under a disproportionate collapse condition.

The U.S. Army Engineer Research and Development Center (ERDC) was tasked by the Department of Homeland Security under the Building Stabilization Program to conduct a full-scale experiment to test a precast concrete beam-column system to failure. This experiment was designed to evaluate the performance of precast frame systems in order to develop a methodology and obtain basic insight for predicting the brittle failure of precast beam-column connections under conditions related to a disproportionate collapse scenario. Understanding the parameters that affect the onset of brittle failure of these systems will lead to the development of new techniques allowing first responders to assess the stability of the structures in real time prior to entering for rescue operations.

15. SUBJECT TERMS

Disproportionate/Progressive Collapses
Pre-Cast Concrete Systems
Earthquake
Crack Propagation in Concrete
Brittle Failure of Beam-Column Connections

16. SECURITY CLASSIFICATION OF:			17. LIMITATION OF ABSTRACT	18. NUMBER OF PAGES	19a. NAME OF RESPONSIBLE PERSON
a. REPORT	b. ABSTRACT	c. THIS PAGE			19b. TELEPHONE NUMBER *(include area code)*
Unclassified	Unclassified	Unclassified		126	